# JET PROPULSION

*A publication of the*

AMERICAN ROCKET SOCIETY

*Research and Development*

VOLUME 27 — OCTOBER 1957 — NUMBER 10

# guiding hand for tomorrow's power

Skilled hands coupled with keen minds made today's rocket powerplants a reality. Minds that formulate new theories in powerplant design . . . and hands that prove these theories by careful experiment, test and application.

Guided by such hands and minds, RMI has led the way for over fifteen years—designing and producing record-breaking powerplants for such supersonic vehicles as the X-1A, Skyrocket and the Viking missile. Today and in the future, RMI engineers and scientists will continue to blaze the trail toward advanced propulsion systems for manned and guided flight.

**Engineers, Scientists**—Perhaps you, too, can work with America's *first* rocket family. You'll find the problems challenging, the rewards great.

*Power for Progress*

RMI®

**REACTION MOTORS, INC.**

*A MEMBER OF THE OMAR TEAM*

DENVILLE, NEW JERSEY

4872

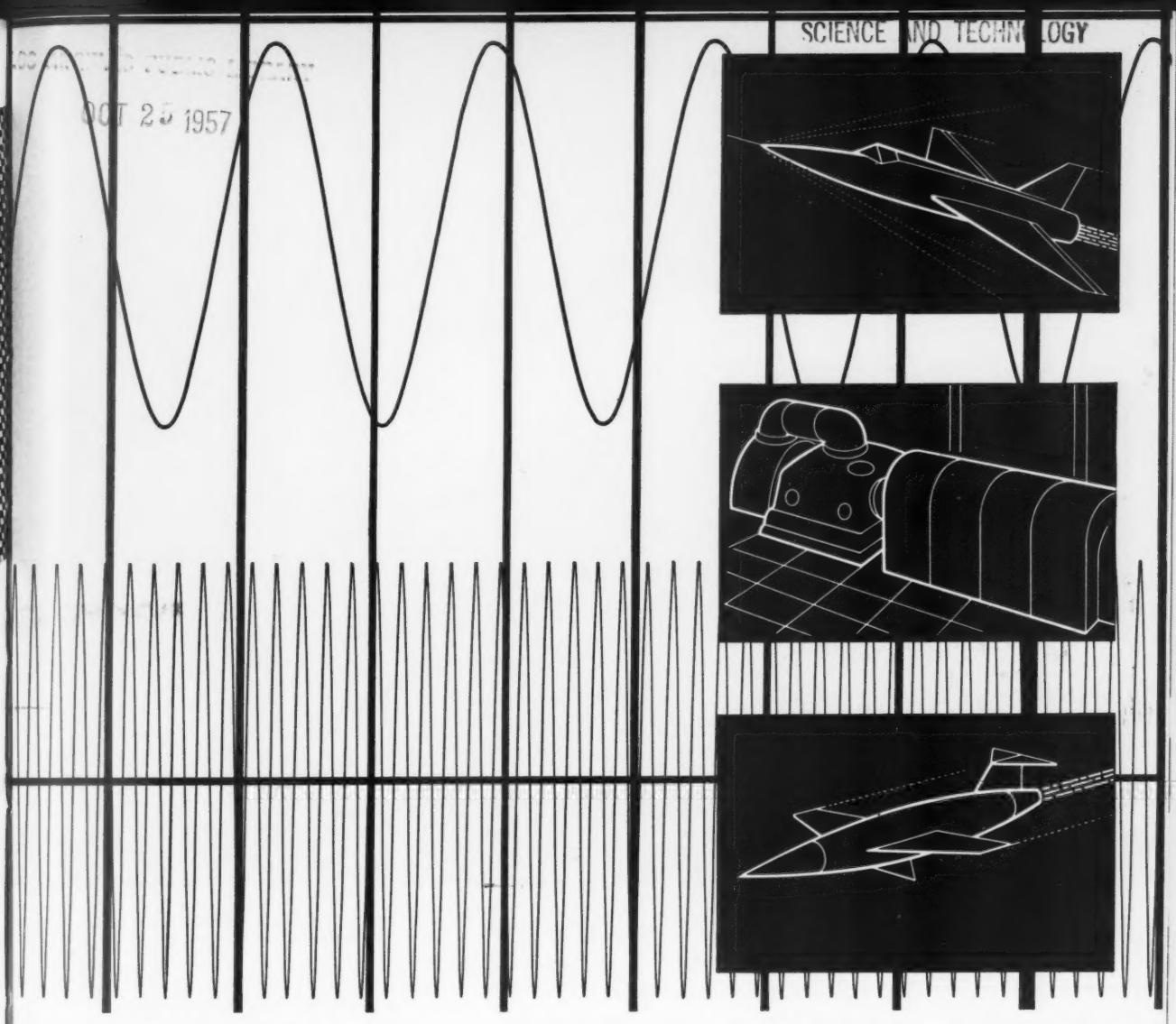

**New from Du Pont!**

# Lino-Writ in 1,000-foot splice-free rolls at no extra cost!

Until now you had to pay premium prices for long splice-free rolls of photorecording paper. Now Du Pont offers the entire line of Lino-Writ in splice-free rolls *in any length* at no extra cost.

With these splice-free rolls, you can put an end to costly losses of records due to traces falling on the splice. Splice-free Lino-Writ gives you accurate, uninterrupted records every time, every test.

Lino-Writ is available in three "speeds" and two thicknesses —plus Lino-Writ 4, the fastest, toughest ultra-thin recording paper made. Whatever your oscillographic requirements, there's a Lino-Writ to fill your needs . . . and now it's splice-free at no extra cost.

For more information on Du Pont Lino-Writ, write the Du Pont Company, Photo Products Department, Wilmington 98, Delaware. In Canada: Du Pont Company of Canada (1956) Limited, Toronto.

DU PONT
REG. U. S. PAT. OFF.
Better Things for Better Living
. . . through Chemistry

**DU PONT OSCILLOGRAPHIC PRODUCTS**
**for Functional Photography**

Photography with a purpose . . . not an end in itself, but a means to an end.

HONEST JOHN, complete except for propellant, warhead and fins, is built of steel by ALCO under prime contract.

# STEEL MAKES A BIRD

**ALCO's unparalleled experience in steel fabrication aids in producing missiles**

For more than a century ALCO has been fabricating steel plate – first into locomotives, then also into heat exchangers, pipe, diesel engines; now into the strong and critical shapes of missiles. ALCO brings to this new problem the special competence that only an experienced steel-plate fabricator can offer.

**A long history** of defense production – both under prime contract and subcontract – is another ALCO asset. Just completed is a contract for M48A2 tanks, now in production is Army's Honest John, as well as Air Force Snark components. On another frontier, ALCO recently completed the Army Package Power Reactor on prime contract; leads in supplying nuclear components under subcontract.

**Seven plants in five states,** with a machine tool inventory of over $50 million, make ALCO defense products. For more information, including a new brochure, "What does it take to make a missile?," write Defense Products, Dept. ONM-2, P. O. Box 1065, Schenectady 1, N. Y.

ALCO

**ALCO PRODUCTS, INC.**
NEW YORK
Sales Offices in Principal Cities

*Locomotives · Diesel Engines · Nuclear Reactors · Heat Exchangers · Springs · Steel Pipe · Forgings · Weldments · Oil-Field Equipment*

## Scope of JET PROPULSION

This Journal is a publication of the American Rocket Society devoted to the advancement of the field of jet propulsion through the dissemination of original papers disclosing new knowledge or new developments. As used herein, the term "jet propulsion" embraces all engines that develop thrust by rearward discharge of a jet through a nozzle or duct, and thus it includes air-consuming engines and underwater systems as well as rockets. JET PROPULSION is open to contributions dealing not only with propulsion but with other aspects of jet-propelled flight, such as flight mechanics, guidance, telemetering, and research instrumentation. Increasing emphasis will be given to the scientific problems of extraterrestrial flight.

## Information for Authors

Manuscripts must be as brief as the proper presentation of the ideas will allow. Exclusion of dispensable material and conciseness of expression will influence the Editors' acceptance of a manuscript. In terms of standard-size double-spaced typed pages, a typical maximum length is 22 pages of text (including equations), 1 page of references, 1 page of abstract, and 12 illustrations. Fewer illustrations permit more text, and vice versa. Greater length will be acceptable only in exceptional cases.

Short manuscripts, not more than one quarter of the maximum length stated for full articles, may qualify for publication as Technical Notes. They may be devoted either to new developments requiring prompt disclosure or to comments on previously published papers. Such manuscripts are usually published within two months of the date of receipt.

Sponsored manuscripts are published occasionally as an ARS service to the industry. A manuscript that does not qualify for publication according to the above-stated requirements as to subject scope or length, but which nevertheless deserves widespread distribution among jet propulsion engineers, may be printed as an extra part of the Journal or as a special supplement if the author or his sponsor will reimburse the Society for actual publication costs. Estimates are available on request. Acknowledgment of such financial sponsorship appears as a footnote on the first page of the article. Publication is prompt since such papers are not in the ordinary backlog.

Manuscripts must be double spaced on one side of paper only with wide margins to allow for instructions to printer. Include a 100 to 200 word abstract. State the authors' positions and affiliations in a footnote on the first page. Do not type equations; write them in ink. Identify unusual symbols or Greek letters for the printer. References are to be grouped at the end of the manuscript and are to be given as follows: for journal articles: authors first, then title, journal, volume, year, page numbers; for books: authors first, then title, publisher, city, edition, and page or chapter numbers. Line drawings must be clear and sharp to make clear engravings. Use black ink on white paper or tracing cloth. Lettering should be large enough to be legible after reduction. Photographs should be glossy prints, not matte or semi-matte. Each illustration must have a legend; legends should be listed in order on a separate sheet.

Manuscripts must be accompanied by written assurance as to security clearance in the event the subject matter lies in a classified area or if the paper originates under government sponsorship. Full responsibility rests with the author.

Submit manuscripts in duplicate (original plus first carbon, with two sets of illustrations) to the Editor, Martin Summerfield, Professor of Aeronautical Engineering, Princeton University, Princeton, N. J. Preprints of papers presented at ARS national meetings are automatically considered for publication.

JET PROPULSION is published monthly by the American Rocket Society, Inc., and the American Interplanetary Society at 20th & Northampton Sts., Easton, Pa., U. S. A. Editorial offices: 500 Fifth Ave., New York 36, N. Y. Price: $12.50 per year, $2.00 per single copy. Entered as second-class matter at the Post Office at Easton, Pa. Notice of change of address should be sent to the Secretary, ARS, at least 30 days prior to publication. Opinions expressed herein are the authors' and do not necessarily reflect the views of the Editors or of the Society.


JET PROPULSION
A publication of the
AMERICAN ROCKET SOCIETY
Research and Development

IRWIN HERSEY—DIRECTOR OF PUBLICATIONS

EDITOR — MARTIN SUMMERFIELD

ASSISTANT EDITORS — LARKIN JOYNER, STANLEY BEITLER

ART EDITOR — JOHN CULIN

ASSOCIATE EDITORS

ALI BULENT CAMBEL, *Northwestern University*
IRVIN GLASSMAN, *Princeton University*
M. H. SMITH, *Princeton University*

CONTRIBUTORS

MARSHALL FISHER, *Princeton University*
GEORGE F. McLAUGHLIN

ADVERTISING & PROMOTION MANAGER

WILLIAM CHENOWETH

ADVERTISING REPRESENTATIVES

D. C. Emery & Associates
155 East 42 St., New York, N. Y.
Telephone: Mu 4-7232

James C. Galloway & Co.
6535 Wilshire Blvd., Los Angeles, Calif.
Telephone: Olive 3-3223

Jim Summers & Asssociates
35 E. Wacker Dr., Chicago, Ill.
Telephone: Andover 3-1154

R. F. Pickrell and Associates
318 Stephenson Bldg., Detroit, Mich.
Telephone: Trinity 1-0790

Harold Short
Holt Rd., Andover, Mass.
Telephone: Andover 2212

Rodney W. Cramer
852 Leader Bldg., Cleveland, Ohio
Telephone: Main 1-9357

"NIMBUS," a new painting by the well-known team of science-artists Simpson-Middleman. In this work, the creators have found new artistic meaning in the Moon and its reflected light. An attempt to capture the polarized nature of moonlight is made. The result, an almost half-light. Collection of the Whitney Museum of American Art, New York.

## Work in the world of supersonic flight—at Boeing

Supersonic flight is still in its infancy, and Boeing engineers are engaged in the adventurous task of pushing forward the frontiers of knowledge in this years-ahead world. Underway at Boeing are design projects for top-secret aircraft and missiles far more advanced than any yet developed. Related explorations delve into the required properties and capabilities of materials, fuels and systems not yet in existence. You'd find working on advanced Boeing projects a true adventure—challenging, rewarding, stature-building. Boeing offers this opportunity today to scientists, and to experienced engineers in many categories.

**BOEING**

*Drop a note now, to John C. Sanders, Engineering Personnel Administrator, Boeing Airplane Company, Department P-68, Seattle 24, Washington.*

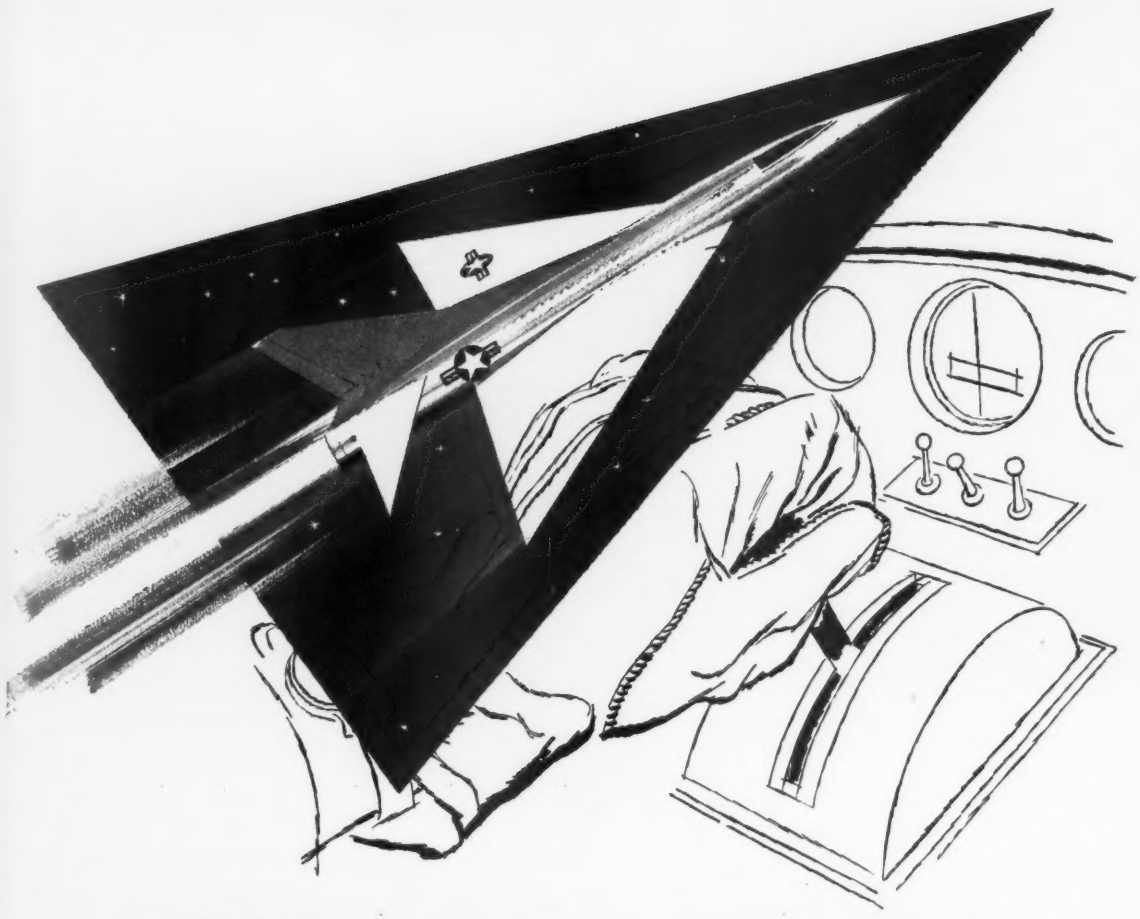

# *Higher and faster than ever before*

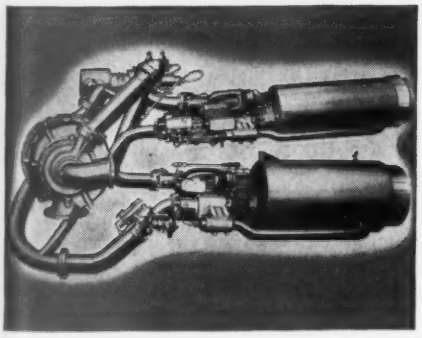

World's first throttleable rocket engine is one of a group of Curtiss-Wright powerplants and missiles capable of several times the speed of sound.

The Curtiss-Wright Rocket Engine would fit under the hood of your car, yet delivers a thrust equal to the power that drives a Navy cruiser at high speeds . . . a thrust that has flown man higher and faster than ever before. And this record-breaking power is controlled, by the hand of the pilot, for the first time in history . . . doesn't burn itself out in ordinary rocket fashion.

The pilot can control his thrust through a wide range, start or stop it at will, conserve fuel or use it all in one prolonged burst. Operating at speeds near the thermal barrier he can explore the advanced problems of supersonic and hypersonic flight.

The Rocket Engine is one of a group of Curtiss-Wright powerplants and missiles capable of several times the speed of sound...a group that includes also the Ram Jet... and the HTV rocket which reaches supersonic speed a fraction of a second after launching.

PROPELLER DIVISION

***Rocket Engines by*** **CURTISS-WRIGHT**

**CORPORATION • CALDWELL, N. J.**

**Divisions and Wholly Owned Subsidiaries of Curtiss-Wright Corporation:**

WRIGHT AERONAUTICAL DIVISION, *Wood-Ridge, N. J.* • PROPELLER DIVISION, *Caldwell, N. J.* • PLASTICS DIVISION, *Quehanna, Pa.* • ELECTRONICS DIVISION, *Carlstadt, N. J.* METALS PROCESSING DIVISION, *Buffalo, N. Y.* • SPECIALTIES DIVISION, *Wood-Ridge, N. J.* • UTICA-BEND CORPORATION, *Utica, Mich* • EXPORT DIVISION, *New York, N. Y.* CALDWELL WRIGHT DIVISION, *Caldwell, N. J.* • AEROPHYSICS DEVELOPMENT CORPORATION, *Santa Barbara, Calif.* • RESEARCH DIVISION, *Clifton, N. J.* & *Quehanna, Pa.* INDUSTRIAL AND SCIENTIFIC PRODUCTS DIVISION, *Caldwell, N. J.* • CURTISS-WRIGHT EUROPA, *N. V., Amsterdam, The Netherlands* • TURBOMOTOR DIVISION, *Princeton, N. J.* MARQUETTE METAL PRODUCTS DIVISION, *Cleveland, Ohio* • CURTISS-WRIGHT OF CANADA LTD., *Montreal, Canada* • PROPULSION RESEARCH CORPORATION, *Santa Monica, Calif.*

for
analog computer
readout:

modern, compact, mobile

# SANBORN

## CONSOLE RECORDING SYSTEMS

Up to eight problem variables can be recorded in inkless, permanent, rectangular-coordinate tracings—with Sanborn's improved six- and eight-channel 156-, 158-5490 Console Systems. Less than four feet high and about two feet in width and depth, these Systems are completely mobile and designed for maximum operating convenience. Controls and indicators on the sloping top panel include individual-channel attenuation, position, balance, sensitivity and stylus heat adjustments; switch for turning off B+ of output amplifiers; chart drive motor switch (can also be remotely controlled); code marker and/or one-second interval timer stylus switch. The Recorder unit, either six or eight channels, features paper loading from the top, and nine precisely controlled speeds from 0.25 to 100 mm/sec. Four dual-channel DC Driver Amplifiers of current feedback design are housed below the Recorder, and are mounted on a chassis which may be withdrawn for inspection.

Electrical specifications of the Console Recording Systems include a basic sensitivity of either .01 volt/chart division (5490 types) or 0.1 volt chart division (5495 types); linearity of 1%; drift less than 1/2 chart division/hour (5490), less than 1/20 chart division/hour (5495); flat frequency response to 20 cps, down 3 db at 60 cps for all amplitudes to 5 cm peak; either single-ended or push-pull input signals of 5 meg. impedance (each input lead to ground).

A useful companion instrument is the new Sanborn Model 183 Programmer, designed to provide a connecting link between an analog computer and the Console Recording System. Shown mounted at the top rear of the Console, the Programmer operates the Console in the following automatic sequence: turns recorder drive on—feeds calibration signals to all channels—reads initial DC levels of computer—closes contacts to start computer problem—records computer output for a preset chart length—turns off recorder drive and resets itself for another cycle.

Further technical data, prices and delivery information—on the 5490/5495 Console Recording Systems and two- to eight-channel 5475/5480 Systems are available on request from your Sanborn Sales-Engineering Representative or the Industrial Division in Waltham.

40th ANNIVERSARY 1917–1957 SANBORN COMPANY

**SANBORN COMPANY**
INDUSTRIAL DIVISION
175 Wyman Street, Waltham 54, Massachusetts

# PRECISE FREQUENCY CONTROL

## Robertshaw-Fulton Crystal Oven

This new compact precision Crystal Oven uses fusion temperatures of crystalline materials to provide extremely constant crystal cavity temperatures.

Completely self-contained, the unit features a continuous proportional control system which eliminates contact noise, power surges, random variations of oven temperatures, and cavity temperature drift.

### SPECIFICATIONS

**CAVITY TEMPERATURE:**
70.6°C at 24°C ambient.

**TEMPERATURE CONTROL:**
Within ±0.5°C from −20°C to +50°C ambient.
Approx. ±0.005°C at fixed ambient.

**HEATER VOLTAGE:**
5 v. a.c. or v. d.c. regulated ±2%.

**HEAT POWER:**
On warm up: approx. 5 watts
Under control: 1.6 w at TA 24°C
3.5 w at TA −20°C

**DIMENSIONS:**
2" O.D. x 4" Length.

**WEIGHT:**
Approximately 12 ounces.

**CRYSTAL HOLDER:**
Accommodates 1 HC-6/U holder.

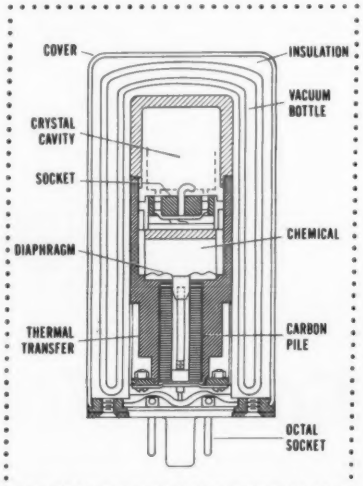


### APPLICATIONS

Temperature control of a crystal or crystal oscillator for secondary frequency standards.

Temperature control of sensitive components, such as resistance-capacitance networks in oscillators or computer circuits.

Temperature control of zener diodes for voltage reference units in d.c. power supplies.

Constant temperature for thermocouple reference junctions.

Reference temperature for calibrating thermistors by using ovens with different cavity temperatures.

*For more information on this compact, extremely reliable Crystal Oven, send for Bulletin No. 1181-1.*

PRODUCTS FOR PROGRESS
BY THE MEN OF
AERONAUTICAL DIVISION
Robertshaw-Fulton
CONTROLS COMPANY
Santa Ana Freeway at Euclid Avenue • Anaheim, California

**OUTSTANDING FACILITIES FOR THE RESEARCH AND DEVELOPMENT OF SPECIALIZED CONTROL DEVICES**


# DOUBLE DIAGNOSIS TO PREVENT "HEART DISEASE"

## ...BY THE B&H JETCAL® ANALYZER

Two of the most important factors that affect jet engine life, efficiency, and safe operation are *Exhaust Gas Temperature (EGT)* and *Engine Speed (RPM)*. Excess heat will reduce "bucket" life as much as 50% and low EGT materially reduces efficiency and thrust. Any of such conditions will make operation of the aircraft both costly and dangerous. The *JETCAL Analyzer pre*determines accuracy of the EGT and (interrelatedly) Tachometer systems and isolates errors if they exist.

### The *JETCAL* ANALYZES JET ENGINES 10 WAYS:

1) The JETCAL Analyzer *functionally* tests EGT thermocouple circuit of a jet aircraft or pilotless aircraft missile for error *without running the engine or disconnecting any wiring*. GUARANTEED ACCURACY is ±4°C. at engine test temperature.

2) Checks individual thermocouples "on the bench" before placement in parallel harness.

3) Checks thermocouples within the harness for continuity.

4) Checks thermocouples *and* paralleling harness for accuracy.

5) Checks resistance of the Exhaust Gas Temperature system.

6) Checks insulation of the EGT circuit for shorts to ground and for shorts between leads.

7) Checks EGT Indicators (in or out of the aircraft).

8) Checks EGT system with engine removed from aircraft (in production line or overhaul shop).

9) Reads jet engine speed while the engine is running with a guaranteed accuracy of ±0.1% in the range of 0-110% RPM. Additionally, the TAKCAL circuit can be used to trouble shoot and isolate errors in the aircraft tachometer system.

10) JETCAL Analyzer enables engine adjustment to proper relationship between engine temperature and engine RPM for maximum thrust and efficiency during engine run (Tabbing or Micing).

ALSO *functionally* checks aircraft Over-Heat Detectors and Wing Anti-Ice Systems (thermal switch and continuous wire) by using TEMPCAL Probes.. Rapid heat rise . . . 3 minutes to 800°F! Fast cycling time of thermal switches . . . 4 to 5 complete cycles per minute for bench checking in production.

**Tests EGT System Accuracy to ±4°C at Test Temperature**

*(functionally, without running the engine)*

**Tests RPM Accuracy to 10 RPM in 10,000 RPM (±0.1%)**

*The JETCAL is in worldwide use . . . by the U. S. Navy and Air Force as well as by major aircraft and engine manufacturers. Write, wire or phone for complete information.*

**B & H INSTRUMENT CO., INC.**

*3479 West Vickery Blvd. • Fort Worth 7, Texas*

*Sales-Engineering Offices:*

VALLEY STREAM, L.I., N. Y.: 108 So. Franklin, LO 1-9220 • DAYTON, O.: 209 Commercial Bldg., MI 4563 • COMPTON, CAL.: 105 N. Bradfield St., NE 6-8970

# TO MAKE THINGS BETTER FOR AMERICA—

Raymond A. Rich, President, Avco Manufacturing Corp.

Avco Manufacturing Corporation is a builder of quality products for the commercial economy and high-performance military systems for national defense. Aircraft engines, electronics systems, farm implements, kitchen components and the nose cone for the Air Force Titan intercontinental ballistic missile are being produced by Avco *today*.

The foundation for Avco tomorrow is being laid at our Research and Advanced Development Division. We know that the technology of the future will be built on scientific research being done now. Amazing new materials and new means for creating useful power hold out the promise of great advances in transportation, in agriculture, in consumer products, in nearly every aspect of our future economy. New scientific knowledge and its imaginative application can turn these promises into reality. Work at the Research and Advanced Development Division has already shown what rapid strides can be taken in a short time.

The division is composed of outstanding scientists and engineers who work in an environment that fosters creative investigation. It is the "breakthrough" division of a progressive manufacturing organization. Avco management recognizes the role of the scientist in modern technology. Avco's determination to make things better for America places the resources of a large, diversified, aggressive company firmly behind the Research and Advanced Development Division.

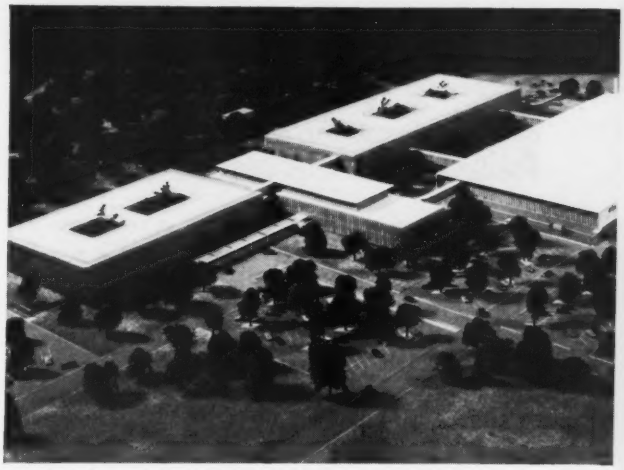

Pictured above is our new Research and Development Center now under construction in Wilmington, Massachusetts. Scheduled for completion in early 1958, this ultramodern laboratory will house the scientific and technical staff of the Avco Research and Advanced Development Division.

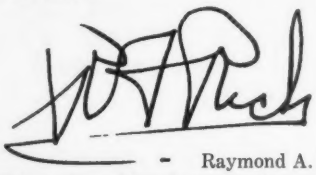

– Raymond A. Rich
President, Avco Manufacturing Corporation

**AVCO**
**Research and Advanced Development**

Avco's new research division now offers unusual and exciting career opportunities for exceptionally qualified and forward-looking scientists and engineers in such fields as:

**Science:**
**Aerodynamics • Electronics • Mathematics • Metallurgy**
**Physical Chemistry • Physics • Thermodynamics**

**Engineering:**
**Aeronautical • Applied Mechanics • Chemical • Electrical**
**Heat Transfer • Mechanical • Reliability • Flight Test**

*Write to Dr. R. W. Johnston, Scientific and Technical Relations, Avco Research and Advanced Development Division, 20 South Union Street, Lawrence, Massachusetts.*

OCTOBER 1957 JET PROPULSION A publication of the AMERICAN ROCKET SOCIETY Research and Development VOLUME 27 NUMBER 10

# Skin Temperatures of a Satellite

CRAIG M. SCHMIDT[1] and ARNOLD J. HANAWALT[2]

Bell Aircraft Corp., Buffalo, N. Y.

**The need for a workable artificial earth satellite has been established both as a reconnaissance vehicle and also as a prerequisite for space travel. One of the attendant problems in the design of such a vehicle is the control and therefore prediction of temperatures that would exist in flight. Previous papers on this topic have brought out many salient features of such predictions but have not been entirely realistic. The present paper attempts to improve on these assumptions and gives numerical computations for a particular configuration that is considered feasible for a satellite design. The example investigated herein is a nonrotating cylindrical shell with one end pointing earthward. The problem of analysis is largely one of geometry, involving spacewise as well as timewise variations in skin temperature. The skin temperatures that would exist are very dependent on the properties of the surface, particularly emissivity and absorptivity, large values producing the widest range in surface temperatures. By proper choice, if possible, of these parameters, this range can be greatly controlled. In particular, the mean temperature of the satellite skin is primarily a function of $\alpha/\epsilon$. For the specific configuration considered herein, nominal limits on the skin temperatures are −200 and +400 F.**

## Nomenclature

$k$ = conductivity
$Q_E$ = radiation emitted from the earth
$Q_R$ = radiation reflected from the earth
$r$ = radius of cylinder
$S$ = solar constant
$T$ = temperature
$t$ = time
$y$ = thickness of skin
$\alpha$ = absorptivity
$\beta$ = angle between the earth-sun line and the orbital plane
$\gamma$ = angle on the cylinder
$\epsilon$ = emissivity
$\theta$ = angle of the satellite in its orbit
$\theta_S$ = angle the satellite enters the earth's shadow
$\rho$ = density
$\sigma$ = Stefan-Boltzmann constant

## Introduction

THE need to predict and control the surface temperatures on a satellite is obvious. The problem is more than merely insuring that the structure of the vehicle is not subjected to too high temperatures or temperature gradients but rather is one of providing an environment suitable for electronic equipment for long periods of time, at a minimum of weight and power. It is the purpose of this paper to investigate the temperatures that exist on a particular satellite configuration and to study the various pertinent parameters in order to determine their relative importance.

Because of the lack of atmosphere in which a satellite would orbit, the means of heat transfer are considerably different than in more conventional aircraft. Whereas convective heating formerly played an important role in determining skin temperatures, particularly for high speed flight, it has long since disappeared at practical orbital altitudes. In fact its replacement, free molecular heating, can be shown to be insignificant for orbital altitudes of 100 miles or higher. This leaves radiation and conduction in the outer skin as the only significant methods of heat transfer. Since the equations of conduction and radiation are well known, the heating problem of a satellite is one of geometry of the vehicle and its orbit.

The configuration chosen for study was a nonrotating (about its own axis) cylindrical shell with one end pointing earthwards at all times. The cylinder was considered to revolve about the earth in a circular orbit such that for the general case it would be exposed to the sun part of an orbit and in the shadow of the earth for the remainder. The primary external sources of heat to the vehicle are radiation from the sun and reflected and emitted radiation from the earth and atmosphere; these heat fluxes to the satellite vary markedly with position in the orbit, that is to say, with time. Since the cylinder is considered not to rotate about its own axis, the heat input also varies with position on the satellite. In addition to these two geometric variables the angle that the earth-sun line makes with the plane of the orbit must be considered. Thus, in general, three variables must be included in any attempt at analysis.

The radiation from the sun is well known but the reflected and emitted radiation from the earth is more open to question. However, reasonable guesses of these latter heat sources were made which necessarily include a variation of heat flux with position in the orbit. It was assumed also that the reflected radiation to the sides of the cylinder is uniform.

Undoubtedly the most uncertain and most important parameters are the emissivity $\epsilon$ and absorptivity $\alpha$ of the skin. Since the skin may well be exposed to high temperatures on its ascent to orbit and to meteor dust while in its orbit, the condition of its surface finish is very difficult to predict. Furthermore, since the absorptivity and emissivity are highly dependent on both the surface condition and temperature,

A form of this paper was presented at the ARS 11th Annual Meeting, New York, N. Y., Nov. 26–29, 1956.

[1] Head, Heat Transfer Group, Development Analysis Department.

[2] Aerodynamicist.

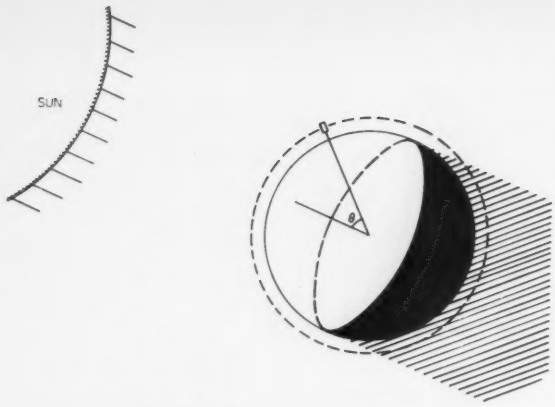


Fig. 1 A pictorial of the sun-earth-satellite orientation

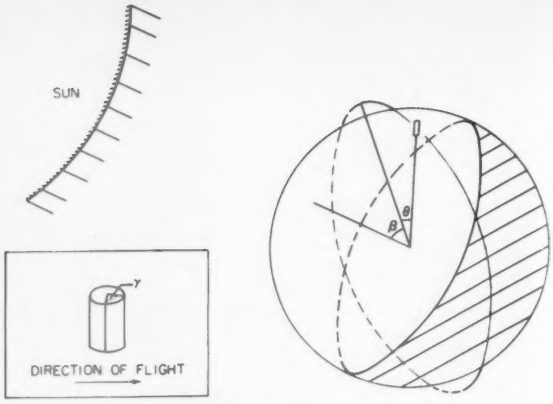


Fig. 2 A schematic of the geometric variables

probable values for $\alpha$ and $\epsilon$ are not known with any degree of certainty. As a result the present study considered several values of these parameters in order to determine their effect on orbital temperatures. It was found that the larger the ratio $\alpha/\epsilon$, the higher the average temperature and the greater the difference between maximum and minimum temperatures.

Many papers (1, 2)[3] that have been written concerning the temperatures of a satellite skin have made the assumption that the temperature is uniform over the satellite at any given time; i.e., the conductivity of the skin is infinite or the satellite is rotating about its own axis at a rapid rate. However, for purposes of reconnaissance a nonspinning vehicle may necessarily be required. Therefore, it is desirable to have a method of analysis available that includes finite or no conduction. Sandorff and Prigge (3) considered finite conduction but only for steady state conditions. The present study undertakes to treat the general time-space temperature distribution on a cylinder, i.e., nonsteady conditions where the vehicle is not a perfect conductor. For vehicles similar to the example considered, conduction can be neglected. Substantiating evidence concerning this assumption is presented in this paper. It should be noted that for a spinning vehicle the method of analysis is a simplified case of that presented herein.

## Method of Analysis

As pointed out in the introduction, the present problem is largely one of geometry. Reference to Figs. 1 and 2 will bring out some of the more important parameters of concern. For a more detailed description of this geometry together with a more comprehensive discussion of results obtained, see (4).

As the satellite revolves about the earth, it passes from the earth's shadow into sunlight and back into the shadow again in a periodic fashion. When the satellite is on the sun side of the earth the amount of incident solar and reflected radiation varies with time and certainly with position on the vehicle, but when it is in the earth's shadow, the incident radiation remains constant. The orbit is considered to be circular and fixed in space with respect to the earth-sun line. The angle $\beta$ is a measure of the orientation of the plane of the orbit with respect to this line, $\beta = 0$ deg corresponding to the earth-sun line lying in the plane of the orbit. The angle $\theta$ denotes the position of the satellite in its orbit, the noon position; i.e., when the satellite is closest to the sun, $\theta$ is given a value of 0 deg. This angle is related to time $t$ by

$$\theta = \frac{360^\circ \times t}{p}$$

[3] Numbers in parentheses indicate References at end of paper.

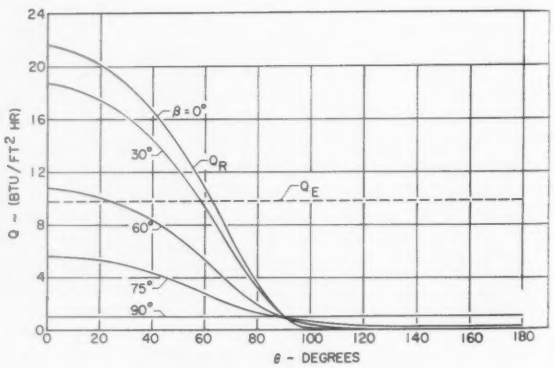


Fig. 3 Variation of reflected and emitted radiation from the earth to the side of a cylinder

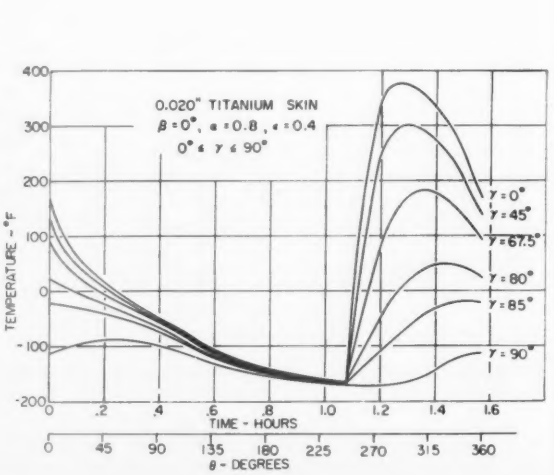


Fig. 4(a) Transient orbital temperatures

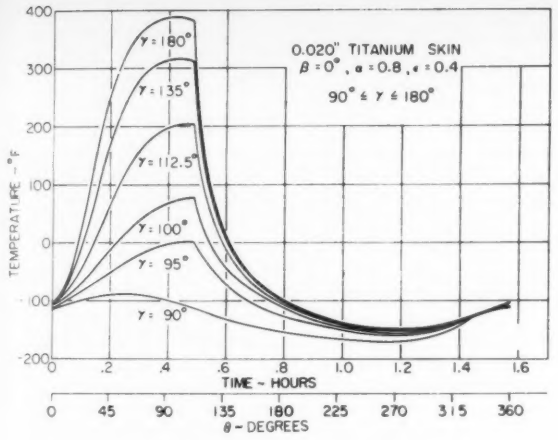


Fig. 4(b) Transient orbital temperatures

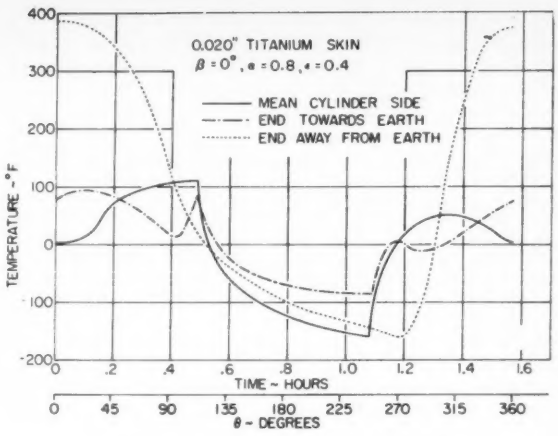


Fig. 5 Transient orbital temperatures

where $p$ is the period of orbit. In the lower left-hand corner of Fig. 2, there is a sketch of the particular satellite configuration considered herein. The angle $\gamma$ measures position on that configuration and has a value of zero for that element called the leading edge. Temperatures are symmetric about the $\gamma = 0$ deg position (leading edge) for the $\beta = 0$ deg orbit, while for the $\beta = 90$ deg orbit they are symmetric about the $\gamma = 90$ or 270 deg positions. For the general orbit, however, there is no plane of symmetry.

The radiation received by a satellite can be divided into three types and is described as follows. First there is the radiation emitted by the earth and atmosphere. This is considered to be constant around the earth and the amount received by a cylinder at an altitude of 300 miles was calculated to be 9.75 Btu/ft²hr for the sides and 31.1 Btu/ft²hr for the end facing the earth. These values were obtained using applicable geometric considerations and the basic radiation emission information from (5). The second source of heat is solar radiation reflected from the earth and atmosphere. This depends on altitude, the distance from the noon position, and the albedo, i.e., the reflectivity of the earth. Using an albedo of ½, calculations were made for the variation of the reflected solar radiation around the earth and the results are shown in Fig. 3. This represents the reflected radiation received by the sides of the cylinder. The amount received by the end of the cylinder facing the earth would vary with $\theta$ in a similar manner but would, however, have a maximum of 61.8 Btu/ft²hr. The last and most important heat source is direct solar radiation and the solar constant used herein was 445 Btu/ft²hr.

In the present analysis no attention has been paid to the relationship between the plane of the orbit and the orientation of the earth. As far as the present temperature calculations are concerned it makes no difference whether the orbit is a polar or an equatorial one or anything in between. In actual practice the amount of radiation reflected and emitted from the earth might vary with the type of orbit, i.e., polar, equatorial, etc., but such differences could easily be included in the analysis. The net result would be to produce only small changes in the surface temperatures.

## Heat Balance Equations

The differential equation expressing the variation of skin temperature with time is not especially complicated, being no more than the usual heat balance equation without the convective term. It can be written

$$\text{thermal capacity} \times \frac{dT}{dt} = \text{solar} + \text{reflected} + \text{emitted} - \epsilon\sigma T^4$$

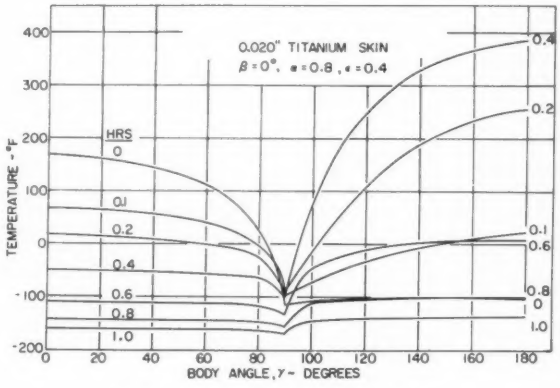


Fig. 6 Temperatures around cylinder

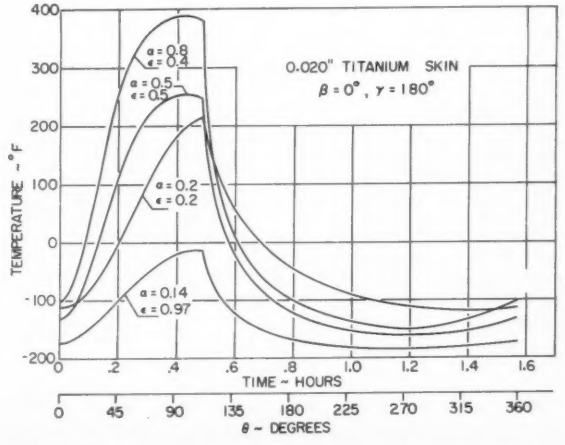


Fig. 7 Effect of variable $\alpha$ and $\epsilon$ on transient orbital temperatures

However, because of the existence of three independent variables and the rather complex boundary conditions that apply, plus the fact that in general an analytic solution does not exist, the solution of this equation for the general orbit is lengthy and of necessity requires numerical integration. The following presents the equations for an orbital altitude of 300 miles. A different altitude would merely result in slightly different regions of validity for the various equations.

The satellite enters the earth's shadow at the angle

$$\theta_S = 90° + \arcsin\left(\frac{\sin 22°}{\cos \beta}\right) \quad [1]$$

and leaves at

$$\theta_S = 270° - \arcsin\left(\frac{\sin 22°}{\cos \beta}\right) \quad [2]$$

For this region the heat balance equation becomes

$$\rho c_p y \frac{dT}{dt} = \epsilon Q_E - \epsilon\sigma T^4 \quad [3]$$

For the remaining $\theta$ the heat balance equation is

$$\rho c_p y \frac{dT}{dt} = \alpha S \cos(\gamma - \gamma_{max}) \sin[\arccos(\cos\theta \cos\beta)] +$$

$$\alpha Q_R + \epsilon Q_E - \epsilon\sigma T^4 \quad [4]$$

where $\gamma_{max}$, the element of the cylinder that receives maximum solar radiation, is given by

$$\gamma_{max} = 180° - \operatorname{arccot}\left(\frac{\sin\theta}{\tan\beta}\right) \quad [5]$$

From Equation [1], for $\beta \geq 68$ deg, $\theta_S = 180$ deg; i.e., the satellite never enters the shadow of the earth. From Equation [5], for $\beta = 90$ deg, $\gamma_{max} = 90$ deg and is independent of time. In fact, for $\beta = 90$ deg, the time dependent term drops out, and temperatures do not vary with time, but only with position on the body. For this case half of the cylinder is in direct sunlight continuously while the other half remains in its own shadow.

Another case of interest, and the one considered in greatest detail in the present study, is the $\beta = 0$ deg case. It is this orbit in which the satellite remains in the earth's shadow the longest and experiences the largest variations in temperatures with time.

## Results

As mentioned above, the particular satellite configuration considered herein was a thin-walled cylindrical shell, nonrotating (about its own axis), revolving about the earth in a 300-mile-high circular orbit with a period of about 1½ hours. The skin was chosen to be 0.020-in.-thick titanium and assumed to be insulated from the interior of the vehicle. Several different values of emissivity and absorptivity were considered in order to illustrate the effect of the parameter $\alpha/\epsilon$ on the skin temperatures.

### Effect of Body Angle

For $\beta = 0$ deg, i.e., when the earth-sun line is in the plane of the orbit, temperatures were obtained over the sides of the cylinder from $\gamma = 0$ to $\gamma = 180$ deg as a function of time,

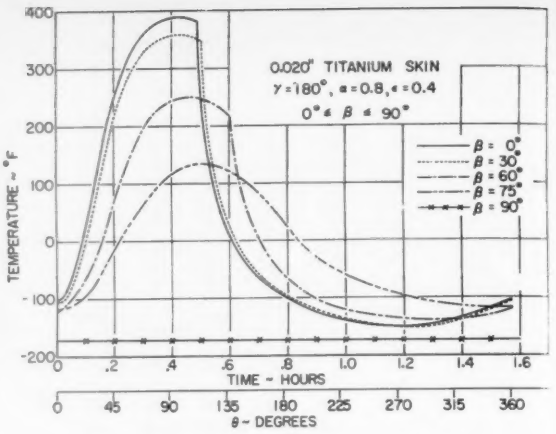


Fig. 8 Effect of varying $\beta$ on transient orbital temperatures

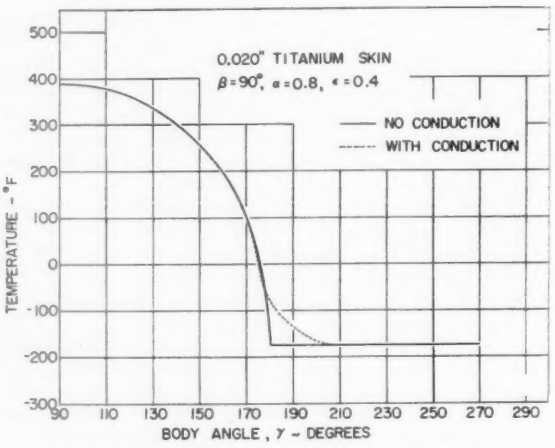


Fig. 9 Effect of conduction on orbital temperatures

see Figs. 4(a) and 4(b). Note that the other side of the vehicle is a mirror image of this side. These results were obtained for $\alpha = 0.8$, $\epsilon = 0.4$. At time zero the sides of the cylinder are all parallel to the sun's rays. Immediately following this, the forward half, $\gamma = 0$ to 90 deg, enters its own shadow, while the aft half from $\gamma = 90$ to 180 deg is in the sun. For this half, the maximum intensity of heating from the sun occurs at $\theta = 90$ deg, shortly before the satellite drops into the shadow of the earth at $\theta = 112$ deg. At this time the whole vehicle starts cooling, the aft part much more quickly because of its relatively high temperature. By the time the vehicle is to come out of the earth's shadow, $\theta = 248$ deg, the temperature of the satellite is nearly down to the equilibrium value of −173 F. During the next phase of flight the forward half of the vehicle is subjected to heating from the sun, the aft is not. The shape of the temperature curves for the forward part of the vehicle in this phase are very different from those of the aft part during the phase from $\theta = 0$ to 112 deg because now the forward part is subjected to the maximum rate of heating almost immediately and this reduces to zero as $\theta$ approaches 360 deg. As a result the maximum temperature reached at $\gamma = 0$ deg is less than it is at $\gamma = 180$ deg.

The mean temperature of the sides of the cylinder is plotted as a function of time in Fig. 5. The maximum temperatures are reduced a good deal in such a mean temperature plot because the maximums for the fore and aft parts of the cylinder occur at different times while the minimums remain low because of the time at which they occur. The over-all mean temperature for a complete orbit for the sides of the cylinder can be obtained from integrating Fig. 5 or 6, found to be −15 F. For comparative purposes a similar investigation was carried out for the case $\alpha = \epsilon = 0.5$, but because of their similarity the resulting curves have not been included in this work. Since the ratio $\alpha/\epsilon$ is one for $\alpha = \epsilon = 0.5$, the over-all mean temperature is lower, by 50 F, than the mean for the $\alpha/\epsilon = 2$ example which has been presented.

Fig. 5 also gives the temperature-time histories of the ends of the vehicle. The curves are rather self-explanatory. Although the end away from the earth receives maximum radiation at $\theta = 0$ deg it does not reach its maximum temperature until slightly later because of the thermal inertia of the system. From that point on it cools until $\theta = 270$ deg at which point the heating cycle starts again. The end toward the earth is much different because it never "sees" the sun except for two intervals—just before the satellite goes into the shadow of the earth and just after it comes out. Thus the amplitudes of temperature cycles of the ends are very different because of their different heating sources.

### Effect of $\alpha$ and $\epsilon$

The effect of varying $\alpha$ and $\epsilon$ is graphically demonstrated in Fig. 7. For this demonstration, one position on the cylinder, $\gamma = 180$ deg, and one orbit, $\beta = 0$ deg, were selected. The two curves $\alpha = \epsilon = 0.5$ and $\alpha = \epsilon = 0.2$ were chosen to demonstrate the effect of varying the magnitudes of the individual values without varying the ratio $\alpha/\epsilon$. As would be expected, the amplitude of the temperature cycle is reduced but the mean value remains nearly constant. The choice of $\alpha = 0.14$, $\epsilon = 0.97$ was made because it would be representative of a magnesium oxide surface and is thought to be one of the lowest possible ratios of $\alpha/\epsilon$. From this figure it can be seen that any desired temperature level and maximum variation can be obtained if the emissivity and absorptivity can be properly chosen.

### Effect of $\beta$

Fig. 8 demonstrates the effect of varying the angle that the orbital plane makes with the earth-sun line. Again this illustration is based on the $\gamma = 180$ deg location with $\alpha = 0.8$, $\epsilon = 0.4$. The amplitude of the time-temperature cycle decreases roughly as the square root of the cosine as $\beta$ increases from 0 to 90 deg. However, the mean temperatures for the sides of the cylinder increase with increasing $\beta$ until the steady condition of $\beta = 90$ deg is reached. The steady state temperature distribution around the cylinder for the $\beta = 90$ deg case is given in Fig. 9. It should be noted that as soon as $\beta$ is chosen other than 0 or 90 deg the temperature distribution about the cylinder is not symmetric.

### Effect of Conduction

The effect of conduction for the particular configuration considered was investigated for the $\beta = 90$ deg orbit and was found to be small (see Fig. 9). This would be true for any configuration having approximately the same relative dimensions. The parameter of importance is $ky/r^2$ so that the applicability of the present analysis embraces a rather large family of materials, skin thicknesses and radii. For any other orbit, the effect of conduction will be less significant than for the one where $\beta = 90$ deg. Also, as the conductivity is increased the amplitudes of the temperature differences are reduced both in time and space while the average temperatures increase with increasing conductivity.

## Conclusions

The skin temperatures of a nonspinning cylindrical satellite pointing earthward have been determined for various $\alpha$ and $\epsilon$ of the skin, for time variable orbits, and for various locations on the vehicle. For the example considered the over-all range of temperatures experienced was −200 to +400 F. The parameters of most importance are the absorptivity and emissivity. The smaller the ratio $\alpha/\epsilon$, the lower the mean temperature and the smaller the cyclic variation. For $\alpha/\epsilon = 2$ the mean temperature is −15 F, while for $\alpha/\epsilon = 1$, it is −65 F. For a constant ratio of $\alpha/\epsilon$ the smaller the individual values of $\alpha$ and $\epsilon$, the less the temperature variation becomes. For example, for $\alpha = \epsilon = 0.5$ this variation is 415 F and for $\alpha = \epsilon = 0.2$ it is reduced to 333 F. Thus, if it is possible to choose $\alpha$ and $\epsilon$, the skin temperatures could be arbitrarily controlled.

The greatest time variation in temperature occurs when the earth-sun line is in the plane of the orbit, $\beta = 0$ deg, and this variation diminishes with increasing $\beta$ until it becomes a steady state condition at $\beta = 90$ deg. The higher the altitude of the orbit, the longer the cylinder remains in the sun both in absolute time and in the percentage of total orbital time. Noncircular orbits can be treated in a similar manner but they present additional geometric complexities. The particular example which has been examined herein treats two shapes—that of a disk or flat plate, i.e., the ends of a cylinder, and the sides of the cylinder. Other shapes such as spheres, cones, etc., can be solved in a similar fashion requiring in many cases the same general equations but slightly different boundary conditions.

## References


1 Seavey, Marden H., "The Temperature of an Object above the Earth's Atmosphere," Internal Report, *Geophysics Research Directorate.*

2 Hibbs, A. R., "The Temperature of an Orbiting Missile," Jet Propulsion Laboratory, California Institute of Technology, March 1956.

3 Sandorff, Paul E., and Prigge, John S. Jr., "Thermal Control of a Space Vehicle," American Astronautical Society meeting, Dec. 1, 1955.

4 Schmidt, Craig M., and Hanawalt, A. J., "Skin Temperatures of a Satellite," ARS Preprint 383–56.

5 Kuiper, G. P., "The Earth as a Planet," vol. II of "The Solar System," published by The University of Chicago.

# Breakup of Water Drops and Sprays With a Shock Wave

RICHARD J. PRIEM[1]

National Advisory Committee for Aeronautics, Cleveland, Ohio

**An apparatus for investigating the effect of shock waves on sprays is described. Shock strengths of 1.32 (Mach number of 1.13) were obtained in a test section at one atmosphere. High speed pictures of 0.030 to 0.160-in. diam water drops show that the drops are broken up by the high gas velocity behind a shock front. Small water jets were not affected by a shock wave. Photographs of impinging jets, parallel sheets and parallel jet types of sprays also show that the breakup of sprays is accomplished by the high velocity gas behind the shock front.**

## Introduction

THE breakup of bulk liquid into sprays of individual drops has been a subject of particular interest and investigation since the advent of the internal combustion engine. From 1920 to 1940, a substantial amount of research was done in Europe and the United States on the atomization of fuel oil in diesel engines. The advent of jet propulsion has intensified studies of fuel atomization because of its importance in determining combustion efficiency.

The present study affirms three important stages in the atomization process: (a) Development of small surface disturbances, (b) air friction and pressure on free liquid to produce drops or ligaments and (c) splitting of the ligaments or drops by the relative air flow.

These stages may occur under two situations. The first is the "steady" case where the relative velocity gradually changes. Falling raindrops exemplify this case. The second case is the "transient" situation where the relative velocity suddenly changes. Drops in an engine having oscillatory combustion (screaming or screeching) fall in this category.

Both cases have recently been investigated by Lane (1)[2] for 500- to 5000-micron drops. He found a critical relative air speed above which the drop is broken up. This was also verified by a group at the University of Minnesota (2).

The problem of pressure oscillations in rocket motors and jet engines (3–5) has increased the demand for information on the "transient" case of drop breakup. Smith and Sprenger (6) have speculated that pressure oscillations break up the propellant in a solid propellant rocket, thereby increasing the burning rate. This could also be a possible means of increased reaction rate in a liquid propellant engine. Consequently, an investigation was undertaken at the NACA Lewis Laboratory to determine experimentally the effect of pressure waves on sprays. This paper shows the effect of single shock waves on various types of water sprays and drops. The effects noted with a reflected shock indicate what may be expected from multiple shocks.

Received Sept. 13, 1956.

[1] Aeronautical Research Scientist, Fuels and Combustion Research Division, Lewis Flight Propulsion Laboratory.

[2] Numbers in parentheses indicate References at end of paper.

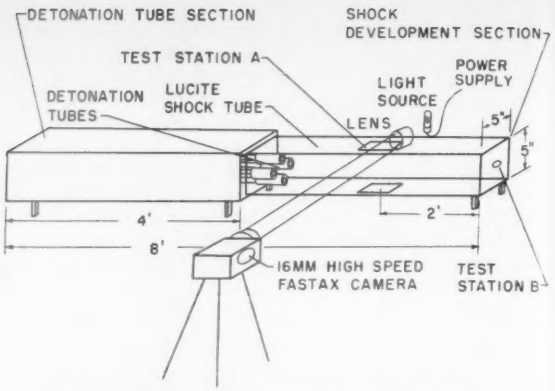


Fig. 1 Schematic of complete shock tube apparatus

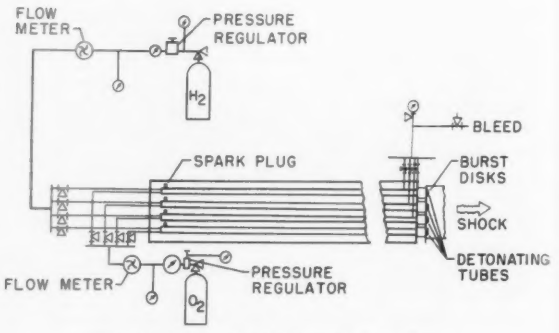


Fig. 2 Schematic of detonation section

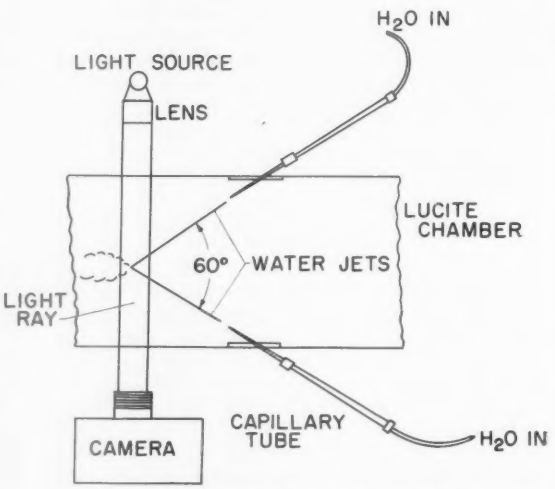


Fig. 3 Detail of test station A with water jets

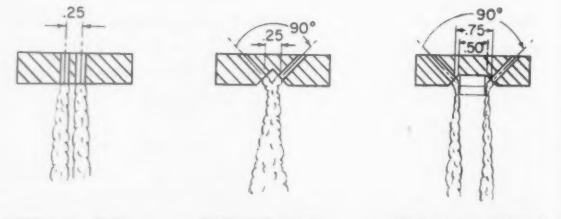


Fig. 4 Schematic of injectors; all orifices, 0.114-in. diam

## Experimental Equipment

The shock tube has two sections, as shown in Fig. 1. The "detonation tubes" section is used to produce the high pressure shock wave. The "shock development" section is 4 ft long and 5 in. square. Midway in this section is one of the test stations; the other station is at the end of the shock development section.

The detonation section has four detonation tubes so that four shocks can be produced at specified time intervals. This section is shown in greater detail in Fig. 2. Each tube is made of $\frac{3}{4}$-in. standard pipe and is connected to a bottle of gaseous hydrogen and oxygen. The gaseous flow is controlled by pressure regulators and metered by rotameters. Flows are adjusted to give the desired mixture ratio in the detonation tubes; after approximately 1 min of flow through the tubes, the valves are closed and the detonation tubes are isolated. Standard burst disks of 0.003-in.-thick aluminum are used to hold the hydrogen-oxygen mixture in the tubes. A spark plug is used to ignite the combustible mixture. A delay circuit also provides a spark to the detonation tubes at various pre-set time intervals.

A schematic view of test station A is shown in Fig. 3. The spray in this case is formed by two capillary tubes with an impingement angle of 60 deg. Each tube is connected to a gas-pressurized water tank. Pictures of the sprays were obtained with a Fastax camera using a standard shadowgraph technique.

Schematic drawings of the injectors for obtaining the various sprays at station B are shown in Fig. 4. The orifices in all the injectors were 0.114-in. in diam.

Shock velocities were measured with two piezoelectric pickups placed 12 in. apart and connected to an oscilloscope. Time required for the shock to travel between pickups was measured from a film record of the oscilloscope trace. Shock strength was obtained from the velocity by applying one-dimensional flow theory.

The shock strengths and velocities obtained with various pressures of the hydrogen-oxygen mixture are shown in Fig. 5. At 1 atm the strength was $1.32 \pm 0.03$, and the Mach number was $1.13 \pm 0.01$. The strength increased with increased mixture pressure.

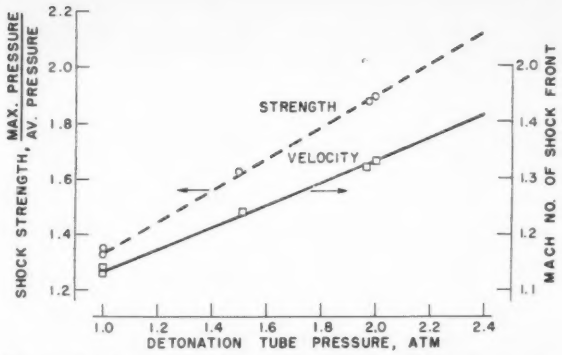


Fig. 5 Shock strengths for various detonation tube pressures; test section pressure, 1 atm

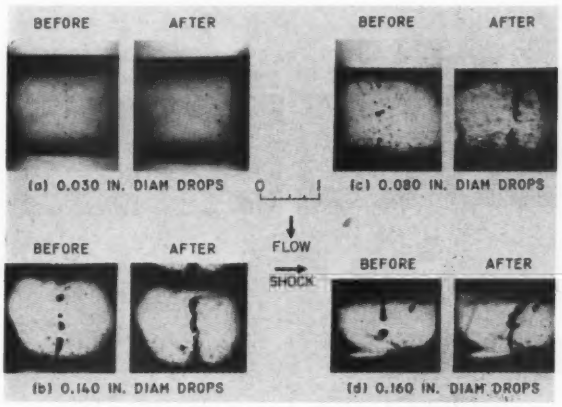


Fig. 6 Effect of shocks on drops of various size

## Experimental Results

All results discussed herein were obtained with a single shock traveling at a Mach number of 1.13 (shock strength of 1.32) with the test section initially at 1 atm. The velocity of the gas behind the shock front was calculated as 240 fps from one-dimensional flow theory.

### Breakup of Drops and Jets by a Single Shock

Photographs of various size water drops, produced by various sized capillary tubes, before and after a shock has passed them, are shown in Fig. 6. The 0.160-in.-diam drops were flattened by the shock wave and small drops were produced on the downstream side of the drop. The number of small drops increased with time, as will be seen later. The condition of small drops being produced from a large bulk of material, like a drop, is called breakup. All the various sized drops shown in Fig. 6 were broken up by the single shock. In the time increment selected in Fig. 6, the 0.080- and 0.030-in.-diam drops were only flattened; however, the original film showed that breakup occurred later, with numerous drops being formed from each large drop.

In (1 and 2) drop breakup was found to be a function of the relative gas velocity, i.e., the velocity of the gas behind the shock wave with respect to the drops. A plot of these results is given in Fig. 7. The shaded area represents the region in which water drops were unstable and would be broken up by the shock. The four points corresponding to the drops

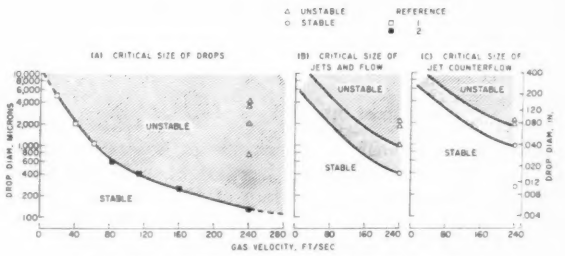


Fig. 7 Critical drop and jet sizes of water

shown in Fig. 6 are included in Fig. 7. Stable drops were not obtained in this investigation because drops smaller than 0.010 in. could not be resolved by the photographic technique.

The effect of a single shock on a jet of water is shown in Fig. 8 for a shock traveling perpendicular to the flow of the jet, and in Fig. 9, for counterflow. For a shock traveling at right angles to the jet, a 0.016-in.-diam (400-micron) jet is stable (not broken up) for a shock strength of 1.30 and a relative gas velocity of 240 fps as shown in Fig. 8. The 0.040-, 0.075- and 0.087-in.-diam jets of Fig. 8 were broken up by the single shock. The critical diameter must therefore be between 0.016 and 0.040 in. This region is shown in Fig. 7(b).

With a shock traveling counterflow to the jet, 0.039- and 0.010-in.-diam jets were stable, as shown in Fig. 9, whereas the 0.075- and 0.087-in.-diam jets were unstable. The critical size must therefore be between 0.039 and 0.075 in. for a counterflow shock. This region is shown in Fig. 7(c).

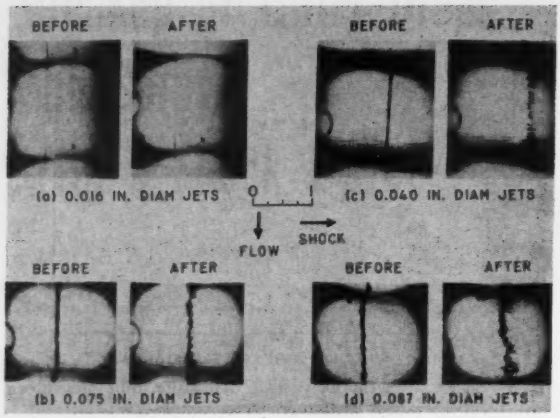


Fig. 8 Effect of shocks on jets of various size; jets perpendicular to shock

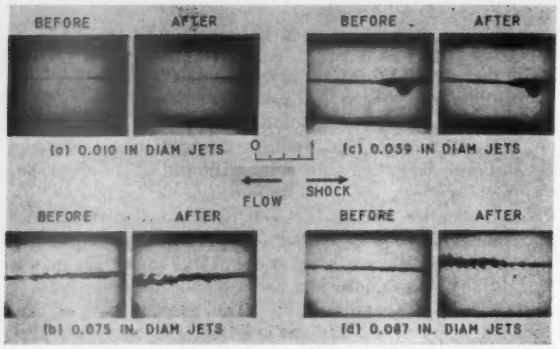


Fig. 9 Effect of shocks on jets of various size; jets parallel to shock

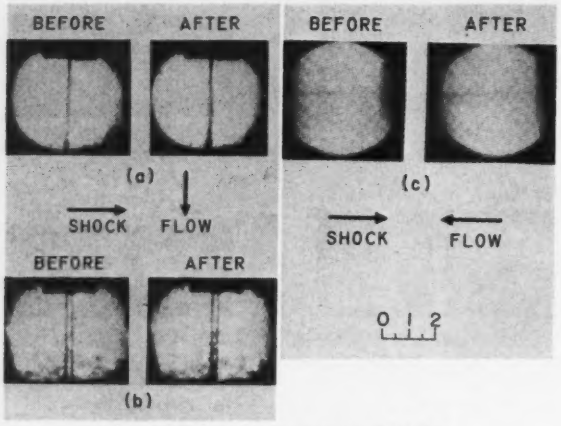


Fig. 10 Effect of shocks on parallel jets

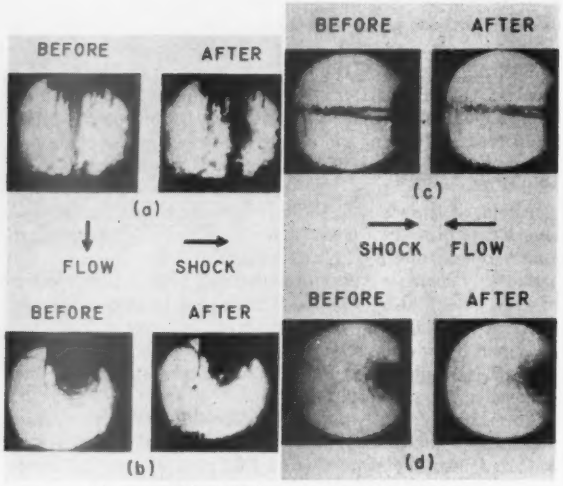


Fig. 11 Effect of shocks on parallel sheets

### Breakup of Sprays by a Single Shock

Atomization of parallel jets by a single shock wave is shown in Fig. 10. Shocks traveling at right angles to the flow appear to produce some breakup of the jets, Fig. 10(a). When the plane of the two jets was in line with the shock, as in Fig. 10(b), the shock also appeared to mix the spray. Shocks traveling against the jet flow produced little or no breakup of the jets, Fig. 10(c). This could be due to the reflection of the shock at the injector face, which greatly reduced the time during which the gases behind the shock reacted with the sprays.

Photographs of the sprays produced by impinging sheets of water before and 0.002 sec after the shock front passed are shown in Fig. 11. When the shock travels at right angles to the flow and the wide side of the sheet, Fig. 11(a), breakup of the spray is definitely obtained from the shock. Mixing is also obtained by the interaction of the shock and spray with this orientation. Rotating the spray 90 deg and presenting the minimum area to the shock, decreased the amount of breakup obtained from the shock, as shown in Fig. 11(b). With counterflow between the shock and spray, very little breakup is obtained, as shown in Figs. 11(c) and (d). The sheets became slightly ruffled and spread out, but breakup was not obtained from the shock.

Breakup of impinging jets of water by shock waves is illustrated in Fig. 12. With perpendicular flow and the wide part of the spray exposed to the shock, Fig. 12(a), breakup is definitely obtained from the shock. Mixing of the spray by the shock is also obtained with this orientation. Rotating the spray 90 deg, as in Fig. 12(b), decreased the effectiveness of the shock in breaking up the spray. One inch from the injector face, where the spray has broken up into drops and ligaments, the shock further breaks up the drops and ligaments. The sheet of liquid next to the injector is widened by the shock. With counterflow as shown in Figs. 12(c) and (d), very little breakup is obtained by the shock.

### Breakup by Repeated Shocks

The effect of repeated shocks on jets and drops is indicated in Fig. 13. Photographs of a 0.087-in.-diam water stream at test station A at various time intervals are shown. The stream originally has one drop and a ligament in the field of view. The first shock front passes the drop between frames 1 and 2. Gas flow behind the shock disintegrates the drop and ligament in increasing amounts with time, until the reflected shock from the end of the test section hits the spray between frames 10 and 11. The second shock breaks up the spray into a fine mist.

A series of photographs showing the breakup of a counterflow impinging jet's spray located at test station A is given in Fig. 14. The first shock front passes the spray between frames 1 and 2 and ruffles the surface and any ligaments ex-

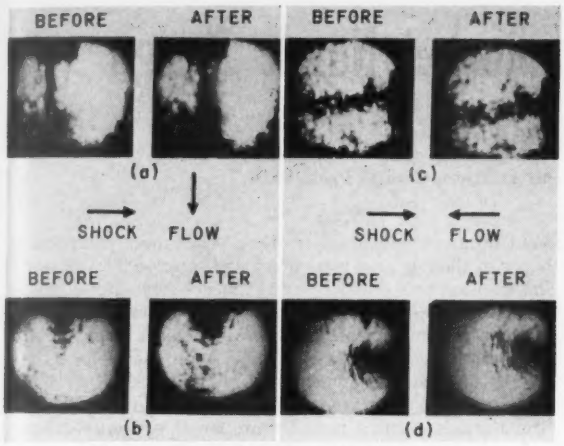


Fig. 12 Effect of shocks on impinging jets

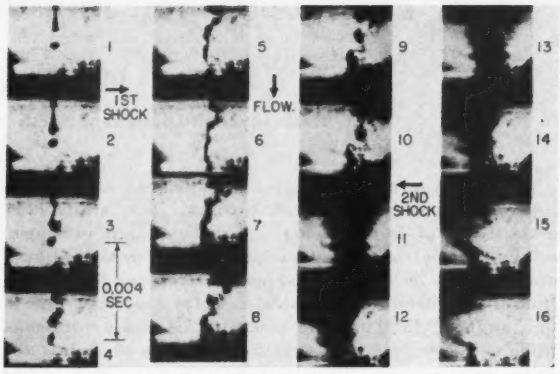


Fig. 13 Effect of reflected shock on drops; jet diameter, 0.087 in.

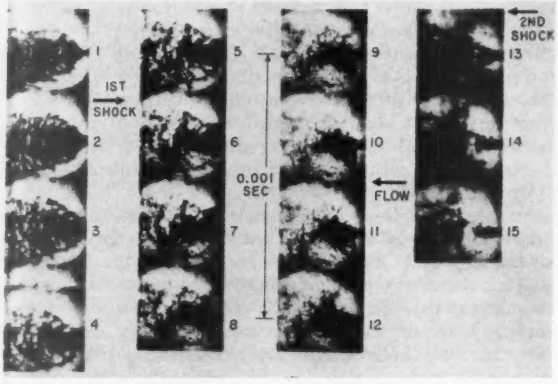


Fig. 14 Effect of reflected shock on spray from impinging jets; jet diameter, 0.087 in.

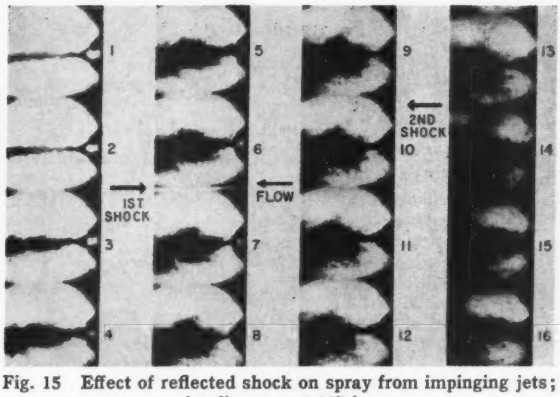


Fig. 15 Effect of reflected shock on spray from impinging jets; jet diameter, 0.087 in.

tending from the sheet. Three thousandths of a second later, the spray is broken up into numerous drops and ligaments. The second shock (reflected from the end of the test section) further breaks up the spray into a fine mist with drops too small to be resolved by the camera.

Photographs of the edge of the spray under the same conditions as in Fig. 14 are presented in Fig. 15. Atomization of the spray increases with time until the second shock passes the spray, at which time the spray is broken up into a fine mist of drops.

## Discussion of Results

There is a critical drop size for a given relative velocity between the drop and the gas behind the shock front (1, 2). Drops larger than the critical size break up into smaller drops, whereas drops smaller than critical are unaffected by the shock. This investigation used drops only in the unstable region, and the results agreed with those of (1, 2).

For jets, the critical diameter is larger than for a single drop. The critical size of a jet is also a function of the angle between the direction of liquid flow and the shock direction. When the flows are perpendicular to the shock travel, the critical sizes are smaller than for counterflow. It appears that the critical size is a function of the area per unit mass exposed to the shock and decreases with increased area. This is verified by comparing the critical size of drops to the critical size of jets. Drops have the smaller size and greater area. Similarly, the counterflow jet has less exposed area than the perpendicular flow jet but a larger critical size. The same reasoning may be applied to the sprays. Orienting the impinging jets and impinging sheets so that the wide part of the spray was exposed to the shock produced the greatest atomization, the 90 deg-rotated orientation was less atomized, and counterflow orientation had negligible atomization.

Photographs showing the histories of the various sprays after the shock front passed further indicate that breakup is obtained through drag from the high velocity gases rather than from the impact of the shock front. The front of the shock undoubtedly flattens or distorts the liquid, thereby increasing the drag that it would have under steady-flow conditions. The importance of the time that a high relative velocity exists between a drop and the gas is indicated by a comparison of Figs. 12(c) and (d) with Figs. 14 and 15. In Figs. 12(c) and (d) the injector face is behind the spray that reflects the shock and, therefore, only a short time exists before the velocities are cancelled. In Figs. 14 and 15 there is a long duration of time before the reflected shock passes the spray. The interaction of the spray and shock in Figs. 14 and 15 was much greater than in Figs. 12(c) and (d), indicating the importance of the length of time that the drop is subjected to high drag forces.

Breakup of liquid under transient conditions produced by a

(*Continued on page 1093*)

# A Philosophy for Improved Rocket Nozzle Design

ROBERT B. DILLAWAY[1]

Rocketdyne, A Division of North American Aviation, Canoga Park, Calif.

**This paper presents a three-dimensional analysis of supersonic contoured rocket nozzles. The study was undertaken in order to arrive at the design of short, axially symmetric nozzles having axially directed exhaust and either, or both, improved performance and less weight than the conventional conical nozzles having a nozzle half angle of 15 deg. The assumptions and approximations used are presented together with the procedure for applying the characteristic method of flow analysis in the nozzle in arriving at a proper nozzle wall contour for axial exhaust. Nozzles equal to or shorter in length by a factor of two compared to conventional 15-deg conical nozzles were analyzed.**

## Nomenclature

$A$ = ratio $\frac{\cot \mu}{M^*}$

$a$ = coefficient

$B', B''$ = $\frac{\sin \theta \sin \mu}{y \sin (\theta \pm \mu)}$ associated with $\lambda'$ and $\lambda''$ respectively

$b$ = coefficient

$c$ = local velocity of sound, fps

$c^*$ = critical velocity of sound, fps

$f(x)$ = function describing nozzle wall curvature

$l$ = coefficient

$M$ = local Mach number

$M^*$ = critical Mach number

$R$ = nozzle wall radius of curvature in throat region, ft

$u_0$ = velocity on the flow axis in nozzle transonic region, fps

$u(x)$ = local fluid velocity, fps

$v(y)$ = local fluid velocity, fps

$x$ = nozzle axial coordinate

$y$ = nozzle radial coordinate

$\epsilon$ = constant; 1 for axisymmetric flow, 0 for two-dimensional flow

$\rho$ = fluid density, slugs/ft$^3$

$\sigma$ = nozzle wall overturning wedge angle, radians

$\delta$ = shock angle relative to upstream flow, radians

$\gamma$ = ratio of specific heats

$\mu$ = Mach angle

$\lambda'\lambda''$ = tan $(\theta \pm \mu)$ characteristic line slope relative to flow axis—rising and falling respectively

$\theta$ = local flow velocity angle relative to horizontal nozzle axis

$\phi$ = potential function $\frac{\partial \phi}{\partial x} = u_x$, $\frac{\partial \phi}{\partial y} = u_y$, radians

***Subscripts and Superscripts***

$'(f', f'')$ = differentiation with respect to independent argument

$1, 2$ = calculation reference point in flow field

$x, xx, y, yy$ = derivative with respect to independent argument

## Introduction

HISTORICALLY the supersonic nozzles used in rocket engines have had conical expansion sections with few exceptions. There is a record of considerable nozzle research on the part of the German scientists at Peenemunde. They found no great advantage in using other more complicated shapes in the low area ratio nozzles of interest for V-2 work. This decision was probably also influenced by ease of engine fabrication considerations. The German investigations resulted in a choice of an optimum divergence angle for the supersonic conical nozzle which has been carried over into American rocket developments.

The continued demand for increased rocket engine performance has resulted in a definite trend to higher exhaust area ratio nozzles for engines operating at high altitudes where the larger nozzle is most effective in increasing engine performance. Conical nozzles, when extended to higher area ratios, become unwieldy in both length and exit diameter. The engine is harder to handle, its weight is increased noticeably, and the nozzle experiences larger stress loads which compound fabrication problems. The increase in weight and stress loads is of added importance if one considers using the engine for thrust vector control by swinging (gimbaling) it on its mount. Increased engine weight and moment of inertia increase the power required to move the engine and thus add to the weight and complexity of the thrust vector control system.

As a result of the foregoing considerations it appears desirable to minimize the nozzle length of the large high performance rocket engine. One immediately thinks of increasing the divergence angle of a conical nozzle in order to accomplish this objective. However, as the divergence angle is increased, the momentum loss, due to nonaxial fluid flow and the associated loss in performance, outweighs any advantages from decreased weight and moment of inertia. Even with current conical nozzle design there is a loss in performance of about 1 per cent due to the partial flow divergence from the axial direction in the nozzle exit plane.

This paper presents the approach taken by Rocketdyne personnel to design short high area ratio supersonic nozzles having performance equal to or superior to present conical nozzle motors at design altitude. The design approach involves no new principles. However, several simplifying assumptions were used to make the required calculations less tedious. The effect on the design philosophy of these simplifying assumptions is discussed in the paper.

## Design Philosophy

Any supersonic nozzle design which produces essentially axial exit of the gas flow will embody an expansion section from the sonic throat followed by an overturning or straightening section. The flow near the wall is deviated from the axis in the expansion section and is redirected toward axial flow in the straightening section.

For years ideal nozzles for wind tunnels have been designed, having uniform axial exhaust without flow disturbance. However, the unique design of these ideal nozzles results in a device which is about twice as long as current rocket nozzles of the same area ratios. This is in direct opposition to the desired length change.

However, it appeared possible to make a nozzle equal to or shorter in length than the conical nozzle of the same area ratio which possessed the required high performance. In such a design it was necessary to first expand the nozzle more radically from the sonic throat (as compared to an ideal nozzle) and then more severely overturn or straighten the flow into approximately axial flow at the exhaust (Fig. 1).

Presented at the ARS 11th Annual Meeting, New York N. Y., Nov. 26–29, 1956.

[1] Supervisor of Basic Studies, Preliminary Design Section. Mem. ARS.

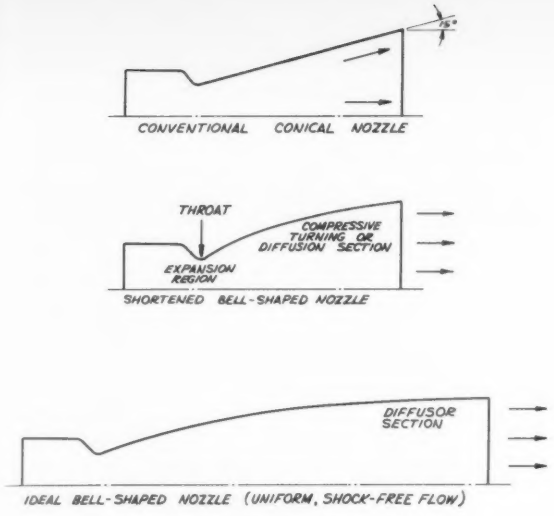


Fig. 1 Typical thrust chamber nozzle types

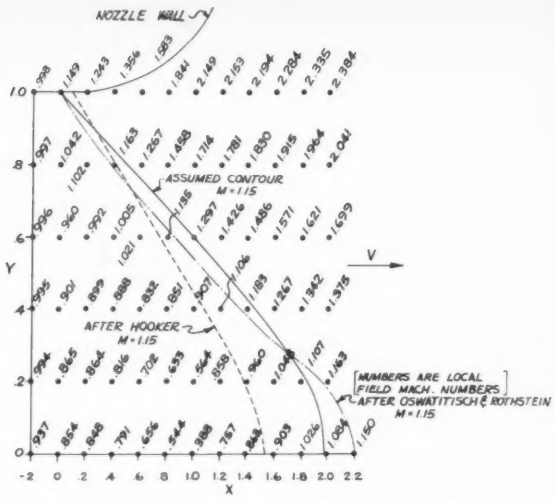


Fig. 2 Nozzle transonic region velocity distribution

The ideal nozzle design has a unique contour which turns the flow of given Mach number without introducing compressive disturbance; it simply eliminates further expansion and guides the gas in its normal flow pattern for such a boundary condition. A nozzle embodying more severe flow turning in the supersonic regime will act as a supersonic diffuser causing shock waves with associated losses, and flow disturbances in the nozzle field. The problem in this design is thus to select properly the minimum required expansion and overturning (or diffusion), thus minimizing the flow losses while providing the desired axial exhaust of the gases.

There is some experimental evidence that if the overturning of the flow can be distributed along the straightening section of the nozzle wall, so that the effective shock wedge angles are limited to 1 or 2 deg, the flow will still behave as though it were isentropic. If this were so the characteristic methods of flow analysis could be employed to give valid flow and pressure distribution patterns throughout the flow field in these short contoured or bell-shaped nozzles. This is what was attempted. If the designs performed as expected, the nozzles would not only show weight and moment of inertia savings over the conical nozzle but might be expected to equal or possibly improve slightly on the conical nozzle performance due to more efficient increase in axial momentum, and possibly to a slight decrease in momentum loss in the boundary layer.

## Nozzle Design Procedure

### Flow Analyses—Transonic Throat Section

The wall curvature at the nozzle throat was kept the same for both the conical and contoured nozzles in the analysis to eliminate all factors but supersonic nozzle contour in the comparative evaluation of nozzle performance. Further, nozzles were designed with the same exit area ratio and various percentages of the length of the reference conical nozzles. Since rocket thrust chambers are built with cylindrical symmetry, the contoured nozzle was designed with cylindrical symmetry.

In order to establish the desirable nozzle expansion angle and wall curvature, the flow field within the nozzle and associated fluid pressure and density had to be established. The "method of characteristics" which is applicable to isentropic axial symmetric flow analysis was used in establishing this flow field. While this technique yields an exact result, it requires stepwise numerical analysis when the flow is axially symmetric.

Numerical analysis of this type requires two initial value lines on which flow criteria $M^*$, $\theta$ are known. One of the loci chosen was the expansion curve representing the supersonic nozzle wall starting from the throat section. The other required curve is a locus of known flow velocities (scalar magnitude and direction) in the throat region across the flow field. It has previously been determined (1, 10)[2] that the numerical determinations of flow field by characteristic methods do not produce accurate results in regions where the Mach number is less than 1.15. Therefore, it was decided to establish this flow field initial value line as the Mach 1.15 locus, if possible by accepted transonic calculational methods, or by resorting to reasonable approximations.

The two power series solutions to the transonic flow field, proposed by Oswatitsch and Rothstein (13) and Hooker (14) were applied to the present boundary conditions with the results shown in Fig. 2 for three-dimensional transonic flow. The major differences between the present problem and the solutions obtained by the above authors are (a) the step change from very large to very small wall curvature at the nozzle throat in going from subsonic to supersonic regions, (b) the nonconstant wall curvature in the region of interest and (c) the small radius of curvature relative to throat diameter in the present problem which results in an undesirable numerical relationship between the wall contour and its first and second derivatives. The last item strongly and adversely influenced the Oswatitsch solution on the flow axis. The applicable potential function

$$\left(1-\left(\frac{v}{c}\right)^2\right)\frac{\partial v}{\partial y}+\left(1-\left(\frac{u}{c}\right)^2\right)\frac{\partial u}{\partial x}-2\,\frac{uv\partial u}{c^2\partial y}+\epsilon\,\frac{v}{y}=0 \quad [1]$$

was solved by Oswatitsch (13) using series expansions for the velocity components,

$$u(x,y)=u_0+\frac{1}{2!}\,(a_2\,y^2)+\frac{1}{4!}\,(a_4\,y^4)+\ldots \quad [2]$$

$$v(x,y)=b_1y_1+\frac{1}{3!}(b_3\,y^3)+\ldots \quad [3]$$

the irrotational flow criteria

$$\frac{\partial u}{\partial y}=\frac{\partial v}{\partial x} \quad [4]$$

[2] Numbers in parentheses indicate References at end of paper.

and the boundary flow conditions

$$v_f/u_f = dy/dx = df/dx = f' \quad [5]$$

The wall shape is given by $y = f(x)$ and all coefficients $a$ and $b$ in Equations [1, 2] are functions of $x$; $u_0$ is a function of the velocity variation along the $x$ (nozzle) axis and is found by use of the conservation of total mass flow relation

$$\int_0^f u\rho \, dy = \text{const} \quad [6]$$

Combining Equations [1 through 6] produces relations for $u$ and $v$ as functions of the wall curvature and its derivatives $(f, f', f'')$.

Using the resulting relations of (13), the flow distribution was found for the nozzle throat region, and a typical distribution is presented in Fig. 2. The solution depends strongly on the nozzle wall characteristics. Since the wall is the flow boundary condition, the flow so determined should be correct near the wall. The unexpected reversal of sign of velocity gradient on the nozzle axis near the throat is probably due to the relative numerical values of the wall functions associated with the small difference in the numerical values of arguments in this region. This odd behavior casts doubt as to the accuracy of the flow picture on the axis found by this approach.

As an alternate solution, the flow field proposed by Hooker (14) was studied. In this case the potential flow equation

$$\phi_{xx} + \frac{1}{y}\phi_y + \phi_{yy} = \frac{1}{2 - (\gamma - 1)(M^{*2} - 1)} \times [M^*_{xx}\phi_x + M^*_{yy}\phi_y] \quad [7]$$

and the critical Mach number relationship

$$M^{*2} = \phi_x^2 + \phi_y^2 \quad [8]$$

were employed. Hooker assumed a power series solution for the potential function

$$\phi = a_1 + a_2 x^2 + b_2 y^2 + a_3 x^3 + b_3 x y^2 + a_4 x^4 + b_4 x^2 y^2 + l_5 y^4 + \ldots \quad [9]$$

together with the boundary condition

$$\frac{\partial\phi}{\partial y}\frac{\partial\phi}{\partial x} = \frac{x}{R} + \tfrac{1}{2}(x^3/R^3) + \ldots \quad [10]$$

Using these two relations [9, 10] and assuming constant wall curvature $(h/R)$ and constant $\gamma$, the coefficients of like powers of $x$ and $y$ are equated after Equation [9] is inserted into Equations [7, 8, 10]. The result is the series function [9] with known coefficients. The $M = 1.15$ locus found by this method was a smooth curve as shown in Fig. 2, with uniformly increasing flow velocity in the field. However, the requirement of constant symmetrical wall curvature does not fit this solution exactly to the problem at hand although the result is not greatly different from that obtained by the Oswatitsch method. Since both approaches were found to be very tedious and time-consuming, the Sauer (11) approximation to the Oswatitsch solution was attempted as it was much simpler. However, the approximation, assuming (a) only small perturbations in $u$ and $v$ from sonic velocity, and (b) constant velocity gradient along the nozzle axis, produced a $M = 1.15$ line in the present problem which never intersected the wall.

Failing to find a straightforward solution for the transonic region, an assumed initial value line was formed. Since the subsonic nozzle wall curvature was relatively small, it was assumed to be zero giving a normal $M = 1$ plane at the true nozzle throat.

The supersonic portion of the expanding nozzle wall was approximated by a series of inscribed chords. The initial chord angle was selected so that the $M = 1.15$ Mach line

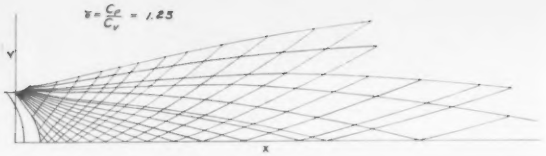


Fig. 3 Characteristic kernel map—kernel calculation for axially symmetric supersonic expanding flow, initial value method with iteration

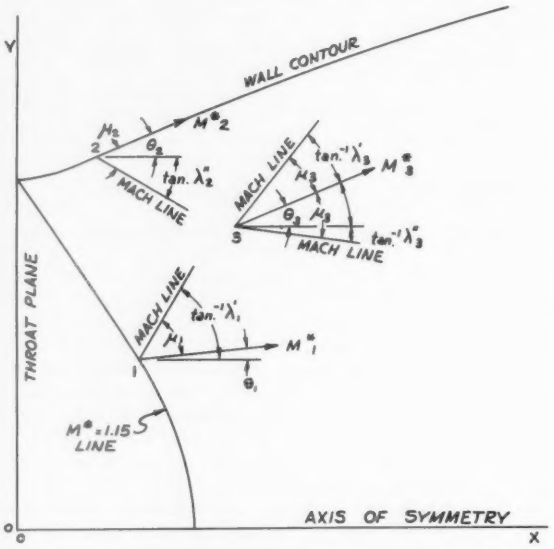


Fig. 4 Flow parameters used in finite difference solution of characteristic equations

intersected the nozzle wall at the throat plane, using the Prandtl-Meyer flow theory. The intersection of the $M = 1.15$ locus on the axis was assumed to occur midway between the points determined by (a) the Sauer method and (b) the extension of the two-dimensional $M = 1.15$ line which intersected the axis. A smooth curve tangent to the Mach line and normal to the flow axis, at the assumed intersection, completed the locus which, as seen in Fig. 2, proved to match very closely and in fact was a compromise between locii obtained by the methods of Oswatitsch and Rothstein and Hooker. It was felt that, based on the error analysis by Oswatitsch, the possible errors in flow field produced by differences between the curves shown in Fig. 2 would be negligible.

## Supersonic Flow Field

The initial value points $(M^*, \theta)$ were chosen on the $M = 1.15$ line at uniformly spaced points from axis to wall. Similar points were chosen on the wall curve where the chords differing by 3-deg angles intersected the true wall curve. The Mach number at each wall point was determined assuming that Prandtl-Meyer type flow existed in the wall region. These results were to be iterated later if it were found necessary, although the small changes in $x$ and $y$ along the wall curve made this seem unlikely.

At each point on both initial value curves the velocity and flow direction were known so that the calculation of the flow field could commence. In using this finite difference approach there is always a quesion of the magnitude of the change in the properties which will produce a sufficiently accurate solution of the flow field. Because of the large fields to be mapped in

this case, only five points were taken on the $M = 1.15$ line including the axis point, and angular expansion increments of 3 deg were chosen along the wall. While the increments were an order of magnitude larger than usually employed in this sort of analysis, successive iteration of each calculation minimized the errors carried throughout the calculation.

The entire flow field developed from the expanding nozzle section was first calculated for total expansion angles up to 40 deg using procedures recommended by Shapiro (10) and Isenberg (1). The ratio of specific heats $\gamma$ was held constant in this analysis. A typical characteristic line mesh for this portion (the "kernel") of the flow field is shown in Fig. 3. In this approach the characteristic equations in the $x$, $y$ and $M^*$, $\theta$ planes

$$dy/dx = \tan(\theta \pm u) = \lambda', \lambda'' \quad [11]$$

$$\frac{dM^*}{M^*} \pm d\theta \tan u - \frac{\sin\theta \sin\mu \tan\mu \, dx}{\cos(\theta \pm \mu)} y = 0 \quad [12]$$

associated with the potential Equation [1] are solved between two known points and the ensuing point of intersection of the two characteristic lines in the physical plane, using the difference relations (see Fig. 4).

$$x_3 = \frac{(\lambda'_1 x_1 - \lambda''_2 x_2) - (y_1 - y_2)}{\lambda'_1 - \lambda''_2} \quad [13]$$

$$y_3 = y_1 + \lambda'_1 (x_3 - x_1) \quad [14]$$

$$M_3^* = \frac{\theta_2 - \theta_1 + A_2 M^*_2 + A_1 M_1^* + B_2''(y_3 - y_2) + B_1'(y_3 - y_1)}{A_1 + A_2} \quad [15]$$

$$\theta_3 = \theta_1 + A_1 (M^*_3 - M^*_1) - B_1'(y_3 - y_1) \quad [16]$$

These relations establish the new flow field point and the local Mach number and flow direction. The Mach angle $\mu$ at the point is obtained from the relation

$$\sin\mu = 1/M \quad [17]$$

The angles $\mu$ and $\theta$ and thus the local values of $\lambda'$, $\lambda''$, $B'$, and $B''$ change between points. Successive iteration of relations [13–16] between points using average $\lambda$'s and $B$'s provides a more accurate picture of the flow field. Fig. 4 shows the physical relations of these values between three typical field points.

In calculating the flow on the axis, $\theta = 0$ from symmetry considerations. Only one upstream point has a characteristic line crossing the axis so that Equations [11–16] must be modified as follows

$$x_3 = x_2 - y_2/\lambda''_{2,3} \quad [18]$$

$$\lambda''_{2,3} = \frac{\lambda''_2 + \lambda''_3}{2} \quad [19]$$

$$\left[\frac{dM^*}{dx}\right]_{3 \text{ at } y=0} = \frac{\theta_2 - A_{2,3}\left[M^*_1 - M^*_2 + \frac{1}{2}\left(\frac{dM^*}{dx}\right)_1 \Delta x_{1,3}\right] + \frac{1}{2}B''_2 y_2}{\frac{1}{2}\left[A_{2,3}\Delta x_{1,3} - \frac{\frac{1}{2}\cot^2\mu_3}{M^*_3} y_2\right]} \quad [20]$$

where points 1 and 3 are succeeding calculation points on the flow axis.

An estimate of $M^*_3$ is obtained by the relation

$$M^*_{3\,est} = M^*_2 + \frac{\theta_2 + B''_2 y_2}{A_2} \quad [21]$$

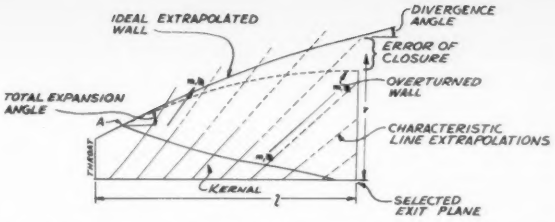


**Fig. 5 Geometric layout for total expansion angle and initia wall curvature in flow-straightening section**

When Equation [20] is solved, a second value of $M^*_3$ is obtained from the relationship

$$M^*_3 = \frac{1}{2}\left[\left(\frac{M^*}{dx}\right)_1 + \left(\frac{M^*}{dx}\right)_3\right] \Delta x_{1,3} \quad [22]$$

Successive iterations are again performed until the value $M^*_3$ converges to a limit within the tolerable error.

Since the flow is irrotational and symmetrical the flow field in only one half of an axial plane cut through the nozzle is calculated.

## Choosing Total Expansion

The field calculation just discussed is straightforward but tedious and is capable of computing machine mechanization. The choice of total expansion angle depends on the desired momentum increase within the nozzle. Since this nozzle generates flow disturbances along its entire wall the flow in the exit plane will not be uniform in velocity magnitude.

An estimate of the momentum in a desired exit plane is made by extending the characteristic line tangents from the kernel for the particular total expansion angle to intersect this desired exit plane. Assuming the values of $M^*$ constant along these characteristic line tangents (Fig. 5) the area averaged momentum is calculated over the desired exit area (assuming constant density) and compared with the ideal one-dimensional increase for a similar area ratio nozzle. This was chosen as the criteria as it was also used in establishing area ratio requirements for conical nozzles. If the exit momentum of the assumed expansion is equal to or slightly larger than the one-dimensional value for the same exit area ratio, the associated expansion angle is used in constructing the remainder of the nozzle wall. While this is the smallest tolerable expansion angle, any larger expansion angle could also be used but would require greater overturning (flow straightening) and thus produce larger losses in the flow system, which is undesirable. The minimum expansion angle producing the desired increase in momentum should produce the nozzle with most nearly ideal flow.

## Nozzle Straightening Section

The remainder of the rising characteristic line tangents are extended from the kernel boundary assuming constant values for $M^*$ and $\theta$ along the extensions. The wall is extended tangent to the expansion arc with the desired total expansion angle until it intersects the first characteristic line tangent. The wall is turned at each characteristic intersection to fit the estimated local flow angle $\theta$ until the desired nozzle exit plane is reached. This procedure approximates crudely a segment of an ideal nozzle with the same total expansion angle, and so will be of too large exit area and will not have a wall parallel to the flow axis in the chosen exit plane as desired. The angle by which the wall deviates from the axial direction in the exit plane is now distributed uniformly at each characteristic line intersection as an overturning angle or compres-

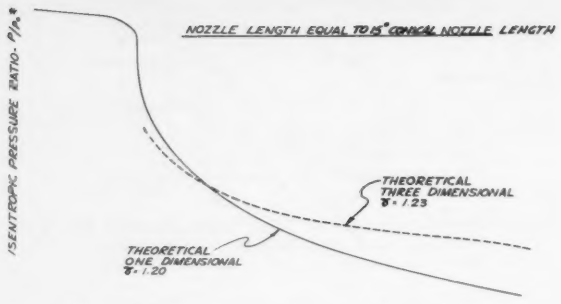


Fig. 6 Wall pressure ratio vs. nozzle area ratio

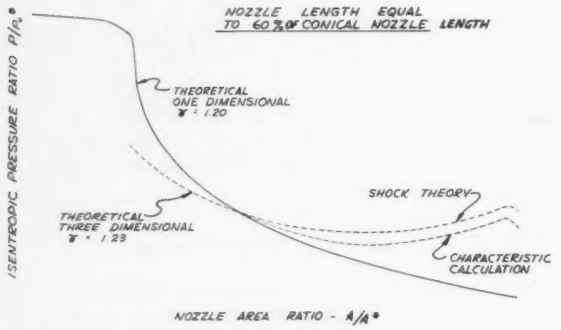


Fig. 7 Wall pressure ratio vs. nozzle area ratio

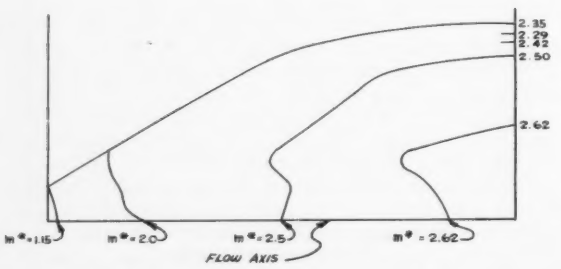


Fig. 8 Theoretical velocity profiles—typical short contoured axially symmetric nozzle

sive wedge. The pattern of uniformly increasing the wedge angle is not necessarily the optimum configuration but was chosen since such a pattern should turn the flow with the least localized flow field disturbance. The nozzle wall constructed on the above pattern ended with zero slope and proper area at the chosen exit plane as shown in Fig. 5.

## Overturned Flow Field

It was necessary to establish the remainder of the internal flow field in order to check the first estimate of the total exit plane momentum and to determine the pressure distribution along the nozzle wall for thrust determination. These pressures also were the best means of checking the flow analysis experimental results.

The flow field in the overturning section was established using the same approach as in the kernel calculations; however, the successive nozzle wall point Mach numbers (as already estimated) were obtained using the relationships

$$y_{wall} - y_1 = (x_{wall} - x_1) \quad [23]$$

$$y_{wall} = f(x_{wall}) \text{ (the wall contour equation)} \quad [24]$$

$$M^*_{wall} = M^*_1 = \frac{(\theta_{wall} - \theta_1 + B_1'(y_{wall} + y_1)}{\frac{\cot \mu}{M^*_1}} \quad [25]$$

Each wall point thus determined in the straightening section became an initial value point for a new descending characteristic $\lambda''$ line in the field. In all cases checked, the initial overturning at the wall altered the flow downstream to a degree that no effective overturning wall angle was materially greater than the smallest (initial) incremental overturning angle used at point A in Fig. 5. Thus, the flows more nearly approached isentropic flow than first estimates predicted.

A check on the momentum increase showed it to be very close to the initial estimate in most cases. If there had been a large discrepancy with the desired momentum increase a new contour with adjusted total expansion angle would have been established. The wall pressure distribution was determined from the local Mach number ($M$) distribution along the wall using ideal one-dimensional relationships. Fig. 1 shows a typical distribution compared with the pressure distribution predicted by one-dimensional analysis.

The overturning wedge angle required naturally increased with increased nozzle contraction (shortening) and/or increased exit area ratio. With nozzles 80 to 100 per cent as long as a similar conical nozzle, the required local overturning wedge angles at the wall were 2–3 deg or less, which produce such weak shocks that the isentropic theory and characteristic equations were used to determine the flow field without much question as to the validity of the assumption.

However, very short nozzles resulted in considerably larger overturning angles wherein the validity of the isentropic relations was questioned. Therefore, the straightening section flow field was also established for a nozzle using oblique shock theory and the relations

$$\frac{1}{M^{*2}_1} = \left[\frac{\sin \sigma \cos \sigma \sin (\sigma - \delta)}{\cos (\sigma - \delta)}\right] + \left(\frac{\gamma - 1}{\gamma + 1}\right) \cos^2 \sigma \quad [26]$$

and

$$M^*_2 = \frac{M^*_1 \cos \sigma}{\cos (\sigma - \delta)} \quad [27]$$

These equations established the changes in flow across the shocks. Characteristic methods were still used to obtain the field variation between the shocks. The predicted wall pressure distribution using the shock theory is higher than predicted by characteristic isentropic analysis as shown in Figs. 6, 7. Preliminary experimental model results indicate that simple characteristic equation determinations predict actual nozzle performance very closely in all cases. The shock theory is evidently too pessimistic. Since the wall curvature is distributed continuously in the wall contour finally laid through the intersections with the characteristic lines, to form a smooth nozzle wall, the overturning will be more distributed, resulting in weaker shocks than expected by the finite step shock analysis.

## Performance Considerations

The flow field of the nozzles designed by the foregoing procedure results in exit velocity which varies in magnitude from axis to wall but has essentially axial flow direction throughout the exit plane. (Fig. 8 shows a typical $M^*$ field distribution for one particular nozzle length.) As the length is further shortened the velocity distribution will vary from that shown in Fig. 8. With extreme nozzle shortening, the peak velocity will in fact shift from the flow axis to an annular ring position within the exit flow plane. Nevertheless, under full flow conditions the performance of the nozzles designed by the approach given in this paper shows promise of exceeding that of conventional conical nozzles of similar length

and area ratio while at the same time producing a noticeable reduction in weight and moment of inertia.

The minimum nozzle length is fixed by maximum useful expansion angle. This value will have to be determined through experiment since it will depend on flow separation tendencies and shock losses in the nozzle associated with excessive expansion and recompression.

The recompression has two detrimental effects to the flow. First the density of the relatively lower velocity gas in the vicinity of the wall is increased relative to the flow on the axis of the nozzle thus increasing the momentum loss relative to an ideal nozzle of similar expansion ratio. Second, the recompression along the wall reduces the wall boundary layer pressure drop with distance along the nozzle wall relative to a conical nozzle. Thus, in use of the nozzles at lower than design altitude (in an adverse pressure gradient) the contoured nozzle would have less tendency to separate at a low altitude resulting in increased drag and reduced performance. The magnitude and importance of this effect will have to be determined experimentally.

The design philosophy presented here is only one of several possible approaches to obtaining shortened rocket nozzles of high performance. For instance, the approach of cutting off ideal nozzle contours so as to have nozzles that flow without loss and exit wall flow angles less than similar conical nozzles but not of zero divergence appears to have merit. This approach is discussed in (15, 16). While the approach presented should have superior performance in very short nozzles of high area ratio, valid comparison will have to await optimization of the nozzle designs presented here and comparison of predicted performance over a wide range of lengths, area ratios, and possibly operating pressure ratios if different from those for which the nozzles were designed.

The present work merely presents an approach to design which based on limited test verification yields accurate results as regards predicted thrust and flow distribution.

### Acknowledgments

The work for this paper was performed at Rocketdyne Div. of North American Aviation, Inc., under the sponsorship of the U. S. Air Force. Their cooperation in the release of this information is greatly appreciated.

The help afforded by A. T. Sutor, V. H. Ransom, W. H. Eng and Mrs. V. Gibbs in the formulation of the program and carrying out the tedious calculations is gratefully acknowledged.

### References

1 Isenberg, J. S., and Lin, C. C., "The Method of Characteristics in Compressible Flow," Part I, Steady Supersonic Flow, Technical Intelligence-Air Materiel Command, Technical Report F-TR-1173A-ND (GDAM A-9-M 11/1) Monograph II, 1947.

2 Ibid, Part Ia, Tables and Charts, Technical Report F-TR-1173B-ND (GDAM A-9-M 11/A).

3 Ferri, Antonio, "Elements of Aerodynamics of Supersonic Flows," MacMillan, New York, 1949, Chapters 10, 12, 13.

4 DeHaller, P., "The Application of a Graphic Method to Some Dynamic Problems in Gases," Sulzer Technical Review, no. 1, 1945.

5 Sibert, Harold W., "High-Speed Aerodynamics," Prentice-Hall, 1948, Chapter 25.

6 Miles, E. R. C., "Supersonic Aerodynamics," McGraw-Hill, 1950, Chapters 8, 9.

7 Courant, R., and Friedricks, K. O., "Supersonic Flow and Shock Waves," Interscience, New York, 1948.

8 Chapman, D. R., "An Analysis of Base Pressure at Supersonic Velocities and Comparison with Experiment," NACA TN 2137, July 1950.

9 Ferri, A., "Application of the Method of Characteristics to Supersonic Flow," NACA TN 1135, 1946.

10 "The Dynamics and Thermodynamics of Compressible Fluid Flow," vols. I, II, A. N. Shapiro, Ronald, 1954.

11 Sauer, R., "General Characteristics of the Flow Through Nozzles at Near Critical Speeds," NACA TN 1147, 1947.

12 Falkovich, S. V., "On the Theory of the Laval Nozzle," NACA TN 1212, 1949.

13 Oswatitsch, K. L., and Rothstein, W., "Flow Pattern in a Converging-Diverging Nozzle," NACA TN 1215, 1949.

14 Hooker, S. C., "Flow of Compressible Fluid in the Neighborhood of the Throat of a Constriction in a Circular Wind Channel," ARC, REM 1429, 1931.

15 Guderley, G., "Beste Formen für Achsensymmetrictre überschallschubdusen," *Zeitschrift für Flugwissenschaften*, Braunschweig, 13, N9, Sept. 1955.

16 Clippinger, R. F., "Supersonic Axially Symmetric Nozzles," B.R.L., Aberdeen Proving Ground, Report 794, Dec. 1951.

---

## Breakup of Water Drops and Sprays

*(Continued from page 1087)*

single shock appears to follow the same three stages mentioned previously for steady-flow conditions, namely, (a) development of small surface disturbances, (b) air friction and pressure on free liquid to produce drops or ligaments and (c) splitting of the ligament or drop by the relative air flow. Preliminary experiments on the effect of reflected shocks have indicated that atomization is greatly increased by the second shock and that all the above stages are not necessarily repeated.

### Summary of Results

The following results were obtained from the investigation of the interaction of single shocks with water sprays and drops:

1 For drops, there is a relation between drop stability and relative gas velocity. At a given relative velocity there is a critical drop size above which drops are shattered by the shock.

2 For jets, there is also a critical size, larger than for drops. Counterflow jets have a larger critical size than perpendicular flow jets.

3 Breakup of sprays formed by impinging jets, parallel sheets and parallel jets is a function of the surface area exposed to the shock and the time of exposure to the high velocity gases behind the shock. The breakup of the spray increases with increased area and time.

4 Shock travel perpendicular to the liquid flow apparently increases the mixing of the spray.

5 A reflected shock greatly increases the breakup of the spray over that produced by a single shock.

### References

1 Lane, W. R., "Shatter of Drops in Streams of Air," *Industrial and Engineering Chemistry*, vol. 43, no. 6, 1951, pp. 1312–1317.

2 Hanson, A. R., Domich, E. G., and Adams, H. S., "An Experimental Investigation of Impact and Shock Wave Breakup of Liquid Drops," University of Minnesota Research Rep. no. 125, Nov. 15, 1955. (Final Report for Bureau of Aeronautics, Navy Dept.)

3 Ellis, H., Odgers, I., Stosik, A. J., Van De Verg, N., and Wick, R. S., "Experimental Investigation of Combustion Instability in Rocket Motors," Fourth Symposium on Combustion, Williams & Wilkins Co., 1953, pp. 880–885.

4 Berman, K., and Logan, S. E., "Combustion Studies with a Rocket Motor Having a Full-Length Observation Window," *Journal of the American Rocket Society*, vol. 22, no. 2, 1952, p. 78.

5 Rogers, D. E., and Marble, F. E., "A Mechanism for High-Frequency Oscillation in Ram-Jet Combustors and Afterburners," JET PROPULSION, vol. 26, June 1956, pp. 456–462.

6 Smith, R. P., and Sprenger, D. F., "Combustion Instability in Solid Propellant Rockets," Fourth Symposium on Combustion, Williams & Wilkins Co., 1953, pp. 893–906.

# Flare Measurements From Rockets

T. A. CHUBB,[1] H. FRIEDMAN,[2] J. E. KUPPERIAN Jr.[3] and J. C. LINDSAY[4]

Naval Research Laboratory, Washington, D. C.

**During the summer of 1956 a series of small rockets were command fired in conjunction with astronomical observations of the sun. The purpose of this program was to make measurements in the D region of the ionosphere during solar flares. This program is a typical example of an integrated research study based on small rocket vehicles. It illustrates how the various specialties of logistics, rocket techniques, electronics and physics all mesh to make possible an upper air investigation. In addition to a description of the rocket system employed, the solutions to three specific problems associated with the small rocket technique will be described—the antenna design problem, the rocket aspect problem and the vertical trajectory problem. Data on the performance of the system are also included.**

## Experiment

BEFORE describing the rocket system, let us first consider the scientific problem which was studied. The program was undertaken to determine the nature of the ionizing radiation produced in solar flares. The program was conceived as a preliminary study to provide data and experience necessary for an expanded study along the same lines during the International Geophysical Year. The solar flare has stood out for a long time as one of the important phenomena of nature about which almost nothing is known. It is the solar event which causes the most striking effects at the earth. When a major flare occurs on the sun there is an immediate cessation of long distance short-wave radio reception. There is a small sharp change in the earth's magnetic field. There is an ejection from the sun of clouds of ionized gas which envelop the earth one to three days after the flare with resulting aurorae, sparking on telegraph wires and a general disturbance of the earth's magnetic field. Five flares in recent years have caused major increases in the intensity of cosmic rays striking the earth's surface. The cosmic ray increases accompanying these flares were many times greater than any fluctuations that have otherwise occurred. Yet the nature of this phenomenon that can cause such major effects is not understood. It is subjected to continuous observation and study by solar observatories and ionosphere monitoring stations scattered around the world. And although much data on flares has been obtained by these various groups, there is no theory of the flare on which there is any agreement.

The particular aspect of the flare selected for study by our group in 1956 was the penetrating radiation produced by large flares and responsible for radio fadeout. The problem is relatively clear-cut. It is known that radio fadeout is caused by ionization of air in the lower D region (about 40 to 50 miles up) where free electrons absorb radio energy because of dissipating collisions with the surrounding gas. At higher altitudes such free electrons act only as reflectors of radio waves. In addition it is known that only two spectral regions of emission from the sun are capable of producing ionization at the required atmospheric depth. The two radiations are the Lyman alpha ultraviolet emission line of hydrogen at 1216 Å and the high temperature x-ray emission from the sun's corona. Previous rocket measurements had pretty definitely confirmed that ionization normally encountered in the D region is caused by resonant Lyman alpha line emission from hydrogen. The normal x-ray radiation from the sun's corona was found to be restricted to wave lengths longer than about 10 Å. These wave lengths are absorbed in the E region (about 70 miles up). However, the large variability in the penetrating power of the normally encountered x-ray spectrum (1, 2)[5] suggested that during a flare there was a good possibility that x-rays of a wave length short enough to penetrate the D region might occur. Thus the first major goal of the flare program was to determine whether an intensification of the normally present Lyman alpha radiation or a hardening of the normally present coronal x-ray spectrum was the primary source of the radio fadeouts occurring during solar flares.

## Rocket System

The approach which we adopted for this program is shown in Fig. 1. This sketch illustrates the use of a command-fired Rockoon system for the study of solar flares. The figure shows a 72-ft Skyhook polyethylene balloon floating at 80,000 ft with a 6-in.-diam solid propellant rocket, the Deacon, suspended beneath the balloon in readiness to be fired. The balloon and rocket were located above an empty area of the Pacific Ocean 400 miles southwest of San Diego. When a flare occurred on the surface of the sun, the rocket was fired by a dual tone command signal transmitted by radio from the control ship to a command receiver suspended below the rocket. The command receiver then turned on the rocket electronics and, after a 30 sec delay, fired the rocket.

The rockets were fired actually at an angle much closer to vertical than that indicated in the drawing. Fired at an angle of 7.5 deg from the vertical, the rocket passed through the balloon on its upward course. After passing through the balloons, the rockets coasted to peak altitudes of 60 to 70 miles. Information from the radiation detectors was transmitted by a 220 mc/s FM FM telemetering link to the instrumentation trailer aboard the command ship. Flares on the sun occur so infrequently that it is very unlikely that a rocket fired at a fixed scheduled time will encounter a flare. Thus, in order to make measurements during a flare it was necessary to have a rocket in readiness for firing while observations of the sun and ionosphere were being made. Since most flares last only 10 to 30 min, it was necessary to fire the rocket promptly as soon as the flare was detected. At the time the 1956 program was planned, safety and scheduling requirements at the available rocket firing ranges prevented the use of a land-based command-fired rocket system. Moreover, since J. A. Van Allen had worked out the Rockoon system and developed it into a reliable technique (3) it seemed to be a good choice for the flare experiment.

The essential components of the rocket program are shown in Fig. 2. Basic to the experiment are the balloon and the rocket with its instrument head and telemetering transmitter. Also suspended below the balloon is the command receiver which turns on the rocket electronics and fires the

Presented at the ARS Spring Meeting, Washington, D. C., April 4–6, 1957.

[1] Physicist.
[2] Head, Electron Optics Branch.
[3] Physicist. Mem. ARS.
[4] Physicist.

Numbers in parentheses indicate References at end of paper.

rocket. Radar reflectors and a pressure measuring radiosonde transmitter are also carried by the balloon to enable the location and altitude of the suspended rocket to be known at all times. Ship-based equipment includes the telemetering receiver and associated signal decoders and recorders. In addition, equipment was required for detecting solar flares. Radio contact was also maintained with the solar observatories at Sacramento Peak, N. Mex., and Climax, Colo. All shipboard components were mounted inside the NRL instrumentation trailer.

The essential features of the rocket experiment are shown in Fig. 3. The instrumentation head was designed to handle signals from four types of detectors carried in the missile and to convert them to suitably coded output signals. The detector complement included aspect photocells, a Lyman alpha ion chamber, a Geiger counter sensitive to x-rays and a scintillation pulse amplitude spectrometer. A conventional four-channel FM FM telemetering system delivering 4 watts was used and was provided with in-flight calibration. The weight of the instrumentation head was 23 lb. Battery power was furnished by silver cells and provided reliable power for over 12 min.

## Special Problems Involved in the Use of Small Rockets

Before considering the performance of the rocket system let us dwell momentarily on the three problems for which we feel we have found interesting solutions. The first problem is the antenna radiation pattern. The theoretical radiation pattern from a crossed dipole antenna array without any rocket is spherical in shape provided proper polarization of the receiving antenna is employed. It seemed to be a good bet to adapt this approach to the Rockoon problem where air drag is small and projection of antennas from the rocket is relatively harmless. The secret to the success of this array, however, is to employ a feeding network which guarantees a reasonably close division of power between the dipoles, which properly phases the dipoles and which protects the driving transmitter from reflected RF power due to slight antenna mismatch. A network accomplishing this feat was developed by R. W. Masters (4) and was adapted to our use by W. R. Nichols. Fig. 4 shows the network employed. The phasing of the antennas is maintained by the extra $\frac{1}{4}$ wave length of 50 Ω coaxial line in the feeds connecting dipole 2,4 as compared to dipole 1,3. The $\frac{1}{4}$ wave length antenna stubs making up each dipole are maintained 180 deg out of phase by the use of an extra $\frac{1}{2}$ wave length of coaxial line in the feeds of stubs 3 and 4. The key to success of the drive network is the resistor R located between points A and B. Power fed to the network from the transmitter causes no voltage drop across R, since points A and B correspond to points of equal phase. For power reflected at the antennas, however, this is not the case. This reflected power returns 180 deg out of phase because of the additional $\lambda/2$ ($\lambda/4$ out + $\lambda/4$ back) in the feed line to 2,4. The reflected power is effectively absorbed in R. With this network standing wave ratios of better than 1.2 were easily and consistently achieved.

The use of this antenna design for ground-based firings poses complications because of aerodynamic drag. Recent radiation pattern measurements indicate that the use of similarly phased antennas consisting of wires or blades bent back at 45 deg is capable of giving a radiation pattern almost as good as the original crossed dipoles. Such aerodynamic antennas are scheduled for testing in a series of Dan firings this coming July.

The second problem of interest is the problem of determining the orientation of the rocket throughout its flight. A knowledge of the rocket aspect is essential to any meaningful interpretation of the experimental data. A detailed description of the method used to determine rocket aspect is given

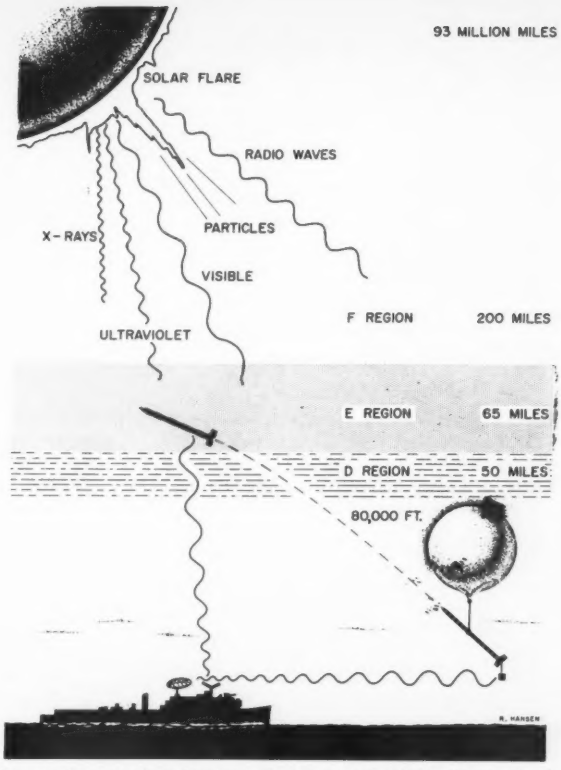


**Fig. 1 Sketch of the Rockoon System as adapted to the study of solar flares. Command firing was used to make possible D layer measurements during the development of the flare. Rocket floating times were limited to about 4 hours because of excessive balloon drift.**

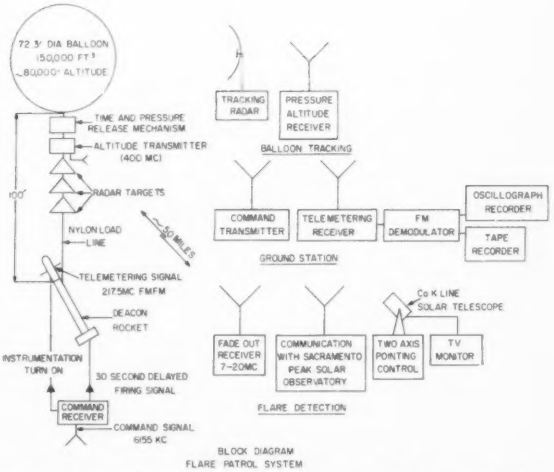


**Fig. 2 Schematic outline of component assemblies employed in the 1956 Rockoon flare studies. Apparatus suspended from the balloon includes instrumented rocket, firing box and equipment for keeping track of the balloon position. Ground-based equipment includes telemetering station, equipment for observing radio fadeout as a flare indicator, and facilities for communication with solar observatories.**

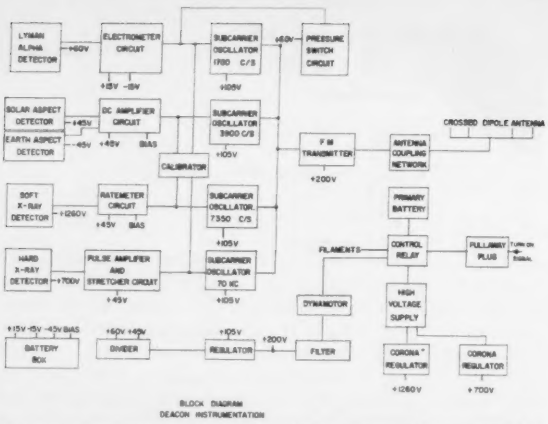


**Fig. 3 Schematic outline of the rocket instrumentation assembly. The equipment incorporates a 4 channel FM FM telemetering system driven by four types of radiation detectors. A calibrator provides in flight calibration on each channel. Power is derived from a silver cell providing 12 min of instrument operation.**

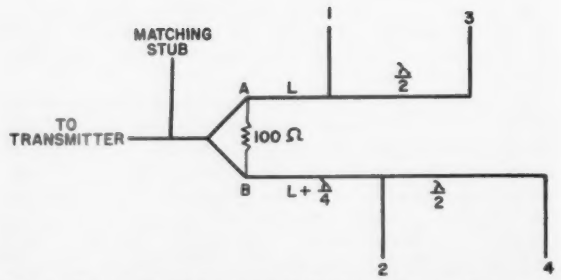


**Fig. 4 Feed network for crossed dipole Rockoon antenna system. The feed network makes matching relatively uncritical by absorbing R. F. power reflected at antenna stubs. The network is made from 50 Ω coaxial cable.**

in (5). In essence the rocket aspect problem for a spinning rocket is solved from information obtained from two photocells. Each of these photocells looks out in a plane perpendicular to the axis of the rocket. Figure 5 shows the responses of these photocells during $1\frac{1}{2}$ rolls of a free-flying rocket. The sun cell is flown uncollimated and measures the angle between the view plane and the sun. The earth cell is tightly collimated so that only by rare coincidence does it see the sun. It responds to earth light and deflects the telemetering signal in a negative direction. By a knowledge of the angle between the view plane and the sun combined with a knowledge of the phase relationship between the subzenith point c and the subsolar point d, the orientation of the rocket axis is determinable with an accuracy of a few degrees.

The third problem for which we have an interesting solution is the problem of determining the altitude of the rocket as a function of time; that is, the rocket's vertical trajectory. This vertical trajectory can be found without using external tracking. The problem is solved by determining the time of rocket peak and the time at which the rocket passed a known altitude above the region of atmospheric drag. A free fall trajectory can be anchored to these points. Both of these pieces of information are obtainable from the response of the Lyman alpha ion chamber. A daytime rocket flying above 100 km sees Lyman alpha radiation from the sun almost unaffected by atmospheric absorption. At an altitude of 74.3 km for a sun 30 deg below zenith, the incident Lyman alpha radiation is attenuated to 30 per cent of its above atmospheric value. An examination of the telemetering record permits a direct determination of the time at which this 30 per cent transmission point was passed. Also a matching of the ascent and descent data of the Lyman alpha detector in the region of strong atmospheric absorption permits an accurate determination of peak time. In making these calculations it is, of course, essential to correct all the Lyman alpha data for variations in rocket aspect. Provided this is done, however, the vertical trajectory of the rocket can be determined in most cases to an accuracy of a few kilometers without the use of tracking data. Since Lyman alpha glow has been observed at night, the method is also applicable for nightflights.

## Results of Project Rockoon

Let us now consider the results of the Rockoon expedition as a whole. Scientifically the expedition was a success in that one rocket was fired during observation of a small flare at Climax, Colo. The rocket firing occurred quite late in the flare and indicated an unusually high intensity of x-ray emission below 10 Å while the Lyman alpha flux was of normal intensity. Operationally, the expedition was less successful. Out of ten rockets, three were lost by failure of the rocket ignition, and one was lost by balloon failure. In contrast, no trouble was encountered in the balloon launchings, shown in Figs. 6 and 7. The villain of the expedition was the rocket igniter. The igniter with which we started was both violent and undependable, despite its having been previously tested at low pressure. The problem of reliable ignition has plagued the Rockoon system because of the difficulty of igniting black powder below 30 mm pressure.

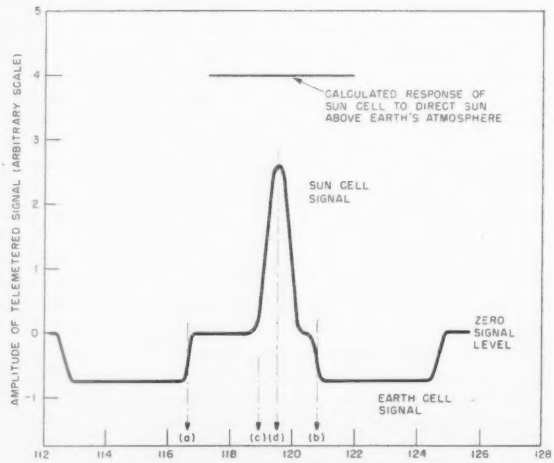


**Fig. 5 Aspect photocell record for rolling rocket. Sun cell peak is the response of an uncollimated photocell. Amplitude of peak measures angle between sun and the plane normal to the rocket axis. Negative response of earth cell appears when a second collimated photocell looks at earth. Phase relationship between c and d combined with sun cell amplitude permits determination of rocket aspect.**

Fig. 6 Launching of a Rockoon from the US Colonial during 1956 Rockoon flare studies

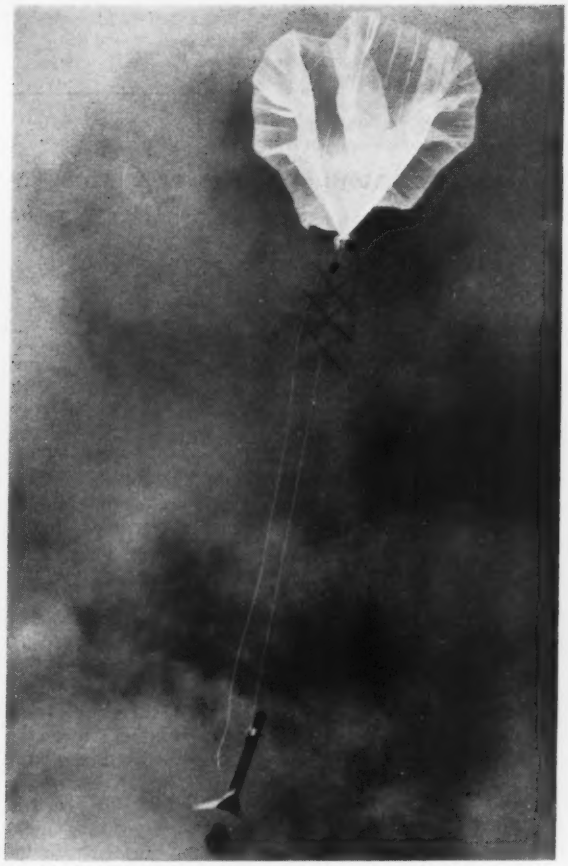

Fig. 7 Deacon rocket and associated equipment a few seconds after launch in 1956 Rockoon flare program

The igniter finally developed and used in the last flight may have provided a satisfactory solution to the problem. This last igniter was made up in a heavy walled brass can, 3-in. in diam. and $1\frac{1}{2}$ in. deep, provided with $\frac{3}{8}$ in. diam blow-out holes covered with 5 mil 2 S aluminum foil. The can was filled with a mixture of crushed black cannon powder (JAN-P-223) and smokeless powder (12 mil T.M.S. $\frac{1}{8}$ in. sq, JAN-P-381). The igniter was fired with a Type MIAl electrical squib surrounded with a paper sack filled with finely crushed black powder. In the flight test, the igniter was satisfactory in every way.

The violent shock produced by most of the igniters caused various types of electronic failure. Despite these difficulties good altitude data was obtained from the Lyman alpha ion chambers in three flights. In these flights, peak altitudes of 100, 102 and 115 km were reached. The length of telemetering time in the other three flights indicated comparable altitudes. These altitudes proved that the rocket performance was at least as good as anticipated. In view of these results, we feel that a command-fired Rockoon system can achieve computed performance.

The scientific results of the 1956 expedition were sufficiently exciting that a considerable extension of the program is planned for 1957. The evidence of flare excitation producing relatively hard x-rays means that it should be possible to follow the development of a flare and its emission character at the critical high energy end of its emission curve. Such a study is capable of distinguishing between thermal and non-thermal types of emission and could well provide a more powerful tool in unraveling the flare mystery than those that have previously been employed.

To exploit these possibilities a series of 14 rockets is being undertaken during the present year. The availability of an island base for launching makes possible ground command firing of a Nike-Deacon (Dan) combination which promises a much better yield of flare data. The use of the Dan rocket system gives adequate altitude with minimal heating. The first firing took place July 1, the beginning of the International Geophysical Year.

## References


1 Byram, E. T., Chubb, T. A., and Friedman, H., "The Solar X-Ray Spectrum and the Density of the Upper Atmosphere," *Journal of Geophysical Research*, vol. 61, 1956, p. 251.

2 Friedman, H., and Chubb, T. A., "Solar X-Ray Emission and the Height of D Layer during Radio Fade-Out," in The Physics of the Ionosphere—Report at 1954 Cambridge Conference, 58; The Physical Society, London S.W. 7, 1955.

3 Van Allen, J. A., and Gottlieb, M. B., "The Inexpensive Attainment of High Altitudes with Balloon-Launched Rockets," in Rocket Exploration of the Upper Atmosphere, edited by RLF Boyd and M. J. Seaton, Pergamon Press, Ltd., London, 1954, p. 53.

4 Masters, R. W., "A Power-Equalizing Network for Antennas," *Proceedings of the Institute of Radio Engineers*, vol. 37, 1949, p. 735.

5 Kupperian Jr., J. E., and Kreplin, R. W., "Optical Aspect System for Rockets," *Review of Scientific Instruments*, vol. 28, Jan. 1957, p. 14.

# Technical Notes

## On Thermonuclear Power Plants

H. J. KAEPPELER[1]

Forschungsinstitut für Physik der Strahlantriebe, Stuttgart, Germany

IN THE July 1956 JET PROPULSION, H. S. Tsien (1)[2] published a study of thermonuclear power generation. Consequently, there appeared comments by J. L. Greenstein (2) and by Shechtman and Larisch (3). While this author essentially agrees with most of the remarks by J. L. Greenstein, he does not concur with those by Shechtman and Larisch. This author believes that radiation pressure does not play an important role in thermonuclear energy production rate in highly diluted plasmas and that in such a plasma the radiation pressure is considerably lower than the values given by Shechtman and Larisch.

The type of thermonuclear power plant as discussed by Tsien (1) was originally investigated by this author for rocket propulsion (4, 5) in 1953 and treated in further papers (6–9). Consequently, E. Sänger studied the energy production of thermonuclear reactions in powerplants (10). The emphasis in the papers (4–9) was on the question of energy transport in reacting plasmas at extreme temperature rather than on the energy production rate itself, which was calculated for a large number of different plasmas by Sänger (10). The effect of radiation on energy transport was included by this author in his studies; however, the effect of radiation pressure on dynamical or energy producing events was neglected with the comment (5) that it would only have to be included in more accurate calculations.

It is the purpose of this note to show that in plasmas at extremely high temperature and technically feasible pressure, the effects of radiation pressure on dynamical and/or energy producing events is actually negligible, and that for technically feasible dimensions of the plasma even the contribution of the radiation pressure to the total pressure can be neglected.

First, the technically feasible dimensions and pressures shall be stated. Technically still feasible dimensions should, in the opinion of this author, not exceed an order of magnitude of $10^4$ cm, while pressures may come into the range of $10^2$ to $10^3$ atm. A plasma at $10^8$ K and 100 atm, e.g., is already highly diluted. Its density ratio $\rho/\rho_0$ ($\rho_0$ = standard density at sea level temperature and pressure) is about $10^{-4}$, its particle density $n = p/kT$ approximately $10^{15}$ cm$^{-3}$. It is very unlikely that such a diluted hydrogen plasma with relatively small dimensions in the order of $10^4$ cm behaves as a black body.

The intensity of the radiation penetrating a plasma body is given by the relation

$$I/I_0 = 1 - e^{-\kappa \cdot r} \quad \ldots\ldots [1]$$

where $r$ is the distance traversed by the radiation, $\kappa$ [cm$^{-1}$] the absorption coefficient, $I = I(r)$ the radiation intensity and $I_0 = \sigma T^4$ the black body radiation intensity, where $\sigma$ is Boltzmann's radiation constant. In a completely ionized plasma, the essential contribution to radiation is from free-free transitions. For these, the absorption coefficient is given by Kramer's formula (11)

$$\kappa_\nu = \frac{4\pi Z^2 e^6}{3\sqrt{3} \cdot h \cdot c \cdot m^2 v} \cdot \frac{1}{\nu^3} \quad \ldots\ldots [2]$$

where $e \cdot Z$ is the ionic charge, $e$ the electronic charge, $m$ the electronic mass, $v$ the velocity of the electron to be retarded in the free-free transition, $h$ Planck's constant, $c$ the velocity of light, and $\nu$ the frequency of the radiation. Integrations must be performed over all velocities and frequencies. This results in (9)

$$\kappa = \frac{15 \cdot 2^4}{3\sqrt{3}\,\pi^3} \frac{h^2 e^6 Z^2}{c(2\pi m)^{3/2}} c_e \cdot c_i \frac{p^2}{(kT)^{11/2}} \quad \ldots\ldots [3]$$

where $p$ is the total pressure, $c_e$ and $c_i$ are the electronic and ionic concentrations, respectively, and $k$ is Boltzmann's constant. For completely ionized hydrogen, $Z = 1$ and $c_e = c_i = \frac{1}{2}$, with $p$ then being the *gas* pressure. Calculations for completely ionized hydrogen at a gas pressure of 100 atm are presented in Fig. 1, the radiation intensity plotted against temperature, with $r$ as a parameter. Similar calculations were already given by Sänger (10). It is immediately evident that hydrogen at $10^8$ K and 100 atm is far from behaving as a black body.

According to Unsöld (12), the radiation pressure is given by the relation

$$p_r = \frac{4\pi}{3c} \cdot I \quad \ldots\ldots [4]$$

where $I$ is the intensity calculated above. This formula is explained in detail by Unsöld. Fig. 2 presents the radiation pressure as a function of the (homogeneous) plasma temperature, with $r$ as a parameter. Taking a plasma body with a (homogeneous) temperature of $10^8$ K and a gas pressure of 100 atm, it is seen from Fig. 2 that the radiation pressure $p_r$ at $r = 100$ $m$ is of the order $10^{-3}$ atm, that is, negligible for a first approximation. As for this plasma state $e^{-\kappa \cdot r} \ll 1$, the relation

$$I/I_0 \approx \kappa \cdot r \quad \ldots\ldots [5]$$

may be used. This shows that $I$ (for constant temperature), and thus also $p_r$, increases linearly with $r$ in this range.

Though Equation [1] is valid for homogeneous temperature distribution only, it may be used to *estimate* the relations in a plasma body with temperature gradient. If $p_r$ is to remain constant for varying $r$ and $T$, the intensity $I$ must remain constant and there follows the condition

$$\kappa r = \text{const for } I = \text{const}, \; p_r = \text{const} \quad \ldots\ldots [6]$$

From Equations [3, 6] follows

$$\left(\frac{r}{r_0}\right) = \text{const}\left(\frac{\kappa_0}{\kappa}\right) = \text{const}\left(\frac{T}{T}\right)^{11/2} \quad \ldots\ldots [7]$$

where $T_0$ and $r_0$ are any associated reference values. As such a temperature profile is consistent with transport considerations (4–7, 9)—in most cases the temperature drop will be

Received April 12, 1957.

[1] Physicist.

[2] Numbers in parentheses indicate References at end of paper.

EDITOR'S NOTE: This section of JET PROPULSION is open to short manuscripts describing new developments or offering comments on papers previously published. Such manuscripts are published without editorial review, usually within two months of the date of receipt. Requirements as to style are the same as for regular contributions (see masthead page of this issue).

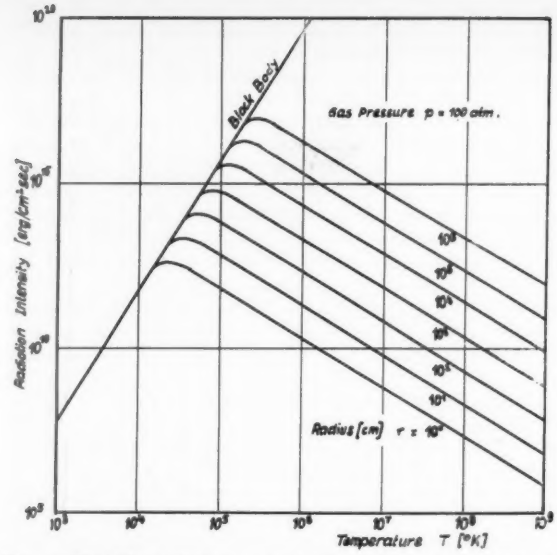


Fig. 1 Radiation intensity $I$ (erg/cm$^2$sec) in completely ionized hydrogen from free-free transitions plotted against temperature $T$, with radius $r$ as a parameter, for a gas pressure of 100 atm

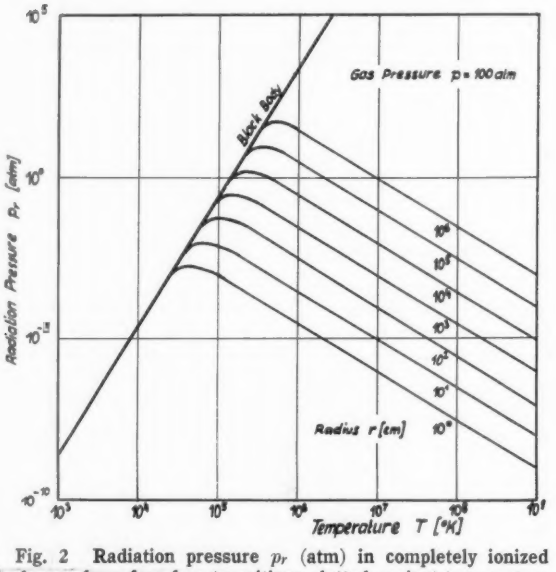


Fig. 2 Radiation pressure $p_r$ (atm) in completely ionized hydrogen from free-free transitions plotted against temperature $T$, with radius $r$ as a parameter, for a gas pressure of 100 atm

even greater—it may well be assumed that also in relatively dense outer layers no strong increase of radiation pressure will have to be expected.

Summarizing, it may be stated that although radiation pressure effects should be considered in a detailed treatment of plasma behavior, they may well be neglected in first approximations for relatively dilute plasmas. Contrary to the calculations of Shechtman and Larisch (3), it is thus shown that radiation pressure has a very small effect on noncatalyzed thermonuclear reactions. For catalyzed thermonuclear reactions (9) this question will have to be studied separately.

### References

1 Tsien, H. S., "Thermonuclear Power Plants," JET PROPULSION, vol. 26, July 1956, p. 559.

2 Greenstein, J. L., "Comments on Hsue-shen Tsien Paper," JET PROPULSION, vol. 26, July 1956, p. 565.

3 Shechtman, I., and Larisch, E., "Comments on Thermonuclear Power Plants," JET PROPULSION, vol. 27, Feb. 1957, p. 176.

4 Kaeppeler, H. J., Forschungsreihe der Gesellschaft für Weltraumforschung, Rep. no. 12, Stuttgart, Sept. 1953.

5 Kaeppeler, H. J., Probleme der Weltraumforschung, Biel, Laubscher, 1954, p. 41.

6 Kaeppeler, H. J., "Problem of Cooling Nuclear Working Fluid Rockets Operating at Extreme Temperatures," JET PROPULSION, vol. 24, 1954, p. 316.

7 Kaeppeler, H. J., *Journa' of the British Interplanetory Society*, vol. 14, 1955, p. 89.

8 Kaeppeler, H. J., *Journal of Astronautics*, vol. 2, 1955, pp. 58, 111.

9 Kaeppeler, H. J., *Raketentechnik und Raumfahrtforschung*, vol. 1, no. 3, 1957, in print.

10 Sänger, E., *Astronautica Acta*, vol. 1, 1955, p. 61.

11 Unsöld, A., "Physik der Sternatmosphären," Springer, Berlin, 1955, p. 167.

12 Unsöld, A., loc. cit., p. 200.

## Apparent Emission Intensities From a Turbulent Flame Composed of Wrinkled Laminar Flames[1]

F. WILLIAMS[2] and A. E. FUHS[3]

Daniel and Florence Guggenheim Jet Propulsion Center, California Institute of Technology, Pasadena, Calif.

THERE has recently been some discussion on the use of the model of a wrinkled laminar flame for an approximate description of turbulent flame structure. In particular, Summerfield has claimed that some of his observations contradict theoretical predictions based on the use of this model.[4] It is the purpose of the following discussion to clarify some of the consequences of the wrinkled laminar flame model.

### Apparent Product and Radical Profiles for Wrinkled Laminar Flames

Consider a turbulent flame. We assume that the structure of the one-dimensional steady-state laminar flame for the given combustible mixture is known, either from theory or experiment. Then the turbulent flame is assumed to consist of an ordinary highly wrinkled laminar flame which moves back and forth very rapidly through the spatial region occupied by the turbulent flame zone. With an instrument, the time resolution of which is long compared with the oscillation time of the wrinkled laminar flame, one sees only the time average of the motion of the laminar flame front, and therefore the turbulent flame pattern appears to be constant in time. Furthermore, regardless of the instrumental time resolution, the measured intensities will always be averaged over space (see Figs. 1 and 2).

The picture implied by the sketches shown in Figs. 1 and 2 is admittedly quite approximate. If a laminar flame front were really oscillating rapidly about a mean position, it would probably not have exactly the same structure as a steady-state laminar flame. Our model does not predict

Received June 28, 1957.

[1] Supported by the Office of Ordnance Research, U. S. Army, under Contract DA-04-495-Ord-446. The authors are indebted to S. S. Penner for suggesting this investigation and for helpful discussions.

[2] National Science Foundation Fellow. Student Mem. ARS.

[3] Guggenheim Jet Propulsion Fellow. Student Mem. ARS.

[4] Summerfield, M., Reiter, S. H., Kebely, V., and Mascolo, R. W., "The Structure and Propagation Mechanism of Turbulent Flames in High Speed Flow," JET PROPULSION, vol. 25, Aug. 1955, pp. 377–384.

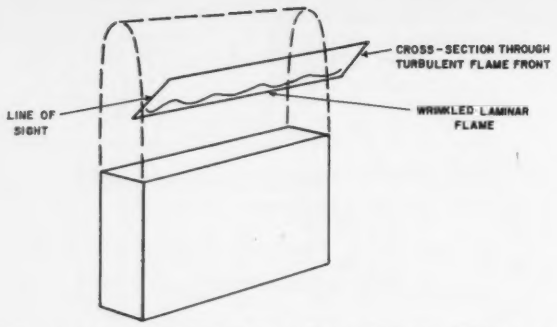


Fig. 1 Schematic illustration of space average obtained by observing an open two-dimensional turbulent flame

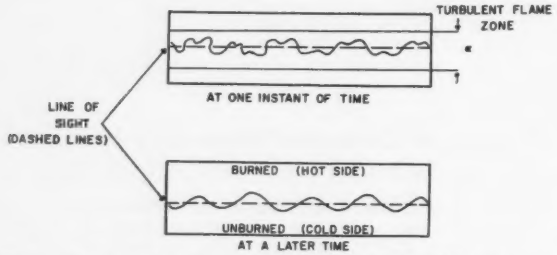


Fig. 2 Plane cutting the wrinkled laminar flame which separates the unburned from the burned gases

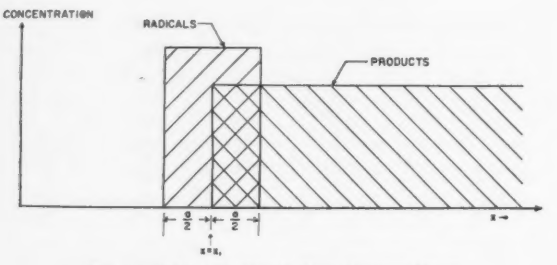


Fig. 3 Model of steady-state laminar flame

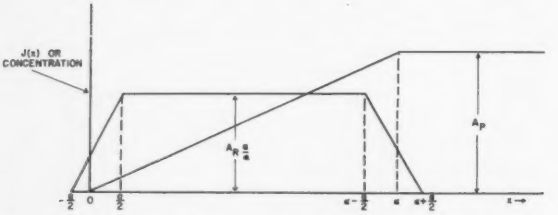


Fig. 4 The quantity $J(x)$ as a function of $x$ for the assumed function $p(x)$

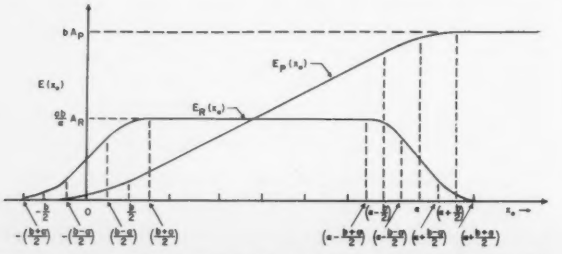

Fig. 5 Instrument response when observations are made with a slit width $b > a$ and $J(x)$ has the $x$-dependence shown in Fig 4

the length of time which the laminar flame spends at each point in the turbulent flame zone.

We shall use approximate representations for the radical distributions in the laminar flame in order to predict the corresponding turbulent flame structure. The roughest approximation to the distribution of radicals and products through a steady-state laminar flame involves radical concentrations which are zero outside an effective width $a$ for the laminar flame and constant within $a$ (see Fig. 3). We also assume that the product concentration is zero to the left of the center of the laminar flame and constant to the right (see Fig. 3).[5]

For the thickness corresponding to ordinary (wrinkled) laminar flames, it is reasonable to assume that a space average is equivalent to a time average. We may assign a probability function $p(x)$ to the turbulent flame in such a way that $p(x)dx$ is the probability that the center of the oscillating laminar flame will be found at a position $x$ in the range $dx$ in the turbulent flame zone. The laminar flame structure and the probability function $p(x)$ determine completely the results of emission intensity measurements on turbulent flames.

Consider the results of intensity measurements for a specified spectral line with an instrument of slit width $b$ for a constant optical path-length $d$ in the flame front perpendicular to the direction of propagation. Neglecting self-absorption, we may then calculate the energy per second received by the instrument, which is equivalent to the intensity reading of the instrument.

The total intensity $I_R(x, x_1)$ emitted from radicals at a position $x$ by a laminar flame with center at $x_1$ is

$$I_R(x, x_1) = \begin{cases} 0 & \text{for } x < x_1 - a/2 \\ A_R & \text{for } x_1 - a/2 \leq x \leq x_1 + a/2 \\ 0 & \text{for } x > x_1 + a/2 \end{cases} \quad [1]$$

similarly, the total intensity emitted from reaction products is

$$I_P(x, x_1) = \begin{cases} 0 & \text{for } x < x_1 \\ A_P & \text{for } x \geq x_1 \end{cases} \quad [2]$$

where the subscripts $R$ and $P$ refer to radicals and products, respectively, and $A_R$ and $A_P$ are constants. Actually the intensity corresponding to the average over-all positions $x_1$ of the center of the laminar flame is observed for a real turbulent flame. If we call $J(x)$ the intensity observed for the turbulent flame at the spatial position $x$, then

$$J(x) = \int_{-\infty}^{\infty} p(x_1) I(x, x_1) dx_1 \quad [3]$$

The probability is, of course, normalized in such a way that $\int_{-\infty}^{\infty} p(x)dx = 1$; $I(x, x_1)$, which depends only on $(x - x_1)$, may be called the intensity kernel. The quantity $J(x)$ is evidently proportional to the average concentration of emitters in the turbulent flame.

Actually, $J(x)$ is proportional to the reading of an instrument with an infinitesimal slit. With an instrument of finite slit width $b$ and uniform sensitivity over $b$, which is centered at the position $x_0$, the energy per second $E(x_0)$ received by the instrument would be

$$E(x_0) = \int_{x_0 - (b/2)}^{x_0 + (b/2)} J(x)dx \quad [4]$$

i.e., the actual reading of the instrument is proportional to

$$E(x_0) = \int_{x_0 - (b/2)}^{x_0 + (b/2)} dx \int_{-\infty}^{\infty} p(x_1) I(x, x_1) dx_1 \quad [5]$$

Once $p(x)$ is known, $E(x_0)$ can be evaluated from Equation [5].

[5] The representation used in Fig. 3 describes roughly the *emission intensity* profiles for CH and $C_2$ ("radicals") and for $H_2O$ ("products") in laminar flames.

A reasonable approximate choice for $p(x)$ is

$$p(x) = \begin{cases} 0 \text{ for } x < 0 \\ \frac{1}{\alpha} \text{ for } 0 \leq x \leq \alpha \\ 0 \text{ for } x > \alpha \end{cases} \quad [6]$$

where $\alpha$ is a constant approximately equal to the turbulent flame width. Equation [6] gives the probability distribution if it is equally likely to find the wrinkled laminar flame anywhere in the turbulent flame zone. Using Equation [6], we find

$$J_P(x) = \begin{cases} 0 & \text{for } x < 0 \\ A_P \left(\frac{x}{\alpha}\right) & \text{for } 0 \leq x \leq \alpha \\ A_P & \text{for } x > \alpha \end{cases} \quad [7]$$

and

$$J_R(x) = \begin{cases} 0 & \text{for } x < -a/2 \\ A_R \dfrac{x + (a/2)}{\alpha} & \text{for } -a/2 \leq x < a/2 \\ A_R \dfrac{a}{\alpha} & \text{for } a/2 \leq x \leq \alpha - a/2 \\ A_R \dfrac{\alpha + (a/2) - x}{\alpha} & \text{for } \alpha - a/2 < x \leq \alpha + a/2 \\ 0 & \text{for } x > \alpha + a/2 \end{cases} \quad [8]$$

These functions $J_P(x)$ and $J_R(x)$ are plotted in Fig. 4.

If one makes a measurement with an instrument of slit width $b > a$, which is often the case, then another integration yields

$$E_P(x_0) = \begin{cases} 0 & \text{for } x_0 < -b/2 \\ \dfrac{A_P}{2\alpha} [x_0 + (b/2)]^2 & \text{for } -b/2 \leq x_0 < b/2 \\ A_P \left(\dfrac{b}{\alpha}\right)_{x_0} & \text{for } b/2 \leq x_0 \leq \alpha - b/2 \\ \dfrac{A_P}{2\alpha} \{2\alpha b - [x_0 - \alpha - (b/2)]^2\} & \text{for } \alpha - b/2 < x_0 \leq \alpha + b/2 \\ A_P b & \text{for } x_0 > \alpha + b/2 \end{cases} \quad [9]$$

and

$$E_R(x_0) = \begin{cases} 0 & \text{for } x_0 < -\left(\dfrac{b+a}{2}\right) \\ \dfrac{A_R}{2\alpha}\left[x_0 + \dfrac{(a+b)}{2}\right]^2 & \text{for } -\left(\dfrac{b+a}{2}\right) \leq x_0 < -\left(\dfrac{b-a}{2}\right) \\ A_R \left(\dfrac{a}{\alpha}\right)[x_0 + (b/2)] & \text{for } -\left(\dfrac{b-a}{2}\right) \leq x_0 < \left(\dfrac{b-a}{2}\right) \\ \dfrac{A_R}{\alpha}\left\{ab - \dfrac{1}{2}\left[x_0 - \dfrac{(b+a)}{2}\right]^2\right\} & \text{for } \dfrac{b-a}{2} \leq x_0 < \dfrac{b+a}{2} \\ A_R \left(\dfrac{ab}{\alpha}\right) & \text{for } \dfrac{b+a}{2} \leq x_0 \leq \alpha - \left(\dfrac{b+a}{2}\right) \end{cases} \quad [10]$$


**Fig. 6 Approximate concentration in the turbulent flame for a continuous function $p(x)$**

Evidently $E_R(x_0)$ is symmetric about $x_0 = \alpha/2$. The functions $E_P(x_0)$ and $E_R(x_0)$ are plotted in Fig. 5. For $b$ somewhat less than $a$ there is only a slight modification of the curves of $E(x_0)$; as $b \to 0$ the corners become sharper and the readings $E(x_0)$ approach $J(x_0)$, which is shown in Fig. 4.

The temperature distribution through a laminar flame follows a curve which is similar to that for the product concentration shown in Fig. 3. Therefore, the resulting average temperature distribution through a turbulent flame would be approximately that shown for the products in Fig. 4, although this quantity is probably unobservable by ordinary spectrographic techniques.

## Discussion

From the preceding simplified analysis a number of conclusions may be drawn regarding apparent intensity profiles for a turbulent flame composed of many wrinkled laminar flames. It is apparent that the wrinkled laminar flame model does not generally predict a rapid rise in the product concentration to its maximum value in a distance of the order of one laminar flame width. On the contrary, with the probability function $p(x)$ used by us, the product concentration rises gradually and does not reach its maximum value until near the end of the turbulent flame zone. Furthermore, it is obvious that a Gaussian distribution for $p(x)$ would lead to an even more gradual rise in the product concentration as is illustrated in Fig. 6. In order to obtain a sharp rise in product concentration one would have to use a $p(x)$ strongly skewed toward the cold end of the turbulent flame zone, which seems physically less attractive.

The wrinkled laminar flame model is also seen to predict that the radical concentration rises to its maximum value over a distance which is of the same order of magnitude as the laminar flame width or the slit width, whichever is larger, and then remains roughly constant throughout the remaining portion of the turbulent flame zone; it decreases to zero over approximately the same distance in which it rose to its maximum value. The distance over which the radical concentration appears to rise or fall is approximately proportional to the slit width for large slit widths ($b \gg a$) and is independent of the slit width for $b \ll a$.

Our particular model for $p(x)$ leads to the conclusion that the product concentration (and also the average temperature) reaches half of its maximum value in the center of the turbulent flame zone, i.e., at $x = \alpha/2$ (compare Fig. 4). It should be possible to check this conclusion experimentally.

The preceding conclusions are valid only for constant $p(x)$; they should remain nearly true for any $p(x)$ which is symmetric about $x = \alpha/2$. However, for skewed distributions the predictions do not apply.

The experiments of Summerfield seem to indicate that the onset of product emission lags the onset of radical emission by more than a laminar flame width. In the experimental studies the time of exposure was adjusted in such a way that the apparent maximum intensities of radical and product emission were the same. For our model the product intensity should increase much more slowly than the radical intensity. Adjusting the exposure time in such a way that radical and product peak intensities are equal will eliminate intensities

below a well-defined minimum value. If this minimum is $(1/m)$ times the maximum intensity, then we predict a separation of about $(1/m)$ times the turbulent flame width in the apparent onset of emission of radicals and products. For most instruments $m$ is a number between 2 and 10. Thus the separation should be $\frac{1}{2}$ to $\frac{1}{10}$ of a turbulent flame width, as has been observed actually by Summerfield and his collaborators.[4]

## Comment on 'Thermonuclear Power Plants'

SLOBODAN P. KRUČIČANIN[1]

Aerotechnical Institute, Beograd, Yugoslavia

IN THE article by H. S. Tsien entitled "Thermonuclear Power Plants" (JET PROPULSION, July 1956, p. 559) the following corrections should be made:

Equation [39], page 561, should be written

$$2 \times 2.014735 - (3.016977 + 1.008142) = 0.004331 \text{ amu} = 4.03 \text{ Mev} = 6.46 \times 10^{-6} \text{ ergs} \quad [39]$$

Equation [40], page 561, should be written

$$2 \times 2.014735 - (1.008982 + 3.01977) = 0.003511 \text{ amu} = 3.27 \text{ Mev} = 5.24 \times 10^{-6} \text{ ergs} \quad [40]$$

Received Nov. 20, 1956.

[1] Bulevar Revolucije 50, Beograd, Yugoslavia.

## Further Comments on 'Thermonuclear Power Plants'

I. SHECHTMAN[1] and E. LARISCH[2]

R. P. R. Academy Bucharest, Roumania

IN FEBRUARY 1957 JET PROPULSION, page 176, our comments on a paper by H. S. Tsien[3] appeared. Our considerations were based on the assumption that thermodynamic equilibrium exists between radiation and matter. These considerations cannot, however, be applied to Dr. Tsien's model where this condition is not satisfied.

Received May 18, 1957.

[1] Institute of Atomic Physics.

[2] Institute of Applied Mechanics.

[3] "Thermonuclear Power Plants," JET PROPULSION, July 1956, p. 559.

## Note on 'Study of Premixed Flames Using Radioactive Tracers'

MARTIN E. GLUCKSTEIN[1]

Ethyl Corp., Detroit, Mich.

REFERENCE is made to "Study of Premixed Flames Using Radioactive Tracers"[2] which according to the authors ". . . is submitted for the purpose of stimulating interchange of speculation on possible techniques for fellow workers." The writer trusts this note will be considered by the authors as one such interchange.

The technique suggested bears careful scrutiny, since there are some basic problems involved in the use of isotope tracers, particularly of the low molecular weight elements. The statement of the authors concerning the equivalence of $T_2$ and $H_2$ in the elemental state and by inference, in flame reactions, is not entirely accurate. Extensive literature exists on the reactions of $H_2$ and $D_2$, and, in general, neither the rates of oxidation of these materials nor their equilibria are the same.

As an example, consider the formation of light and heavy water. The Bureau of Standards (1)[3] reports these values for the free energy of formation ($\Delta F_f^0$) of "water" in the gaseous state at 25 C

$H_2O$: $\Delta F_{f0} = -54.6352$ kcal/mol
HDO: $\Delta F_{f0} = -55.828$ kcal/mol
$D_2O$ $\Delta F_{f0} = -56.067$ kcal/mol

From these values, the inequality of the equilibrium constants is apparent.

The effect of $T_2$ on the equilibrium of the water formation reactions may be examined by comparing the partition functions of the various compounds by the usual methods of statistical thermodynamics.

The rates of reaction of $H_2$ and $D_2$ may differ since there exists a difference in the zero point energy of the isotopes. Following Glasstone, the ratio of the reaction rates for reactions involving the molecular isotopic forms may be found from the exponential term in the Arrhenius rate expression (2). This ratio is

$$\frac{k_1}{k_2} = e^{+(\epsilon_1 - \epsilon_2)/RT} \quad [1]$$

where $k_1$, $k_2$ and $\epsilon_1$, $\epsilon_2$ are the rate constants and the zero point energies of $H_2$ and $D_2$, respectively. The zero point energies are related to each other nearly as the inverse square roots of the reduced masses or

$$\epsilon_{H_2} : \epsilon_{D_2} : \epsilon_{T_2} = \sqrt{2} : 1 : \sqrt{\tfrac{2}{3}} \quad [2]$$

Using Glasstone's value of $\epsilon_{H_2} - \epsilon_{D_2} \approx 1790$ cal, the value $\epsilon_{H_2} - \epsilon_{T_2} \approx 2500$ cal is obtained, or the ratio of reaction rates is

$$\frac{k_{H_2}}{k_{T_2}} = e^{+1320/T} \quad [3]$$

where $T$ is in degrees Kelvin. At 1725 C $k_{H_2}/k_{T_2} \approx 2$, and at 4000 K has only dropped to 1.39. This pronounced difference in reaction rate constants should certainly not be neglected.

Further, due to the large proportional difference in molecular weights, the diffusional characteristics of these isotopes are quite different. If the binary diffusion coefficients are calculated by the approximate equation [3]

$$D_{ij} = \frac{2.628 \times 10^{-3} \sqrt{T^3 (M_i + M_j)/2M_iM_j}}{P\sigma_{ij}^2}, \text{ cm}^2/\text{sec} \quad [4]$$

(where $M_i$, $M_j$ are the molecular weights of the diffusing specie, $P$ is the pressure, $\sigma_{ij}$ the effective molecular diameter, $\sigma_{ij} = \frac{1}{2}(\sigma_i + \sigma_j)$ and $T$ temperature) then the ratio of diffusion coefficients for $H_2$ and $T_2$ may be found. For oxygen as the second component this ratio is

$$\frac{D_{H_2-O_2}}{D_{T_2-O_2}} = \left[\frac{(M_{H_2} + M_{O_2})(2M_{T_2}M_{O_2})}{(2M_{H_2}M_{O_2})(M_{T_2} + M_{O_2})}\right]^{\frac{1}{2}} \quad [5]$$

since $M_{H_2} = 2$, $M_{T_2} = 6$, $M_{O_2} = 32$ assuming equal effective diameters for $H_2$ and $T_2$. The extension of this argument to other transport properties is relatively direct, and in addition

Received April 19, 1957.

[1] Research Laboratories, Research and Development Department.

[2] Kopytoff, V., Bell, C. G., and Cambel, A. B., JET PROPULSION, vol. 26, June 1956, p. 501.

[3] Numbers in parentheses indicate References at end of paper.

to the more frequently required properties of thermal conductivity and viscosity should also include the (usually neglected) thermal diffusion.

The writer recognizes the approximate nature of the examples presented. However, they do serve to indicate the care that should be exercised in attempting to extrapolate data taken with an $H_2$-$T_2$-air system to that of $H_2$ alone. The design of the experiment must be such that the transport, equilibrium and kinetic effects due to isotopic substitution may be corrected.

The suggested use of tagged compounds would materially lessen these undesirable effects but they cannot be eliminated. In the study of properties as elusive as those of simple flames, it is essential that the yardsticks employed be precise.

It is my hope that the authors may find the time and/or the funds to proceed with a program such as they have outlined. With proper precautions, data of this type should prove valuable.

EDITOR'S NOTE: The effects of isotopic substitutions mentioned by Dr. Gluckstein is the subject of a paper by Friedman, R., and Burke, E., "Burning Velocities," *Industrial and Engineering Chemistry*, vol. 43, 1951, p. 2772.

### References


1 Rossini, F. D., et al., "Selected Values of Thermodynamic Properties," Bureau of Standards Circular 500, U. S. Government Printing Office, Washington, D. C., 1952.

2 Glasstone, S., "Textbook of Physical Chemistry," 2nd edit., D. Van Nostrand, New York, 1946.

3 Hirschfelder, J. O., Curtiss, C. F., and Bird, R. B., "Molecular Theory of Gases and Liquids," Wiley, New York, 1954.


## The Free Vibration of a Variable Mass[1]


**C. C. MIESSE**[2]

**Armour Research Foundation, Chicago, Ill.**


THE free vibration of a tank in which the weight of liquid decreases linearly with time can be determined by considering the basic differential equation, as obtained from Newton's Second Law

$$\text{force} = \frac{d}{dt}(\text{momentum})$$

$$Kx + c\frac{dx}{dt} = -\frac{d}{dt}\,M_0(1 - t/G)\frac{dx}{dt} \quad \ldots\ldots [1]$$

where

$G$ = $M_0T/M_L$
$K$ = spring constant, lb/in.
$x$ = displacement, in.
$c$ = damping coefficient, lb-sec/in.
$t$ = time, sec
$M_0$ = mass of full tank, slugs
$M_L$ = mass of liquid in full tank, slugs
$T$ = time required for emptying tank

By defining the dimensionless variable

$$u = 1 - t/G = \frac{M}{M_0} \quad \ldots\ldots [2]$$

Equation [1] can be written

$$u\ddot{x} + (1 - Gc/M_0)\dot{x} + KG^2x/M_0 = 0 \quad \ldots\ldots [3]$$

where the dots represent differentiation with respect to $u$.

Substitution of the dimensionless variables

$$v = 2G\sqrt{K_u/M_0} = 2w_nG\sqrt{u} \quad \ldots\ldots [4]$$

and

$$x = v^pf(v) \quad \ldots\ldots [5]$$

where $w_n$ is the natural frequency of the system (in rad/sec) at time $t = 0$, and $p = cG/M_0$, into Equation [3] yields for $f(v)$

$$v^2f'' + vf' + (v^2 - p^2)f = 0 \quad \ldots\ldots [6]$$

where the primes represent differentiation with respect to $v$. Since Equation [6] is readily recognized as Bessel's equation, the solution can be expressed as

$$f = AJ_p(v) + BY_p(v) \quad \ldots\ldots [7]$$

where $J_p(v)$ and $Y_p(v)$ are the Bessel functions of the first and second kind, respectively, and of the $p$th order. The complete solution of Equation [3] thus is

$$x = Av^p[J_p(v) + B'Y_p(v)] \quad \ldots\ldots [8]$$

where the arbitrary constants $A$ and $B'$ are determined by the boundary conditions. Since the initial conditions are unessential for the determination of the "frequency," $B'$ can be set equal to zero and $A = 1$, and the problem becomes one of determining the zeros of the Bessel function $J_p(v)$ for

$$2w_nG\sqrt{1 - M_L/M_0} \leq v \leq 2w_nG \quad \ldots\ldots [9]$$

For $w_n = 300$ rad/sec, $G = 200$ sec, and $M_L/M_0 = 0.84$, inequality [9] becomes

$$4.8 \times 10^4 \leq v \leq 12 \times 10^4$$

which indicates immediately that very high values of the argument are involved. One method for evaluating the large zeros of $J_0(x)$—this would be the case for $p = 0$, i.e., no damping—has been presented by Stokes (1).[3] The zeros of $J_0(x)$ are the roots of the equation

$$\cot(x - \pi/4) = Q(x, 0)/P(x, 0) \quad \ldots\ldots [10]$$

where

$$P(x, 0) = 1 - \frac{1\cdot9}{2!(8x)^2} + \frac{1\cdot9\cdot25\cdot49}{4!(8x)^4} - \ldots\ldots [11]$$

and

$$Q(x, 0) = -\frac{1}{1!8x} + \frac{1\cdot9\cdot25}{3!(8x)^3} - \ldots\ldots [12]$$

A single series solution for the zeros of $J_0(x)$ was subsequently derived by Watson (2)

$$x = h + \frac{1}{8h} - \frac{31}{384h^3} + \frac{3779}{15360h^5} \quad \ldots\ldots [13]$$

where

$$h = \pi(n - \tfrac{1}{4}) \quad \ldots\ldots [14]$$

and $n$ is the number of the zero.

The extension of Watson's analysis to Bessel functions of higher order ($r$) led to the general equation

$$x = H - \frac{4r^2 - 1}{8H} - \frac{(4r^2 - 1)(26r^2 - 31)}{384H^3} - \ldots\ldots [15]$$

where

$$H = \pi(n + \tfrac{1}{2}r - \tfrac{1}{4}) \quad \ldots\ldots [16]$$


[1] The work reported in this paper was performed at Aerojet-General Corp., under the sponsorship of the U. S. Air Force.


[2] Supervisor, Combustion Research Section. Mem. ARS.

[3] Numbers in parentheses indicate References at end of paper.

From Equations [15, 16], it is apparent that the zeros of $J_p(v)$ can be represented by the equation

$$v = \pi(n + \tfrac{1}{2}p - \tfrac{1}{4}) - \frac{4p^2 - 1}{8\pi(n + \tfrac{1}{2}p - \tfrac{1}{4})} + \dots \quad [17]$$

The "period" of oscillation ($\Delta v$) can then be represented by twice the interval between two successive zeros

$$\Delta v = 2dv = 2\left(\pi + \frac{4p^2 - 1}{8\pi(n + \tfrac{1}{2}p - \tfrac{1}{4})^2} - \dots\right)$$

$$\approx 2\pi\left(1 + \frac{4p^2 - 1}{8v^2}\right) \quad [18]$$

and the period of oscillation, in terms of time, is obtained from Equations [2, 4, 17, 18] as

$$|\Delta t| = G\Delta u = \frac{2Gv\Delta v}{(2w_nG)^2} \approx \frac{2\pi}{w_n}\left(1 + \frac{4p^2 - 1}{8v^2}\right)\sqrt{u} =$$

$$2\pi\left(1 + \frac{4p^2 - 1}{8v^2}\right)\sqrt{\frac{M}{K}} \quad [19]$$

Since the frequency is the reciprocal of the period

$$f \approx \frac{1}{2\pi}\sqrt{\frac{K}{M}}\left(1 - \frac{4p^2 - 1}{8v^2}\right) \quad [20]$$

It is thus seen that the instantaneous values of the resonant frequency of a system with variable mass can be obtained by determining the steady-state frequency corresponding to the instantaneous mass ($M$), and multiplying by the correction factor represented by the quantity in parentheses in Equation [20]. For large values of $v$, as indicated in the foregoing example, and relatively small values of $p$ (corresponding to small damping), it is apparent that the correction will be negligible.

The variation in amplitude can be determined from an equation given by Copson (3): For large values of $v$

$$J_p(v) \leq \frac{1}{\sqrt{\tfrac{1}{2}\pi v}} \quad [21]$$

and

$$v^p J_p(v) \leq \sqrt{\frac{2}{\pi}}\, v^{p - 1/2} \quad [22]$$

Equation [22] thus indicates that the amplitude of oscillation will increase with time for $p < \frac{1}{2}$, and will decrease with time for larger values of $p$, which represents the degree of damping in the oscillatory system.

### References


1 Stokes, G. G., "On the Effect of the Internal Friction of Fluids on Motion of Pendulum," *Cambridge Philosophical Transactions*, vol. 9, 1856, p. 63.

2 Watson, G. N., "A Treatise on the Theory of Bessel Functions," Cambridge University Press, Cambridge, 1952, p. 503.

3 Copson, E. T., "Theory of Functions of a Complex Variable," Oxford University Press, 1946, Chapter XII; See also Jahnke, E., and Emde, F., "Tables of Functions," Dover, New York, 1945, p. 138.


# Test of a Heat Transfer Correlation for Boiling Liquid Metals[1]


**W. G. CAMACK[2] and H. K. FORSTER[3]**
**Lockheed Aircraft Corp., Palo Alto, Calif.**


### Nomenclature

$Nu, Re, Pr$ = Nusselt, Reynolds and Prandtl number, respectively
$q/A$ = heat flux, Btu/hr-sq ft
$\sigma$ = surface tension
$\rho$ = density
$k$ = heat conductivity
$\mu$ = viscosity
$c_L$ = specific heat
$B$ = coefficient for bubble growth, given in Equation [4]
$a$ = thermal diffusivity
$K_1, K_2$ = coefficients given in terms of properties of liquid and vapor
$\Delta p$ = vapor pressure difference corresponding to superheat $\Delta T$

***Subscripts***

$L, v, w$ = liquid, vapor and heating surface, respectively

THE process of heat transfer to a boiling liquid is quite complex and the formulas which have been presented in the literature are mainly in the nature of empirical correlations. A compilation of many of these correlations may be found in J. W. Westwater's review article in (1).[4] There seem to be two types:

(a) Purely empirical correlations like that of Cryder and Finalborgo (2)

$$h = C(\Delta T)^n.b^T \quad [1]$$

in which $C$ and $b$ and $n$, changing from liquid to liquid, have to be determined from experiment.

(b) Relations like those of Jakob and Linke (3), and of Insinger and Bliss (4), or of Rohsenow(5), in which dimensionless groups are derived from theoretical considerations and the exponents of these groups are then empirically determined. The value of any of these correlations depends entirely on how widely the experimental conditions may be varied without necessitating changes in the constants and exponents.

A year ago another such correlation of the form

$$(Nu) = \alpha\,(Re)^m \cdot (Pr) \quad [2]$$

was proposed by Forster and Zuber(6) for maximum (burnout) heat flux in a boiling liquid at rest

$$\frac{q/A}{(T_W - T_L)k_L}\, B\sqrt[4]{\frac{4\sigma^2\rho_L}{\Delta p^3}} = 0.0015\left(\frac{\rho_L B^2}{\mu_L}\right)^{0.62}\left(\frac{\mu_L c_L}{k_L}\right)^{\frac{1}{3}} \quad [3]$$

The Prandtl number is the same as usually employed and the Nusselt group was obtained from dimensional analysis; following some ideas of Ellion(7), the Reynolds group was "derived" from previous calculations of the growth of vapor bubbles close to the heating surface, which showed that the bubble radius is closely approximated by

$$R(t) = B\sqrt{t} \text{ with } B = \frac{c_L\rho_L}{L\rho_v}\sqrt{\pi\alpha}\,\Delta T \quad [4]$$

Thereby the product $R\dot{R}$ becomes independent of both time and radius. Consequently, this product which equals $B^2/2$ was used as the characteristic product of linear dimension times velocity in a Reynolds number.

Equation [3], which was originally tested for correlating *burnout* heat flux with burnout superheat of four liquids, was later tested by Perkins and Westwater(8) for correlating heat flux and superheat for one liquid (methanol) over a *range* of superheats. The results were encouraging in the sense that all these data were well correlated by Equation [3] for different


Received May 6, 1957.

[1] This study was performed in part under AEC Contract No. AT(04-3)-98 and Air Force Contract No. AF 33(616)-3441.


[2] Research Engineer.

[3] Consultant. Professsor of Engineering, University of California, Los Angeles, Calif.

[4] Numbers in parentheses indicate References at end of paper.

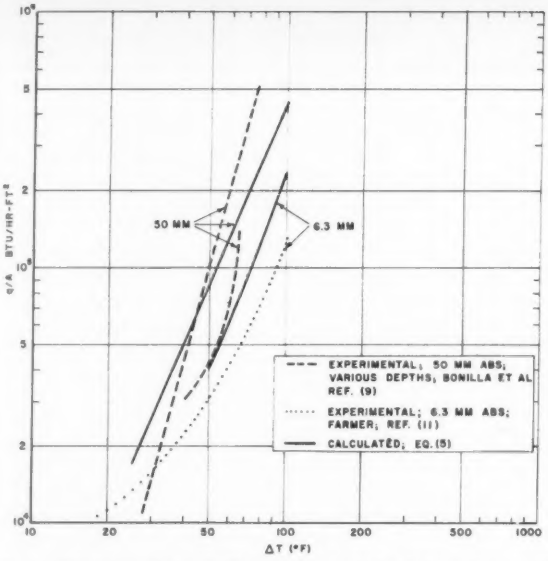


Fig. 1 **Heat transfer to boiling mercury at absolute pressure of vapor 6.3 mm and 50 mm (nucleate boiling)**

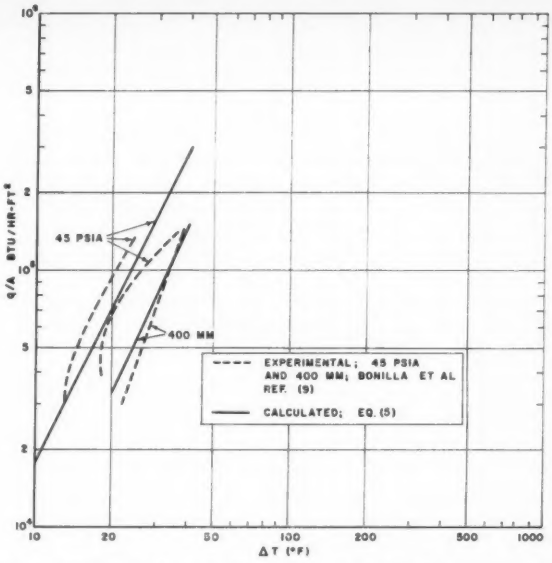


Fig. 2 **Heat transfer to boiling mercury at absolute pressure of vapor 400 mm and 45 psia (nucleate boiling)**

liquids without necessitating any change in the constant or the exponent.

A crucial test of a correlation like Equation [3] would be afforded by comparing it with heat flux data in a liquid of thermal properties as different as possible from those of water, methanol, etc. Fortunately, C. F. Bonilla and co-workers(9) have recently published excellent data on the variation with pressure and superheat of heat flux in boiling mercury; also, a few data on boiling heat transfer of liquid sodium and of sodium potassium were reported by Lyon, Foust, and Katz (10). We have therefore set out to compare these data with Equation [3]; the results were good and we believe them to be of more general interest.

For purposes of computation it is advantageous to write Equation [3] in expanded form for thermal flux $q/A$ in Btu/hr-sq ft. Grouping together the liquid properties which are to be taken at saturation plus superheat temperature and $\rho_v$ which is evaluated at saturation temperature, yields a coefficient $K_1$

$$k_1 = 0.172 \frac{k_L^{0.8}\, \rho_L^{0.5}\, c_L^{0.45}}{L^{0.25}\, \sigma^{0.5}\, \mu_L^{0.3}\, \rho_v^{0.25}}$$

which may be computed just once for each run since the values of the properties of the liquid phase change but little with variation in superheat. The thermal flux as a function of superheat can then be readily computed on the slide rule by expressing Equation [3] in the form

$$\frac{q}{A} = K_1\, \Delta T^{1.25}\, \Delta p^{0.75} \qquad [5]$$

where the exponent of $\Delta T$ was increased by 0.01 for convenience in computation; $\Delta p$, the pressure above saturation corresponding to superheat $\Delta T$, is to be obtained from the vapor pressure relation of the liquid metal.

In Figs. 1, 2, and 3 some experimental data reported by Professor Bonilla for mercury are compared with values calculated from Equation [5]; a few data for boiling sodium,

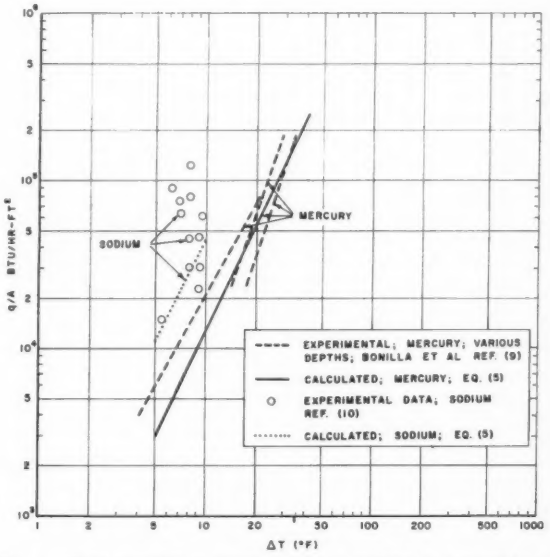


Fig. 3 **Heat transfer to mercury and to sodium at atmospheric pressure (nucleate boiling)**

reported by Lyon, Foust and Katz (10) and data by Farmer (11) are also included in Fig. 3.

In our opinion it is encouraging that Equation [5] holds as well as it does for liquids as *different* physically as methanol and the liquid metals. When comparing these data with the various curves presented in (9) due attention must be given to the fact that the problem of "wetting" is quite critical for liquid metals and that a low slope of heat flux $q/A$ vs. superheat indicates the presence of film boiling for which Equation [5] is inapplicable. For instance, Farmer's data in Fig. 3 represent film boiling for low superheat, developing more into nucleate boiling for larger superheat.

*Dependence on Superheat:* The slope of heat flux vs. superheat can be computed from Equation [5] by inserting the appropriate relationship for the vapor pressure in terms of

the superheat. Since the (absolute) temperature $T$ is large compared to the superheat $\Delta T$, Clapeyron's equation gives a first approximation

$$\Delta p = \frac{pL}{RT^2}\,\Delta T$$

which, inserted in Equation [5], shows that $q/A$ increases as $\Delta T^2$ for small superheat and increases exponentially as $\Delta T$ increases. This agrees well with the statement by Professor Bonilla (9, p. 7) that the slope of (log $q/A$) vs. (log $\Delta T$) ranges between 2 and 3 in the nucleate boiling region.

*Dependence on Pressure:* Cryder and Finalborgo (2) presented an empirical relation for the dependence of heat flux on pressure *at constant superheat* which is, from Equation [1]

$$\log \frac{q}{q_0} = b(T - T_0) \qquad [6]$$

In words: if a liquid boils either at pressure $p$ and temperature $T$ or at pressure $p_0$ and temperature $T_0$, then, if the superheat $\Delta T$ is the same in both cases, the heat fluxes are in the relation given by Equation [6]. We shall show that Equation [6] is a special case of Equation [5], namely, for small variations in boiling temperature.

Let us write $K_1\rho_v^{0.25} = K_2$ ($K_2$ then depends on the properties of the liquid only and varies little with pressure), and use Clapeyron's equation for $\Delta p$

$$\frac{q}{A} = K_2\,\Delta T^2 \left(\frac{pL}{RT^2}\right)^{0.75} \Big/ \left(\frac{p}{RT}\right)^{0.25} \qquad [7]$$

and the ratio of heat flux $q/A$ at $(T;p)$ and at $(T_0;p_0)$ becomes

$$\frac{q}{q_0} = \left(\frac{p}{p_0}\right)^{0.5} \Big/ \left(\frac{T}{T_0}\right)^{1.25} \qquad [8]$$

To the extent to which $L$ may be considered constant

$$p = p_0 \exp\left\{\frac{L}{R}\,\frac{T - T_0}{TT_0}\right\} \qquad [9]$$

and the logarithm of Equation [8] becomes

$$\log \frac{q}{q_0} = \frac{L}{2RT}\,\frac{T - T_0}{T_0} - \frac{5}{4}\log\frac{T}{T_0} \qquad [10]$$

To the extent to which the range of boiling temperatures $(T - T_0)$ may be considered small compared to the absolute boiling temperature, $(T - T_0)/T_0$ is small and $\log(1 + x) = x$ for small $x$; thereby Equation [10] attains the *form* of Equation [6] of Cryder and Finalborgo

$$\log \frac{q}{q_0} \approx \left[\frac{L}{2RTT_0} - \frac{5}{4T_0}\right](T - T_0) \qquad [11]$$

While the numerical data in (2) have since been recognized to be too high, we may comment on the fact that the coefficient $b$ in Equation [6] had been found not to vary too much for some liquids. One may see from Equation [11] that such is a consequence of Trouton's rule (12), which states that $L/T$ has a fairly constant value for many liquids.

Another relation between superheat, pressure and heat flux which is of interest to the designer is the following: How does the superheat $\Delta T$ vary with pressure $p$ while keeping the heat flux *constant?* The relation is, directly from Equation [7]

$$\frac{\Delta T^2\, p^{\frac{1}{2}}}{T^{\frac{5}{4}}} = K_3 \text{ with } K_3 = \frac{q}{AK_2}\left(\frac{R}{L}\right)^{\frac{1}{2}} \qquad [12]$$

Experimental values for $\Delta T$ vs. $p$, when plotted on a log-log scale, gave nearly straight lines for low pressure; it is interesting that Equation [12] reproduces correctly the slope of these lines for mercury (9, Fig. 10) as well as for other liquids (13). By taking the logarithm of Equation [12] and differentiating with respect to log $p$ we obtain

$$\frac{d(\log \Delta T)}{d(\log p)} = -\frac{1}{4} + \frac{5}{8}\,\frac{RT}{L} \qquad [13]$$

where use was made of Equation [9] in differentiation of

$$\frac{d(\log T)}{d(\log p)} = \frac{1}{T}\,\frac{dT}{d(\log p)} = \frac{1}{T}\,\frac{RT^2}{L}$$

According to Equation [13], for boiling at low pressure where $RT/L$ is small, the slope of (log $\Delta T$) vs. (log $p$) should be $-0.25$ and independent of the liquid. This is borne out by experiment: The slope of the curve for mercury (9, Fig. 10) is found to be $-0.28$, while for several other liquids a slope of $-0.25$ is reported in (13). It is interesting to note that the experimental data in (9) do show a slight positive curvature in agreement with the second term of Equation [13].

In conclusion we may say that the heat transfer correlation, Equation [3], has now been tested for methanol and for some liquid metals, and that fair agreement was obtained for dependence on both pressure and superheat without any change in exponent or constant. Tests for other liquids will show that changes have to be affixed but it may now be assumed that such changes will be minor. The geometric arrangement for which Equation [3] was derived is that of pool boiling from the horizontal (not vertical) heating surface, and the surface conditions are to be such that good wetting of the surface prevails.

We wish to express our sincere gratitude to Professor Bonilla who gave us his kind permission to reproduce his experimental data in this paper.

### References

1 "Advances in Chemical Engineering," edited by T. B. Drew and J. W. Hoopes, vol. 1, Academic Press, 1956.

2 Cryder, D. S., and Finalborgo, A. C., *Transactions of the American Institute of Chemical Engineers*, vol. 33, 1937, p. 346.

3 Jakob, M., and Linke, W., *Physik Zeitschrift*, vol. 36, 1935, p. 267.

4 Insinger, T. H., and Bliss, H., *Transactions of the American Institute of Chemical Engineers*, vol. 36, 1940.

5 Rohsenow, W. M., *Trans. ASME*, vol. 74, 1952, p. 969.

6 Forster, H. K. and Zuber, N., *American Institute of Chemical Engineers Journal*, 1, 1955, p. 531.

7 Ellion, M. E., Memo. 20–88, California Institute of Technology, Jet Propulsion Laboratory, March 1954.

8 Perkins, A. S. and Westwater, J. W., *American Institute of Chemical Engineers Journal*, vol. 2, 1956, p. 471.

9 Bonilla, C. F., Bush, Y. S., Stalder, A., Shaikhmahmud, N. S., and Ramachandran, A., "Pool Boiling Heat Transfer with Mercury," Reactor Heat Transfer Conference, New York, Nov. 1956; also Report NYO-7638.

10 Lyon, R. E., Foust, A. S., and Katz, D. L. Ann. Mtg *American Institute of Chemical Engineers*, St. Louis, Prepr. 6, 1953.

11 Poppendick, H. F., "Heat Transfer Symposium," University of Michigan Press, 1952, p. 90.

12 See, for instance, Epstein, P. S., "Thermodynamics," 5th edit., Wiley, 1949, p. 125.

13 Bonilla, C. F., and Perry, C. W., *Transactions of the American Institute of Chemical Engineers*, vol. 37, 1941, p. 685.

# Ultimate Design of High Altitude Sounding Rockets

IRVING MICHELSON[1]

Odin Associates, Pasadena, Calif.

## Introduction

THE principal design features and performance capabilities of a number of current American and foreign high altitude sounding rockets have been reported in the March 1957 issue of JET PROPULSION, in what may reasonably be taken as an index of the present state of the art. We note that none of these rockets will attain altitudes as great even as a small fraction of one per cent of the distance to the moon, notwithstanding statements published almost daily which assert that flight to the moon is possible now; that we are "committed" to space flight; etc. Engineering-type calculations to support these claims are usually omitted, however, so that some doubts must linger in the minds of many.

It is the purpose of this note to point out that techniques are available which determine optimum sounding rocket capability as a function of fuels and materials limitations, for the types of multistaged rockets which are of greatest importance with respect to space flight. Calculation results are presented, moreover, for two examples representing extreme altitude sounding to a summit height of one earth diameter, and minimal lunar flight. These are interpreted as confirming, on the whole, the immediate feasibility, using presently available fuels and structural materials, of sounding rockets which surpass by an entire magnitude, the performance of the announced rockets.

## Discussion

The crucial importance of multiple staging for escape vehicles which depend on chemical fuels for propulsion has long been known in rocketry, and is hardly less essential for extreme altitude rockets which do not escape, but return to earth. The fact that current sounding rocket designs usually involve not more than two stages, however, can be ascribed to greater developmental interest in liquid rockets and the severe weight and reliability penalties associated with such systems. The numerous advantages of modern solid fuels, including suitability for multiple staging, requires their consideration from the standpoint of space flight. The thrust optimization problem for multistage, solid propellant rockets is essentially different from the classical treatments, all of which are oriented toward liquid rockets and therefore do not serve as useful guides for optimization of the currently most interesting configurations. The analysis of optimum staging is much simplified when air drag is neglected and thrust is considered piecewise-constant, and permits the inclusion of structural design efficiency parameters for the several stages. The theory has been presented by M. Vertregt,[2] and the results are immediately applicable to the direct problem of computing the minimum value of over-all payload ratio for a rocket of prescribed fuel and structural properties which can attain prescribed altitude.

For a sounding rocket arbitrarily assumed to consist of four stages, the explicit determination of optimized over-all payload ratio becomes most simple when both the structure ratio

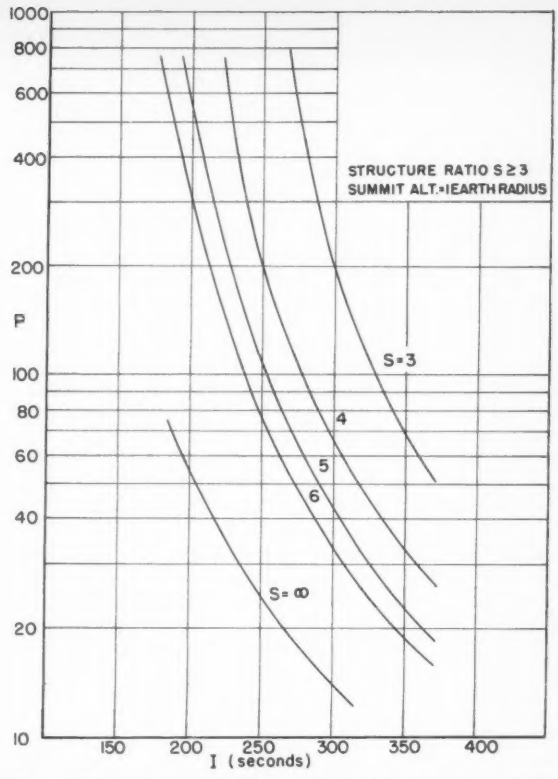


**Fig. 1 Optimized over-all payload ratio $P$ of four-stage sounding rocket vs. specific impulse I**

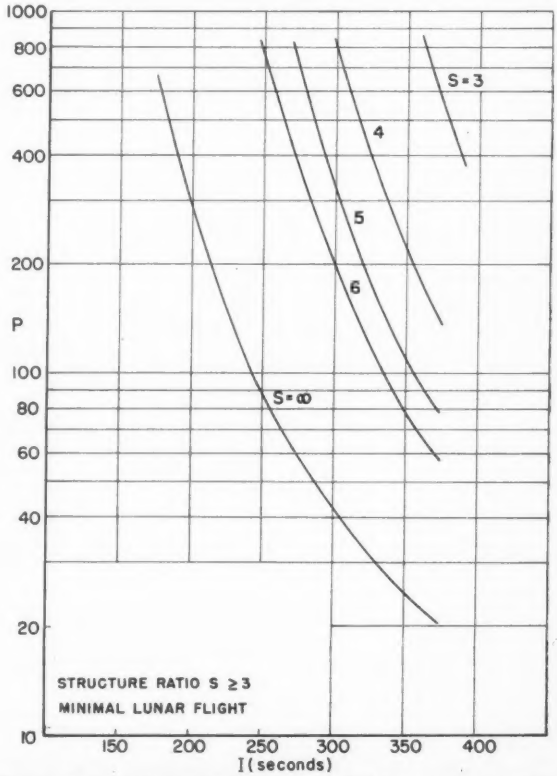


**Fig. 2 Optimized over-all payload ratio $P$ of four-stage sounding rocket vs. specific impulse $I$**

Received April 29, 1957.

[1] Research Engineer. Now Professor of Aeronautical Engineering, Pennsylvania State University. Mem. ARS.

[2] Vertregt, M., "A Method for Calculating the Mass Ratios of Step-Rockets," *Journal of the British Interplanetary Society*, vol. 15, 1956, p. 95.

$s$ and the fuel specific impulse $I$ have the same values for each step; then

$$P = e^{V/gI}\left(\frac{s-1}{s-e^{V/4gI}}\right)^4 \quad \ldots\ldots\ldots\ldots [1]$$

The ideal velocity $V$ is determined by the summit altitude $h$, measured in units of one earth radius, by the equation

$$V = V_e\sqrt{\frac{h}{h+1}} \quad \ldots\ldots\ldots\ldots [2]$$

$V_e$ denotes escape velocity from earth, 36,693 fps, and the mean effective jet exhaust velocity $gI$ is related to specific impulse through the sea-level gravity constant $g$. The more general equations, for an arbitrary number of stages and unrestricted values of $s$ and $I$ for each step, are briefly indicated in Appendix A. The notation system of weights and ratios is shown in Appendix B. It will be seen that aside from its compactness, this system affords such conveniences as values for the ratios all greater than one, and equations of symmetrical structure, avoiding the use of negative powers.

The values of over-all payload ratio $P$ are plotted against specific impulse in Fig. 1 for a summit altitude of one earth radius (equal to $20.926 \times 10^6$ ft), for which $V$ equals the maximum earth satellite speed 25,946 fps. Values of structure ratio from 3 upward appear parametrically, the larger values representing more efficient utilization of structural weight. As an absolute upper limit of structural efficiency, the curve (marked $s = \infty$) is shown which corresponds to a design composed of fuel and payload alone, no weight at all being assigned to structure. In Fig. 2 analagous curves are shown for a minimal lunar flight requiring an ideal velocity of 36,400 fps.

If, following Krause[3], we accept as a reasonable upper limit for over-all payload ratio the value $P = 500$, Fig. 1 then shows, for example, that a sounding rocket may be expected to reach one earth radius when specific impulse and structure ratio values of 230 and 4, respectively, can be attained; alternatively, the pair of values $I = 276$, $s = 3$ are equally good. From Fig. 2 it appears that a minimal lunar flight requires $I = 316$ and $s = 4$, or the equivalent. As an aid in assessing the significance of the values quoted for structure ratio, it may be noted that published data indicate that for the ASP rocket, $s = 3.14$, while for the (admittedly less comparable) Aerobee-Hi, a value of $s = 4.82$ represents current design. Structure ratio values of 4 or greater appear highly desirable and may be expected with current materials, for well-designed solid rocket casings.

[3] Krause, H. G. L., "Allgemeine Theore der Stufenrakete," *Weltraumfahrt*, x:52, 1953.



## Conclusions

Comparing fuel and structural design requirements with realistic current values in this manner therefore confirms that at least we may regard present technological capability as being quite far ahead of announced sounding rocket developments, and perhaps even ready for lunar flight or escape from earth. More accurate calculations are certainly indicated which would make allowance, for example, for depressed values of structure ratio for first and last steps (reflecting payload housing weight and fin weights), and which would consider problems associated with launching; but these calculations should be based on actual designs and can hardly be carried through in completely general form.

## APPENDIX A

### General Equations of Multiple Staging Optimization

The over-all payload ratio $P$ is related to mass ratio $r_i$ and structure ratio $s_i$ ($i = 1, 2, \ldots, n$), of the individual steps of a sounding rocket containing $n$ steps, by definition, according to the equation

$$P = r_1 r_2 \ldots\ldots r_n \cdot \frac{s_1 - 1}{s_1 - r_1} \cdot \frac{s_2 - 1}{s_2 - r_2} \ldots\ldots \frac{s_n - 1}{s_n - r_n} \quad \ldots [A1]$$

M. Vertregt[2] has shown that the optimum staging (viz., minimized value of $P$) is obtained when the step mass ratios are determined by the structure ratios and specific impulse, according to the equations

$$\left.\begin{aligned} r_i &= s_i - \frac{s_i}{s_1}\frac{I_1}{I_i}(s_1 - r_1);\ i = 2, 3, \ldots, n \\ V &= \sum_{i=1}^{n} gI_i \ln r_i \end{aligned}\right\} \quad \ldots\ldots [A2]$$

## APPENDIX B

### Vertregt's Nomenclature System for Step Rockets

$M_p$ = weight of payload
$M_{ci}$ = dry weight of step $i$ of complete rocket
$M_{bi}$ = weight of propellants of step $i$
$M_i$ = total weight of subrocket $i$, consisting of payload and steps $1, 2, \ldots, i$.

$$M_i = \begin{cases} M_{i-1} + M_{ci} + M_{bi} & (i > 1) \\ M_p + M_{ci} + M_{bi} & (i = 1) \end{cases}$$

$p_i$ = payload ratio of subrocket $i$

$$p_i = \begin{cases} \dfrac{M_i}{M_{i-1}} & (i > 1) \\ M_1 \div M_p & (i = 1) \end{cases}$$

$P$ = over-all payload ratio of complete n-stage rocket = $M_n/M_p = p_1 \cdot p_2 \cdot \ldots\ldots p_n$
$s_i$ = structure ratio of step $i = (M_{ci} + M_{bi})/M_{ci}$
$r_i$ = mass ratio of step $i = M_i/(M_i - M_{bi})$
= over-all mass ratio $= r_1 \cdot r_2 \cdot \ldots\ldots r_n$

*New positions in*

## MISSILE SYSTEMS PROPULSION

Weapon systems management activities at Lockheed's Palo Alto and Sunnyvale organizations call for significant achievement in propulsion. Areas include design analysis, evaluation of test information and technical management of propulsion subcontractors. Inquiries are invited from those possessing a high order of systems ability and strong familiarity with solid and liquid propellant rockets and ramjets. Please address the Research and Development Staff, Sunnyvale 20, California.

*Here Propulsion Staff members discuss problems relating to accurate positioning of a vehicle in the upper atmosphere. Left to right: J. F. Houle, propellant feed systems analysis; B. Ellis, Propulsion Department manager; J. J. Donhan, control force generators.*


*Lockheed*

**MISSILE SYSTEMS**

A DIVISION OF LOCKHEED AIRCRAFT CORPORATION

PALO ALTO • SUNNYVALE • VAN NUYS

CALIFORNIA

# Book Reviews

**Ali Bulent Cambel, Northwestern University, *Associate Editor***

**Viscous Flow Theory,** by Shih-I Pai, D. Van Nostrand Co., Inc., Princeton, N. J. Vol. I, Laminar Flow, 1956, 384 +xvi pp. $7.75. Vol. II, Turbulent Flow, 1957, 277 + xi pp. $7.75.

Reviewed by W. H. Reid
Yerkes Observatory

The motion of a viscous fluid may be laminar or turbulent depending, roughly speaking, on whether or not the Reynolds number exceeds some critical value. This motion, whether laminar or turbulent, is governed by a well-established set of dynamical equations which hold under all but the most extreme conditions, and these equations, together with appropriate boundary or initial conditions suffice to determine a well-defined mathematical problem. Unfortunately, we are not yet able to solve these equations in any general way, even in the laminar case, and the theory of viscous flows is largely concerned therefore with various methods of approximation which hold in certain limiting cases.

In the first of these volumes dealing with laminar flow, the author begins with a discussion of the equations which govern the motion of a viscous compressible fluid. Some exact solutions of the Navier-Stokes equations are then given, followed by a discussion of dimensional methods. The remainder of the volume is then devoted to approximate methods of solution, and includes the methods of Stokes and Oseen for slow motion in which one can linearize the convective term, and to the methods of boundary layer theory for flows near solid bodies at high Reynolds numbers.

As an introduction to the subject, this book does not provide so deep a physical insight into the mechanics of a viscous fluid as can be found, for example, in Volume I of Goldstein's "Modern Developments," nor so detailed a discussion of boundary layer theory as can be found in Schlichting's treatise.

The turbulent motion of a viscous fluid presents an even more formidable problem. Not only are those difficulties which were present in the laminar case—nonlinearity, energy dissipation, and unsteadiness—still present, but also there arises a further difficulty, incompleteness. We are of course not interested in the detailed velocity fluctuations themselves but only in some mean values—to this extent all theories of turbulence are statistical—and the effect of taking mean values of the Navier-Stokes equations is to introduce further unknowns such as the Reynolds stresses or the triple velocity correlations.

To overcome this incompleteness, various assumptions have been made which lead on the one hand to the mixing-length theories and on the other to the so-called statistical theories. While it is true that the statistical theories are not yet able to provide solutions to many practical problems, they do provide an insight into the mechanism of turbulence and a descriptive framework not possessed by the mixing length theories. These two approaches to the problem are here dealt with as if they had little in common. The limitations of the mixing length theories are briefly noted but no attempt is made to incorporate any of the more general statistical concepts into this part of the subject. At one point the situation is just the reverse. Thus, in discussing the turbulent flow in a circular pipe and between parallel walls, the author presents an ad hoc polynomial expression for the mean velocity and Reynolds stress distribution. As a convenient analytical representation of the experimental data this may have some use, but it can hardly be regarded as a theoretical deduction.

The second half of Volume II, which is devoted to the statistical theory, begins with a general discussion of stationary random functions, probability distributions, correlation functions and spectra, and then goes on to discuss turbulent diffusion, decaying homogeneous turbulence and the separate effects of compressibility and of a magnetic field. Throughout this part of the book, the author has drawn rather freely from the lecture notes which he prepared in 1950–1951 based on lectures given at the University of Maryland by Goldstein, Kampé de Fériet, and others. As a result, his treatment of the subject reflects the situation as it existed at that time, little cognizance having been taken of more recent developments in the subject. A single example must suffice. Under suitable assumptions, the Kármán-Howarth equation which governs the behavior of the double correlation function can be integrated to obtain the so-called Loitsiansky "invariant." It is now known, however, that the assumptions under which this result is usually obtained are not satisfied; no mention is made of this fact although, curiously enough, a reference is given to the most recent work on this problem in which the lack of invariance is clearly established.

The problem of turbulence has remained unsolved for many years and its full solution may yet be many years off. But the stage has at least been reached when, having recognized the inadequacy of the mixing length theories, an attempt must be made to apply the statistical methods to the more practical and much more difficult problems of shear flow—if not in detail, at least in spirit. On such a task the present volume will provide little help.

In both volumes the style is very uneven and is marred by grammatical errors throughout, as if a series of lecture notes had simply been put directly into print without any detailed revision. There is very little originality in the treatment of the subject matter so that those who are familiar with the subject will find little to interest them here, while those seeking an introduction to the subject can find more instructive accounts elsewhere.

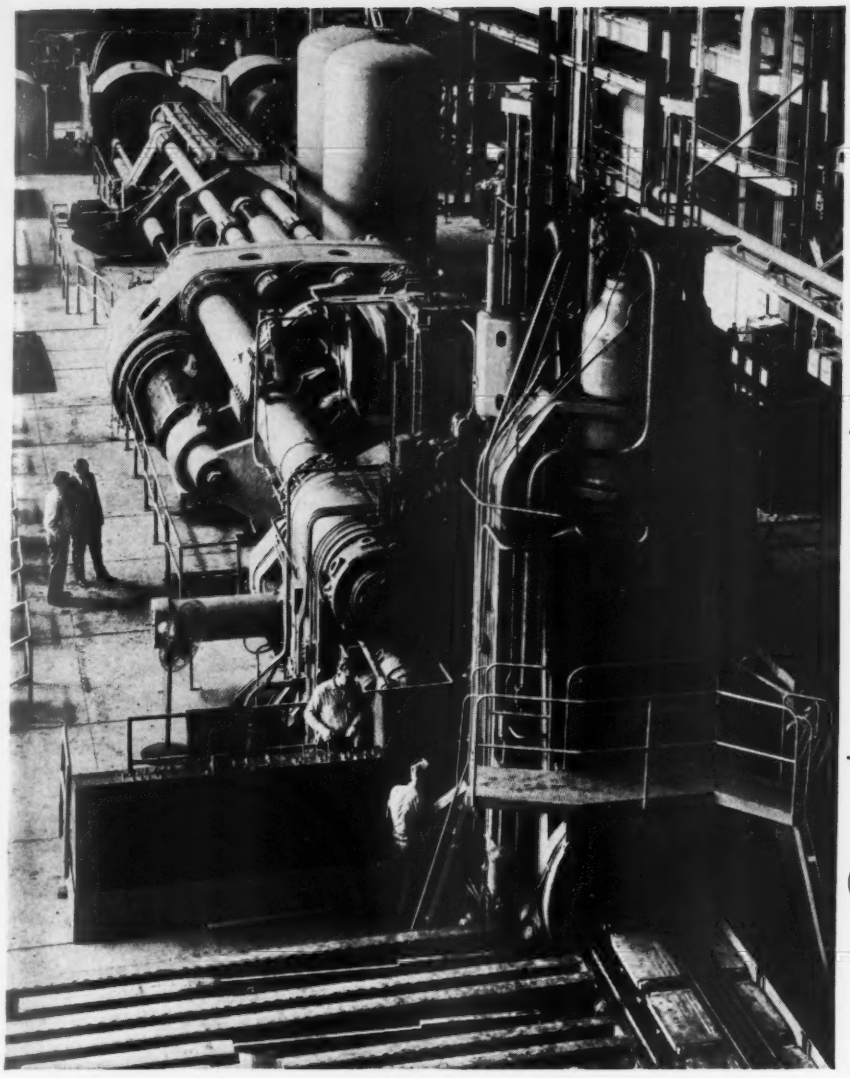

**HOW THE 13,200-TON PRESS BOOSTS EXTRUSION CAPACITY**

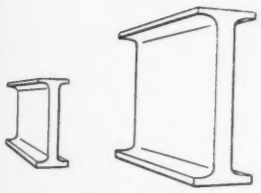

FROM 11″ TO 28″

**STRUCTURAL SHAPES**

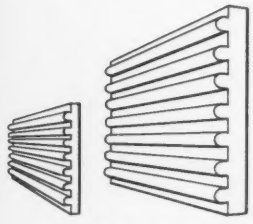

FROM 9″ TO 20″

**STIFFENED SECTIONS**

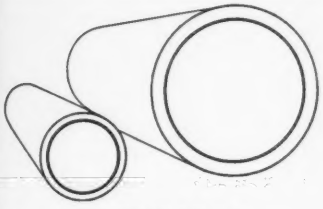

FROM 10″ TO 24″ O. D.

**TUBING**

# DOW'S NEW EXTRUSION PRESS PACKS 13,200-TON PUNCH

**Here's a whole new range of large magnesium extrusions:**
**24-inch O. D. Tubing  28-inch I-Beams  80-foot-long sections**

This mammoth press, newest addition to The Dow Chemical Company's rolling and extrusion mill at Madison, Illinois, is the world's largest magnesium extrusion facility. Its vastly increased capacities afford new opportunities for designers working with light metals. A wide variety of new magnesium applications for aircraft, missile, military and general industrial use are now possible and practical. In addition to extruding magnesium, the press is also available for large aluminum extrusions.

Here's how the big press will increase maximum dimensions of representative magnesium extrusions: Integrally stiffened sections, from 9 to 20 inches wide; I-Beams from 11 to 28 inches high; round tubing from 10 to 24 inches outside diameter; and maximum lengths of 80 feet. A large number of shapes and forms can be produced, limited only by the design of the die through which the metal is extruded. Many complex shapes that formerly required separate operations can now be formed in one operation.

If your design calls for large magnesium or aluminum extrusions, contact the nearest Dow Sales Office or write to THE DOW CHEMICAL COMPANY, Midland, Michigan, Department MA 1406F.

*YOU CAN DEPEND ON* DOW

# Technical Literature Digest

**M. H. Smith,** *Associate Editor,* **and M. H. Fisher,** *Contributor*
The James Forrestal Research Center, Princeton University

## Jet and Rocket Propulsion Engines

**Design and Experimental Evaluation of a Light-Weight Turbine-Wheel Assembly,** by W. C. Morgan and R. H. Kemp, *NACA TN* 4023, June 1956, 25 pp.

**The Measurement of High Frequency Alternating Pressures in Gas Turbines,** by J. R. Forschaw and H. Taylor, *Gt. Brit., Aeron. Res. Council, R&M* 2990 (formerly *Nat. Gas. Turb. Estab. Mem.* M. 213), 1957, 14 pp.

**Combustion Processes in Liquid Propellent Rocket Motors,** Sixth Quarterly Progress Report, Jan. 1–March 31, 1957, *Princeton Univ. Dept. Aeron. Engng., Rep.* 334f, June 1957, 11 pp.

**The Component Pressure Losses in Combustion Chambers,** by H. A. Knight and R. B. Walker, *Gt. Brit. Aeron. Res. Council, R&M* 2987 (formerly *Nat. Gas Turb. Rep.* R. 143), 1957, 34 pp.

**Thermodynamic Investigation of the Benzene Turbine Cycle,** by N. A. Beldecos and J. D. Lokay, *Atomic Energy Commission,* WIAP-M-24, July 1953, 28 pp.

**Tests of Two Models of Eclipse Pioneer Rocket Driven Turbo Pumps,** by R. Fearn, *Naval Air Missile Test Center, Tech. Rep.* 42, March 1949, 53 pp. (Declassified from Confidential by authority of NAMTC letter A9/Ser. 362, 7/20/56.)

**Fire Safety Tests for Jets Needed Now,** by Richard van Osten, *American Aviation,* vol. 21, June 17, 1957, p. 89.

**Small Turbojets Put Life into "Flying Boxcar,"** *American Aviation,* vol. 21, June 17, 1957, p. 90.

**Design Progress: Combustion Starter Fills Interceptor Needs,** by Victor DeBiasi, *Aviation Age,* Vol. 27, June 1957, pp. 106–107.

**On Generalized Scaling Procedures for Liquid-Fuel Rocket Engines,** by S. S. Penner and A. E. Fuhs, *Combustion and Flame,* vol. 1, no. 2, June 1957, pp. 229–240.

**Rotating Stall in Axial Single Stage Compressors: Laws of Similitude,** by Simon Goldstein and Andre L. Jaumotte, *Z. Angew. Math. Physik,* vol. 8, no. 3, May 25, 1957, pp. 235–251 (in French).

**The Influence of Pressure and Temperature Variations on the Thrust of Ramjet, Turbojet, and Turboprop Engines,** by Rudolf Schmidt, *Z. Flugwissenschaften,* vol. 5, May 1957, pp. 139–149 (in German).

**Some Aspects of Compressor Stage Design,** by J. F. Louis and J. H. Horlock, *Gt. Brit., Aeron. Res. Council, Current Paper* 319 (Formerly *ARC Tech. Rep.* 18333), 1957, 12 pp., 7 figs.

**Determination of Turbine Stage Performance for an Automotive Power Plant,** by L. B. Mann Jr., A. H. Bell, and G. W. Thebert, *ASME, Pap.* 57-GTP-10, March 1957, 19 pp., 18 figs.

**A Generalized Presentation of Gas Turbine Combustor Performance,** by A. E. Noreen, and W. T. Martin, *ASME, Pap.* 57-GTP-5, March 1957, 9 pp.

**Analytical Methods for Performance Estimates of Free Piston Gasifiers,** by A. R. Bobrowsky, *ASME, Pap.* 57-GTP-6, March 1957, 15 pp., 8 figs.

**Over-all Performance of J35-A-23 Two-Stage Turbine** (revised version), by John J. Rebeske Jr., William E. Berkey and Robert E. Forrette, *NACA RM* E51E22, Dec. 1951, 20 pp. (Declassified from Confidential by authority of *NACA Res. Abstracts* 115, p. 11, 5/22/57.)

**An Analysis of the Potentialities of a Two-Stage Counterrotating Supersonic Compressor,** by Ward W. Wilcox, *NACA RM* E52E01, July 1952, 41 pp. (Declassified from Confidential by authority of *NACA Res. Abstracts* 115, p. 11, 5/22/57.

**Investigation of Losses in the XJ35-A-23 Two-Stage Turbine,** by John J. Rebeske Jr. and Robert E. Forrette, *NACA RM* E52E15, Aug. 1952, 25 pp. (Declassified from Confidential by authority of *NACA Res. Abstracts* 115, p. 12, 5/22/57.)

**Determination of Surge and Stall Limits of an Axial-Flow Turbojet Engine for Control Applications,** by Ross D. Schmidt, George Basu and Edward M. McGraw, *NACA RM* E53B10, Aug. 1953, 30 pp. (Declassified from Confidential by authority of *NACA Res. Abstracts* 115, p. 12, 5/22/57.)

## Heat Transfer and Fluid Flow

**Theoretical Analysis of Incompressible Flow through a Radial-Inlet Centrifugal Impeller at Various Weight Flows,** by James J. Kramer, Vasily D. Prian and Chung-Hua Wu, *NACA Rep.* 1279, 1956, 16 pp. (supersedes *NACA TN* 3448, and 3449).

**Thermodynamic Study of a Roots Compressor as a Source of High-Temperature Air,** by Clarence B. Cohen, Richard R. Woollett and Kenneth C. Weston, *NACA TN* 4025, June 1957, 34 pp.

**Hypersonic Gas Dynamic Charts for Equilibrium Air,** by Saul Feldman, *AVCO Mfg. Corp., AVCO Res. Lab.,* Jan. 1957, 123 pp.

**Free Convection in Narrow Vertical Liquid Metal Annuli,** by D. P. Timo, *Atomic Energy Commission,* KAPL-M-DPT-8, March 1955, 32 pp.

**The Effect of Chemical Nature of Heating Surfaces on the Heat Transfer Coefficients of Pool Boiling Liquids; Final Report for February 1, 1952–June 15, 1955,** by George W. Preckshot, *Atomic Energy Commission,* AECU-3183, Dec. 1955, 61 pp.

**Determination of Burnout Limits of Polyphenyl Coolants,** by K. Sato, *Atomic Energy Commission, Rep.* AGC-AE-32 (*Aerojet General Corp. Rep.* 1225), Feb. 1957, 51 pp.

**Thermal Conductivity Measurements,** by J. M. Davidson, *Atomic Energy Commission, Res. and Dev. Rep.,* HW 47063, Dec. 1956, 18 pp.

**Circumferential Inlet Distortions in Axial Flow Turbo-Machinery,** by Fredric Ehrich, *J. Aeron. Sci.,* vol. 24, June 1957, pp. 413–417.

EDITOR'S NOTE: Contributions from E. R. G. Eckert, J. P. Hartnett, T. F. Irvine Jr. and P. J. Schneider of the Heat Transfer Laboratory, University of Minnesota, are gratefully acknowledged.

# Electronic Cooling Package...by AiResearch

**SPECIFICATIONS OF TYPICAL AIRESEARCH COOLING PACKAGE**

| | |
|---|---|
| Air Flow | 60 CFM |
| Fan Air Inlet Pressure | 18 PSIA |
| Fan Pressure Rise | 1.2 inches water |
| Heat Exchanger Pressure Drop | 1.0 inches water |
| Liquid | Water Methanol (70% Methanol) |
| Liquid Flow | 0.4 GPM |
| Heat Rejection* | 300 Watts |
| Fan Power | 30 Watts, 110 V., single phase, 400 cycle |
| Package envelope dimensions | 7 x 6 x 3 inches |
| Package wet weight | 2.5 lbs. |

*Assumes Class A (85°C.) electronic components, liquid inlet temperature to heat exchanger, 55°C. Includes heat from fan motor.

This high performance AiResearch package cools sealed and pressurized electronic equipment. The fan circulates air through the liquid cooled heat exchanger and over electronic components in a hermetically sealed module. Air cooled units are also available. Fan and heat exchanger are designed, built and packaged by AiResearch for matched performance. Package size is tailored to your individual cooling requirements.

The Garrett Corporation, through its AiResearch Manufacturing divisions, is an industry leader in components and cooling systems for aircraft, missiles and nuclear applications. This wide experience is now being offered to the electronics industry to provide a cooling package to meet any cooling requirement. Send us details of your problem or contact the nearest Airsupply or Aero Engineering office for further information.

**THE GARRETT CORPORATION**

AiResearch Manufacturing Divisions

*Los Angeles 45, California • Phoenix, Arizona*

**AERO ENGINEERING OFFICES:**

MINEOLA • ATLANTA • BALTIMORE • BOSTON • CHICAGO • CINCINNATI • COLUMBUS
DETROIT • INDIANAPOLIS • PHILADELPHIA • ST. LOUIS • SYRACUSE • WINTER PARK

**AIRSUPPLY OFFICES:**

BEVERLY HILLS • DENVER • FT. WORTH • KANSAS CITY • SAN DIEGO • SAN FRANCISCO
SEATTLE • TULSA • WICHITA

**A Water Cooled Nozzle for a Large Solid Propellant Rocket Motor,** by Wayne J. Colahan Jr., *Calif. Inst. Techn., Jet Propulsion Lab., Mem.* 20-134, Sept. 1956, 22 pp.

## Aerodynamics of Jet Propelled Missiles

**Flight Investigations at Low Supersonic Speeds to Determine the Effectiveness of Cones and a Wedge in Reducing the Drag of Round Nose Bodies and Airfoils,** by Sidney R. Alexander, *NACA RM* L8L07a, March 1949, 15 pp. (Declassified from Confidential by authority of *NACA Res. Abstracts* 57, 1/29/54, p. 26.)

**Photographic Method of Determining the Aerodynamic Resistance of Missiles in Flight,** by C. E. Cremona, *Astronautica Acta,* vol. 3, no. 1, 1957, pp. 52–66 (in Italian).

**On Magnus Effects Caused by the Boundary-Layer Displacement Thickness on Bodies of Revolution at Small Angles of Attack,** by John C. Martin, *J. Aeron. Sci.,* vol. 24, June 1957, pp. 421–429.

**Laminar Boundary Layer on a Spinning Cone at Small Angles of Attack in a Supersonic Flow,** by R. Sedney, *J. Aeron. Sci.,* vol. 24, June 1957, pp. 430–436, 455.

**Newtonian Flow Theory for Slender Bodies,** by J. D. Cole, *J. Aeron. Sci.,* vol. 24, June 1957, pp. 448–455.

**Free Molecular Flow Forces and Heat Transfer for an Infinite Circular Cylinder at Angle of Attack,** by L. Talbot, *J. Aeron. Sci.,* vol. 24, June 1957, pp. 458–459.

**Flight Investigation of the Drag of Round-Nosed Bodies of Revolution at Mach Numbers from 0.6 to 1.5 Using Rocket-Propelled Test Vehicles,** by Roger G. Hart, *NACA RM* L51E25, July 1951, 9 pp. (Declassified from Confidential by authority of *NACA Res. Abstracts* 115, p. 15, 5/22/57.)

**Wind Tunnel Investigation of a Ramjet Canard Missile Model Having a Wing and Canard Surfaces of Delta Plan Form with 70° Swept Leading Edges; Longitudinal and Lateral Stability and Control Characteristics at a Mach Number of 1.60,** by M. Leroy Spearman and Ross B. Robinson, *NACA RM* L52E15, Aug. 1952, 63 pp. (Declassified from Confidential by authority of *NACA Res. Abstracts* 115, p. 16, 5/22/57.)

**On the Transonic Flow of a Compressible Fluid Past an Axisymmetric Slender Body at Zero Incidence,** by Ken-ichi Kusukawa, *J. Physical Soc. Japan,* vol. 12, April 1957, pp. 401–410.

**On the Transonic Flow of a Compressible Fluid Past a Nearly Axisymmetric Slender Body,** by Ken-ichi Kusukawa, *J. Physical Soc. Japan,* vol. 12, April 1957, pp. 411–419.

**Effect of Bluntness on Transition for a Cone and a Hollow Cylinder at Mach 3.1,** by Paul F. Brinich and Norman Sands, *NACA TN* 3979, May 1957, 42 pp.

**Detached Shock Waves Ahead of Bluff Nosed Cylinders,** by Jerome R. Katz, *NAVORD Rep.* 5423 (*NOTS* 1686), April 1957, 38 pp.

**Temperature Attained by a Missile at Great Speeds in the High Atmosphere,** by Marcel Devienne, *Fusées et Recherche Aeronautique,* vol. 2, no. 1, March 1957, pp. 43–47, (in French).

**Correlation of Cone-Cylinder Normal Force and Pitching Moment Data by the Hypersonic Similarity Rule,** by William H. Dorrance and Robert G. Norell, *J.*


# SOLID POWER FROM PETROLEUM

The "PRODUCER"—a new Phillips-designed rocket—develops higher thrust than any other known single solid propellant motor available today. Creative engineering which made this rocket a reality has also made possible other advances in design including the longest duration large solid propellant motor ever fired.

The "PRODUCER" uses composite solid propellant made of low-cost ammonium nitrate oxidizer, synthetic rubber fuel binder and additives. Low-cost components, reliable ignition and stable combustion make this motor attractive for a variety of applications.

In addition to the "PRODUCER" Phillips offers a wide range of off-the-shelf solid propellant motors for military use such as the M15 JATO, the "PUSHER" and sled booster motors and very long duration types. These versatile, economical propulsion units can be engineered to meet a variety of thrust, duration and total impulse requirements. The superior reliability, stability and shelf life of Phillips propellants are a "solid" argument for solid propulsion!

**We invite you to write and discuss your technical and production problems with us. Or call one of our regional representatives: Washington, D. C.—E. L. Klein, EXecutive 3-3050; Los Angeles—R. O. Gose, GRanite 2-0218; Dayton, Ohio—C. W. Strayer, YOrktown 3263.**

**Address all inquiries to:**
Rocket Fuels Division
**Bartlesville, Oklahoma**

Phillips 66

**PHILLIPS PETROLEUM COMPANY**
Bartlesville, Oklahoma

*Aeron. Sci.*, vol. 24, May 1957, pp. 371–377, 392.

**Vortex Interference Effects on the Aerodynamics of Slender Airplanes and Missiles,** by Alvin H. Sacks, *J. Aeron. Sci.*, vol. 24, June 1957, pp. 393–402, 412.

## Combustion, Fuels and Propellants

**Propagation of a Free Flame in a Turbulent Gas Stream,** by William R. Mickelson and Norman E. Ernstein, *NACA Rep.* 1286, 1956, 26 pp. (supersedes *NACA TN* 3456).

**Research on the Safety Characteristics of Normal Propyl Nitrate II; Terminal Report,** by Adolph B. Amster, George D. Edwards and Joseph B. Levy, *NAVORD Rep.* 4493, March 1957, 19 pp., 4 fig.

**Quarterly Periodic Status Report,** *Mass Inst. Tech., Depts. Chem. and Chem. Engng., Hydrogen Peroxide Labs.*, March 1957, 10 pp.

**National Annual Survey of Aviation Fuels, 1956,** by O. C. Blade, *Bur. Mines, Info. Circ.* 7782, March 1957, 16 pp., 5 fig.

**Production of Boron Trichloride by Means of a High Intensity Electric Arc Process,** by Charles Sheer, A. W. Diniac, J. A. Dyer and S. Korman, *Wright Air Dev. Center. Tech. Rep.* 56-487 (*ASTIA AD* 118305), March 1957, 59 pp.

**Mechanism and Kinetics of the Reaction between Fuming Nitric Acid and/or Its Decomposition Products and Gaseous Hydrocarbons,** *Franklin Inst., Labs. Res. and Dev., Final Tech. Rep.*, F-2452 (*WACD TR* 57-138; *ASTIA AD* 118105), July 11, 1954–Dec. 31, 1956, 54 pp.

**Factors Which Influence the Suitability of Liquid Propellants as Rocket Motor Regenerative Coolants,** by D. R. Bartz, *Calif. Inst. Tech., Jet Propulsion Lab., Mem.* 20-139, Dec. 1956, 21 pp.

**Free Radicals as Fuels,** by Karl Scheller, Henry C. Thacker Jr. and James A. Bierlein, *Wright Air Dev. Center, Tech. Note* 56-538 (*ASTIA AD* 118101), Feb. 1957, 25 pp.

**Hydrogen,** *Atomic Energy Commission, Safety and Fire Protection Bull.* 5, 1956, 10 pp.

**Ignition Reactions in the Hydrogen Oxygen Water System at Elevated Temperatures,** by Elmer F. Stephan, Nathan S. Hatfield, Robert S. Peoples and H. A. Pray, *Atomic Energy Commission*, BMI-1138, Oct. 1956, 56 pp.

**Research on the Combustion and Explosion Hazards of Hydrogen Water Vapor Air Mixtures,** by Michael G. Zabetakis, *Atomic Energy Commission*, AECU-3327, Sept. 1956, 11 pp.

**Evaluation of RMI Servicing Equipment,** by Guy G. Wooten, *Naval Air Missile Test Center, Tech. Rep.* 29, May 1948, 27 pp. (Declassified from Confidential by authority of NAMTC letter A9/Ser. 362, 7/20/56.)

**Dimethylamino Radical,** by Francis Owen Rice and Chester J. Grelecki, *J. American Chem. Soc.*, vol. 79, June 5, 1957, pp. 2679–2680.

**Chemically Reacting Systems in Equilibrium, I: Calculation of Mixture Strengths,** by H. J. Kaeppeler and G. Baumann, *Astronautica Acta*, vol. 3, no. 1, 1957, pp. 28–46 (in German).

**Some Limiting Oxygen Concentrations for Diffusion Flames in Air Diluted with Nitrogen,** by R. F. Simmons and H. G. Wolfhard, *Combustion and Flame*, vol. 1, no. 2, June 1957, pp. 155–161.

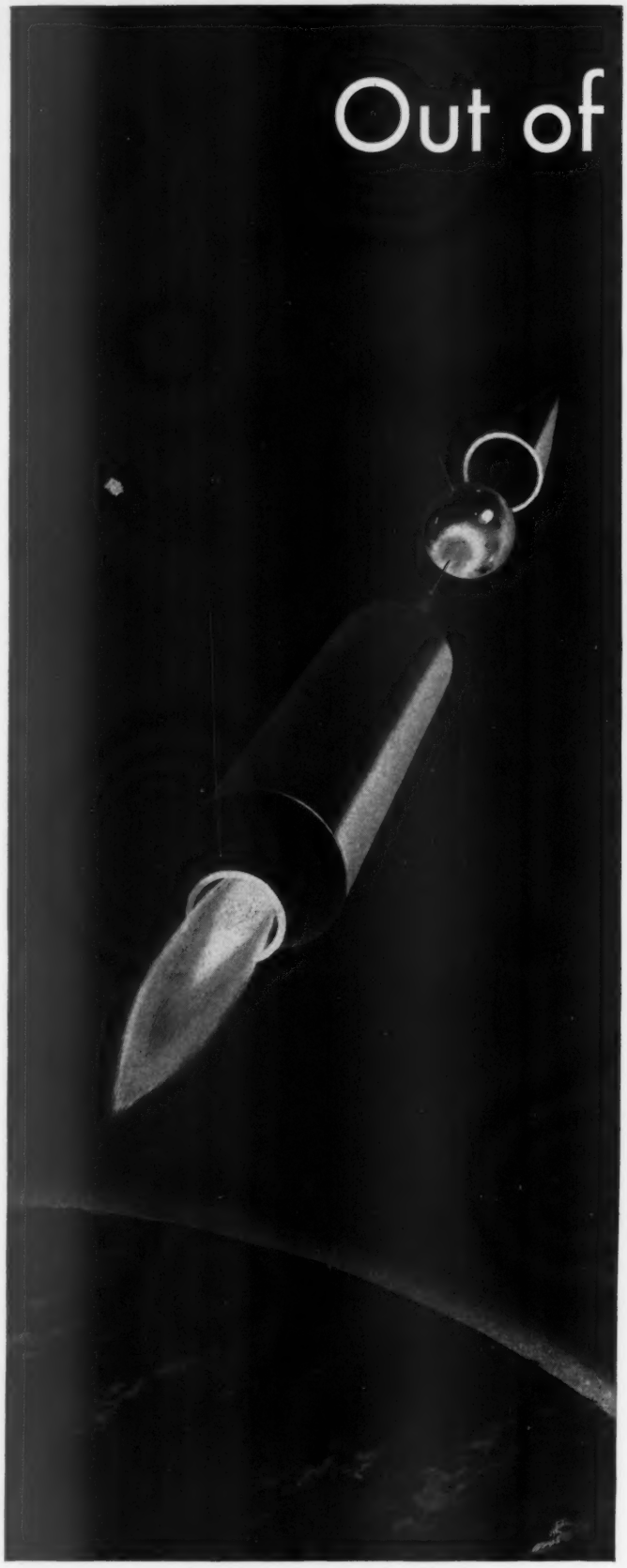

# Out of this world!

## *Norton ROKIDE* coating may aid in launching the satellite at the end of its final rocket ride — 300 miles high*

In the Defense Department's *Project Vanguard*, a three-stage rocket is planned to carry a shining satellite into an orbit hundreds of miles above the earth. The third and last stage of the rocket will reach approximately 18,000 miles per hour when it releases the satellite 300 miles above the earth.

*One of the third-stage rocket engines being tested for Project Vanguard — and successfully flown last May 1st — was manufactured by The Grand Central Rocket Company of Redlands, California. To help contain the terrific*

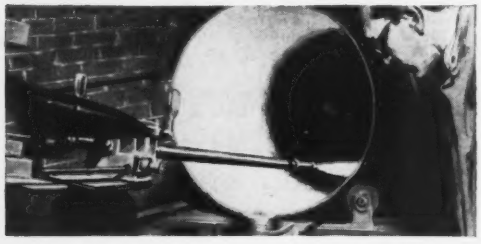

*energy release required to reach this supersonic speed, the inside of its nozzle is protected with* ROKIDE *"A" aluminum oxide coating applied by the Metallizing Company of Los Angeles.*

Besides ROKIDE "A" other Norton ROKIDE spray coatings include "ZS" zirconium silicate and "Z" zirconium oxide. All are hard, adherent crystalline refractory materials. All can be applied to base materials, particularly metals, of a wide variety of shapes and sizes.

Parts on which ROKIDE coatings are especially useful are those requiring thermal or electrical insulation . . . refractoriness . . . resistance to wear or corrosion . . . high melting points . . . excellent mechanical strength . . . dimensional stability . . . relative chemical inertness.

Proved in such critical applications as reaction motors and some A.E.C. projects, ROKIDE coatings are also of great value to general industry. Other Norton high-purity, chemically-stable refractory materials are helping industry to break through the "thermal barrier."

Facilities for applying ROKIDE coatings are available at Norton Company, Worcester, Mass., and Santa Clara, Cal., and at strategically located licensee plants. For complete facts, write to NORTON COMPANY, New Products Department, 729 New Bond Street, Worcester 6, Massachusetts.

**NORTON**

**NEW PRODUCTS**

*Making better products . . . to make your products better*

**NORTON PRODUCTS**
Abrasives • Grinding Wheels
Grinding Machines • Refractories
**BEHR-MANNING DIVISION**
Coated Abrasives • Sharpening Stones
Pressure-Sensitive Tapes

*Trade-Mark Reg. U. S. Pat. Off. and Foreign Countries

# New Patents

George F. McLaughlin, *Contributor*

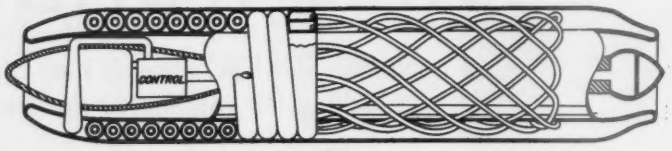


2,798,361

**Internal combustion engines (2,798,361).** Frederick A. Hiersch, Detroit, Mich., assignor to Continental Aviation and Engineering Corp.

Jet engine with a coiled fuel storage tank ahead of annular headers at the mid-section. Fuel from the outer header discharges preheated fuel to the inner header, and from there to the combustion chamber.

**Means for slowing down an aircraft during landing when powered by a turbojet (2,798,362).** H. S. Rainbow and D. Pym, Coventry, England, assignors to Armstrong Siddeley Motors, Ltd.

Pairs of flaps pivotally mounted near their downstream ends around the jet nozzle. Adjacent flaps, when opened, provide a V-section in which one flange extends well into the path of the jet gases, and the other outside the nozzle, to change the flow direction of part of the gases.

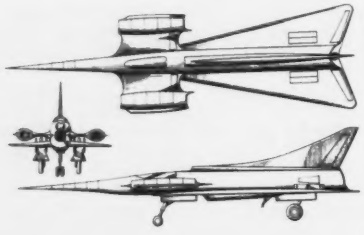

**Aircraft design 180,846.** Andrew Rocco, El Segundo, Calif.

**Gas turbine power plant apparatus (2,798,661).** Arthur Willenbrock Jr. and Arnold H. Redding, Wallingford, Pa., assignors to Westinghouse Electric Corp.

Sets of curved radial vanes for guiding currents of fluid uniformly throughout the flow area. Each set includes two left-hand and two right-hand vanes. Left-hand vanes are disposed adjacent to each other, and right-hand vanes adjacent to each other.

**Flexible coupling for connecting jet-engine-powered aircraft (or guided missiles) to ground mounted silencers (2,798,743).** Nils-Olof Olesten, Linkoping, Sweden, assignor to Svenska Aeroplan Aktiebolaget.

Vehicle discharge pipe opens into a tubular connecting member of the silencer to form a continuous duct. A flexible bellows encircles the connector, its rear part encompassing the front of the silencer with a gas-tight connection.

**Jet-driven helicopter rotor system (2,799,353).** Edward T. Andrews, Belleair Beach, Largo, Fla.

Automatic interruption of jet discharge at the rotor tip while the blade is opposite the horizontal movement of the helicopter. The discharge is re-established when blade movement is in the same general direction as horizontal movement of the helicopter.

**Propellant powder (2,799,566).** Ralph L. Cook, Alton, Ill., assignor to Olin Mathieson Chemical Corp.

Smokeless powder grain coated with a mixture of 1 to 4 parts (by weight) of potassium sulfate and 1 to 4 parts of alkaline metal nitrates consisting of the nitrates of potassium and sodium. The coating is between 0.10 to 1.50 per cent.

**Acoustic jet engine with flow deflection fluid pumping characteristics (2,796,735).** Albert G. Bodine Jr., Van Nuys, Calif.

Jet flow apparatus with a resonant fluid conduit and pressure pulse generating means in part of the conduit for creating periodic pressure pulses in the fluid. A net pumping gradient is created in response to flow in the conduit, inwardly of the inlet and outwardly of the outlet.

**Critical aerodynamic limit indicator (2,796,763).** Grosse-Lohmann, Montgomery County, Md.

Instrument with hands arranged to cross each other to indicate at their intersection values of Mach number and angle of attack. A reference correlates the intersection of hands with respect to allowable aircraft performance.

**Jet deflecting device for discharge nozzles of propulsion units (2,797,547).** H. L. P. Meulien, L. J. Bauger and H. Turinetti, Paris, France.

Grid of deflecting blades placed outside the normal path of the jet. A cowling covers the blades during nondeflecting periods, and uncovers them when deflection of the jet stream is desired.

**Apparatus for simulating aircraft turbojet engine operation (2,798,308).** Robert G. Stern and Thomas C. Wakefield, Denville, N. J., assignors to Curtiss-Wright Corp.

Throttle controlling a quantity representing rpm. Electrical systems operated according to functions of simulated altitude and Mach number produce quantities representing temperature functions. The combined quantities result in an indication of turbine outlet temperature.

**Ducted fan type jet propulsion engine (2,798,360).** Ronald M. Hazen and Otaker P. Prachar, Indianapolis, Ind., assignors to General Motors Corp.

Means for reducing the capacity of a first compressor during starting of a turbine, and for varying the area of the exhaust nozzle for the second combustion chamber. An igniter tube extending between the two chambers conducts hot gas for ignition of the fuel.

EDITORS NOTE: Patents listed above were selected from the Official Gazette of the U. S. Patent Office. Printed copies of Patents may be obtained from the Commissioner of Patents, Washington 25, D. C., at a cost of 25 cents each; design patents, 10 cents.

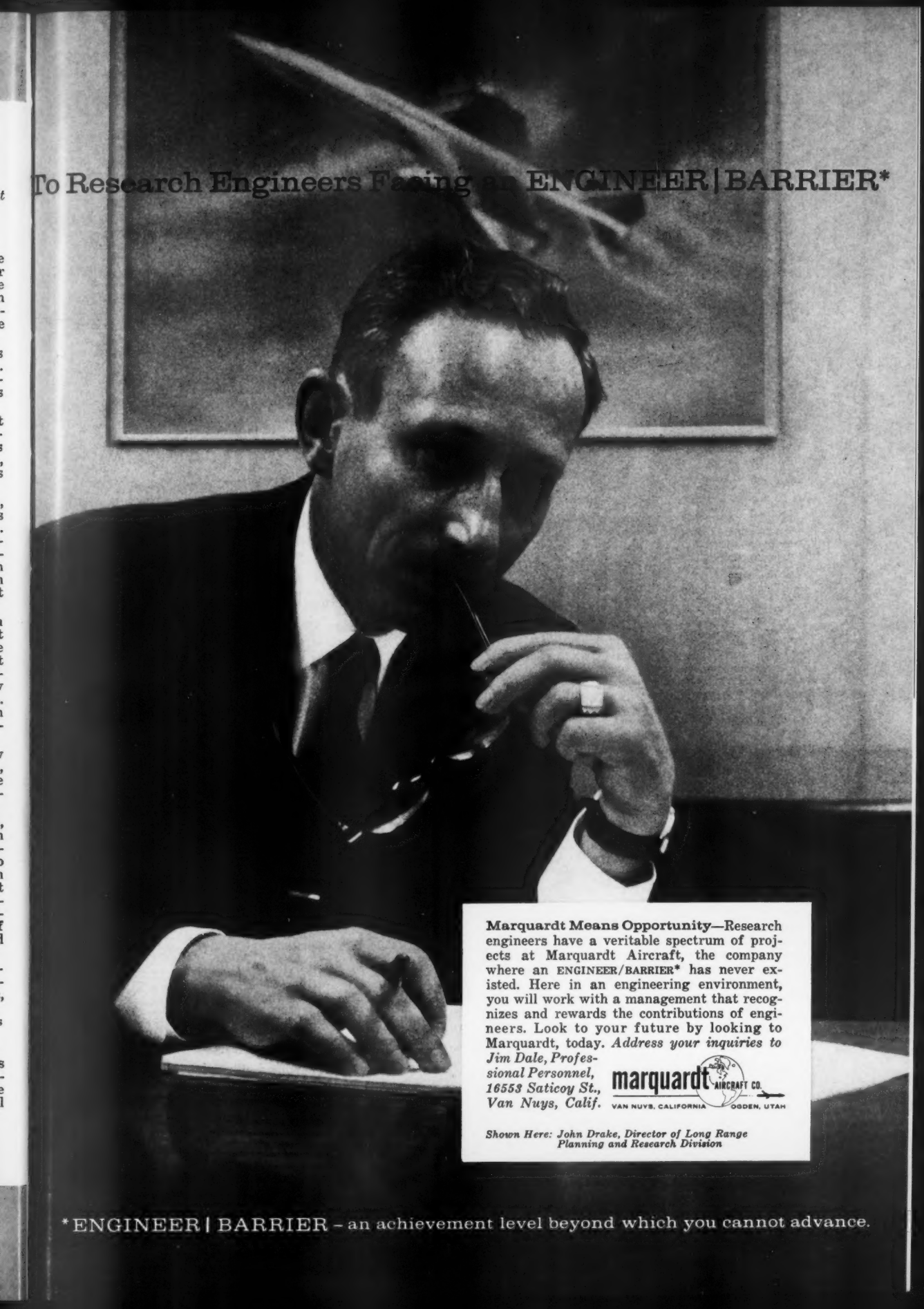
To Research Engineers Facing an ENGINEER | BARRIER*
Marquardt Means Opportunity—Research engineers have a veritable spectrum of projects at Marquardt Aircraft, the company where an ENGINEER/BARRIER* has never existed. Here in an engineering environment, you will work with a management that recognizes and rewards the contributions of engineers. Look to your future by looking to Marquardt, today. Address your inquiries to Jim Dale, Professional Personnel, 16553 Saticoy St., Van Nuys, Calif.
marquardt AIRCRAFT CO.
VAN NUYS, CALIFORNIA
OGDEN, UTAH
Shown Here: John Drake, Director of Long Range Planning and Research Division
*ENGINEER | BARRIER – an achievement level beyond which you cannot advance.

**Means for controlling the speed of jet propelled aircraft, missiles or other aerial bodies** (2,796,730). O. N. Lawrence, Dorridge, England, assignor to Joseph Lucas, Ltd.

Ramjet-propelled body, with propulsion means movable at or above sonic speed. When a change in the position the shock wave produces causes the motion of the body to exceed a predetermined value, a detecting means causes a reduction in the fuel supply.

**Variable area jet propulsion nozzle** (2,796,731). F. W. W. Morley and A. A. Rubbra, Littleover, England, assignors to Rolls-Royce, Ltd.

Arcuate flaps in overlapping positions form a wall and are pivotally mounted at their upstream ends. Pairs of elements are angularly disposed, supported in circumferential relation, and are moved to vary the nozzle area.

**Gas producing apparatus of the gas turbine type** (2,796,732). A. J. Penn, Northwood, England, assignor to D. Napier & Son, Ltd.

Turbine, driven by the products of combustion, driving a first compressor and a second air compressor. The exhaust from turbine and compressor air are delivered into a duct from which they are discharged through a single conduit to form the required power gas.

**Sonic burner heat engine with acoustic reflector for augmentation** (2,796,734). Albert G. Bodine Jr., Van Nuys, Calif.

Burner with a gas conduit forming a resonant guide for a fundamental frequency acoustic pattern. The pattern has high and low impedance regions spaced longitudinally of the conduit. The combustion chamber is located in the high impedance region of the pattern, and a gas discharge port at the low impedance region.

**Launcher** (2,800,836). Aden B. Meinel, Pasadena, Calif., assignor to the U. S. Navy.

Rocket launcher on which a removably mounted main launching track is supported on releasable triangular legs, brace members and base plates.

**Detonation trap for liquid explosives using frangible coupling** (2,801,517). Maurice J. Zucrow and Thorpe B. Walker, Pasadena, Calif., assignors to Aerojet-General Corp.

Device for arresting a detonation wave traveling through a fluid in the conduit between a reservoir and a jet motor. A frangible section with a closed end is included in the conduit downstream from the section. A loop section provides fluid continuity between the frangible section and the side outlet of a cylindrical tube in the conduit.

**Remote control system** (2,801,815). Everard M. Williams and Edwin V. Cousy, Dayton, Ohio.

System for controlling the flight of a missile along the axis of a solid cone radiation pattern in accordance with the resultants of differentially combined received energy flow during the first and second two pulse intervals.

**Supersonic airplane cooling system** (2,801,829). John E. M. Taylor, Cleveland Heights, Ohio.

A heat exchanger movably mounted for cooling selected portions of an aircraft moving at speeds high enough to produce a frictional, high temperature fluid boundary on its external surfaces. The system reduces the relative velocity between the exchanger and the external free air to prevent formation of the boundary layer on portions of the exchanger.

# New Bendix SM-E Connector

*(smaller, lighter than AN-E but equally dependable)*

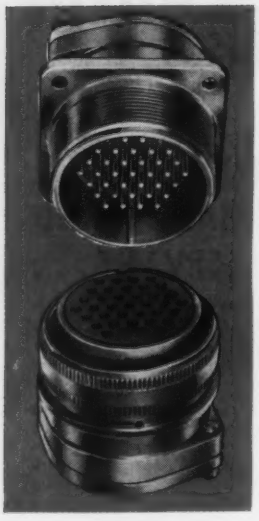

Here is the newest in the ever growing family of Bendix* environment resistant connectors. The new SM-E Series (Short "E") will provide the same performance as the standard AN-E connectors, but is shorter, lighter and more easily serviced. Not only does this connector conform to the vibration resistant requirements of the "E" connector in the MIL-C-5015C government specification, but it also provides effective moisture barriers both at the solder well ends and mating surfaces using the full range of wire sizes. Of particular interest to production and maintenance people is the back nut design, which provides a jacking action on the grommet during disassembly, thereby lifting it free of the solder wells. This feature when combined with the new Bendix "slippery rubber" grommets makes easy work of wire threading and grommet travel over the wire bundles.

Available in all standard AN shell sizes and tooled for most of the popular AN configurations.

Write for complete descriptive folder.

*TRADEMARK

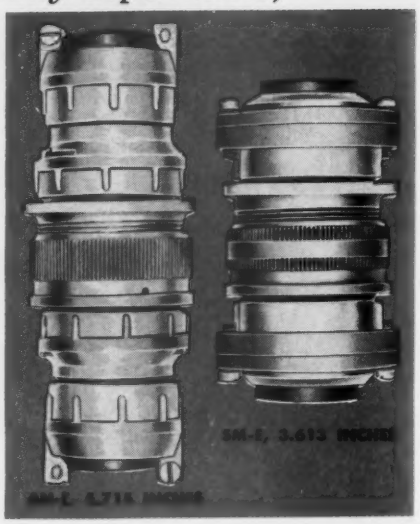


Comparison based on size 40 mated assemblies. Space savings for smaller sizes are proportional.

Bendix **SCINTILLA DIVISION of** Bendix AVIATION CORPORATION
**SIDNEY, NEW YORK**

Export Sales and Service: Bendix International Division, 205 East 42nd St., New York 17, N. Y.
FACTORY BRANCH OFFICES:
117 E. Providencia Ave., Burbank, Calif. • Paterson Building, 18038 Mack Ave., Detroit 24, Mich. • 545 Cedar Lane, Teaneck, N. J. • 5906 North Port Washington Rd., Milwaukee 17, Wisc.
Hulman Building, 120 W. Second St., Dayton 2, Ohio • 2608 Inwood Road, Dallas 19, Texas • 8425 First Ave., South, Seattle 8, Washington • 1701 "K" Street, N.W., Washington 6, D. C.

---

# NORTHAM

**HIGH SENSITIVITY, LOW RANGE**
**PRESSURE TRANSDUCER**

Diameter: 2¼"

Weight: 12 oz.

An extremely sensitive variable inductance instrument for measurement of steady and transient pressure in full scale ranges as low as ± 4 inches of water. Permissible pressure overload in either direction up to maximum line pressure, 100 psi, for difficult flow-metering applications. A light diaphragm sensing element free from external mechanical linkage results in high natural frequency for dynamic measurements.

**MODEL DP-7 SPECIFICATIONS:**

Pressure Ranges:....± 0.15 to ± 15 psid
Maximum Line Pressure:.....100 psi
Accuracy:.....± 1% full scale
Excitation Frequency: From 60 to 20,000 cps
Natural Frequency: From 250 cps for 0.15 psi range to 2500 cps for 15 psi range

**WRITE FOR BULLETIN NO. JP-7**

**Northam Engineering Facilities Are Available To Assist You With Any Application Problems.**

**NORTHAM PRODUCTS INCLUDE . . .**

Transducers for pressure, acceleration and displacement measurement and auxiliary electronic equipment for complete systems.

**NORTHAM ELECTRONICS, INC.**
*A Subsidiary of Norris-Thermador Corp.*
2420 North Lake Avenue, Altadena, Calif.

---

# SPECIAL PURPOSE RECEIVERS

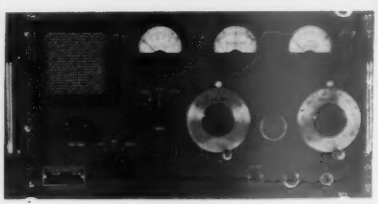

(TYPE 1400)

**NEMS-CLARKE is the recognized leader in the design and production of Special Purpose Receivers. We have a receiver to meet your requirements, whether it be for laboratory applications, telemetry reception, propagation study, guided missile monitoring, television and sound rebroadcasting, or as a general communication receiver where superior performance is required.**

## NEMS • CLARKE INC.

A DIVISION OF VITRO CORP. OF AMERICA
919 JESUP-BLAIR DRIVE
SILVER SPRING, MARYLAND

*For further information write Dept. V-1*

---

**PRECISE CURRENT for your TESTING NEEDS!**

**VARIABLE FREQUENCY MOTOR GENERATOR SETS ADJUST 360 TO 440 CPS.**

Generator mounted controls include reset buttons, limit switch. Motor and generator remain stationary. Vari-drive pulley adjustment controlled by small motor. Remote control panels available.

Units can be equipped with synchronous motor starter and magnetic amplifier, automatic voltage regulator.

**KATO 400 CYCLE MOTOR GENERATOR SETS**
***NOW UP TO 250 KW!***

KATO MOTOR GENERATOR SETS are available in frequencies, speeds and sizes for every specialized use . . . operating high cycle tools, testing components and electronic equipment.

**INPUT 60 CYCLES**
**OUTPUT 400 CYCLES**

**WRITE FOR NEW FOLDER!**

**Builders of fine Electrical Machinery Since 1928**

## KATO Engineering Company

**1498 First Ave., Mankato, Minn.**

# Solar's Missile Capabilities Start with Basic Design

SOLAR'S EXPERIENCED missile engineering group is made up of qualified experts in the many sciences related to missile development. It is a versatile organization devoted entirely to guided missile technology—from basic design to highly precise, top-quality production. And underlying Solar's missile capabilities is a ten-year backlog of experience. For more than a decade the company has been actively engaged in building fuselages, controls, propulsion units and components of stainless steel, titanium and other high-temperature super alloys. Solar's creative missile team is available *now* to assist in your important missile program.

SOLAR AIRCRAFT COMPANY — SAN DIEGO, DES MOINES

**FOR COMPLETE INFORMATION** write to Missile Engineering, Dept. D-91, Solar Aircraft Company, San Diego 12, Calif.

**ENGINEERS WANTED.** Unlimited opportunities, challenging projects, good living with Solar! Write for new brochure.


JANUS:
*protector of doors to heaven*

# Temperature, Pressure, Moisture, Dust

Expanding aircraft performance creates new problems in protecting electronic equipment under extreme altitude and ambient conditions. Eastern's long experience in the field helps you to recommend electronic gear with confidence that performance will be reliable at temperatures from — 55°C to +55°C; from zero to over 70,000 feet.

Cooling Units, with or without refrigeration cycles, provide safe operating temperature limits in electronic equipment. Pressurization Units that meet government specifications maintain proper operating pressures at various altitudes, and utilize dehydrators that remove moisture and dust from ambient air. A program of research and development continually expands performance ranges to provide customized units to meet your needs.

When your problem is to make your electronic equipment perform efficiently under tough conditions, meet the challenge by asking Eastern for complete and creative engineering help.

*Write for Eastern*
*AVIONICS BULLETIN 340*

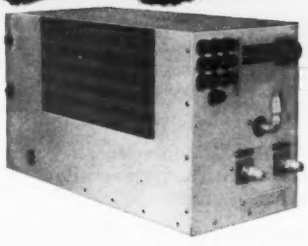

REFRIGERATION COOLING UNIT

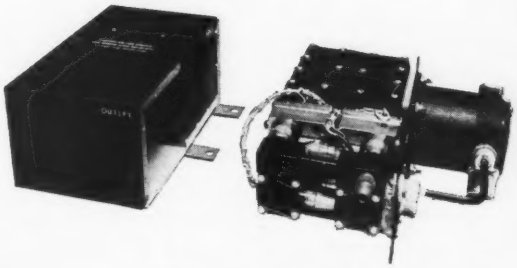

1500 SERIES PRESSURIZATION UNIT

EASTERN AVIATION PRODUCTS

**Eastern INDUSTRIES, INC.**
100 Skiff St. Hamden 14, Conn.

*West Coast Office: 1608 Centinela Avenue — Inglewood 3, California — Phone ORegon 8-3958*


# The rivet that rides the hot seat of the F-102A Delta Dagger

***How Convair solved a red-hot fastening problem with Du Pont Aircraft Blind Expansion Rivets***

Convair had to find a blind fastener that would give dependable service at elevated temperatures.

They found that Du Pont High Temperature Nickel Rivets solved the problem—fastening the asbestos edge gasket on the access door in the shroud for the afterburner assembly of the F-102A Delta Dagger.

But that's only part of the story. Here are some other important reasons for Convair's choice of Du Pont Rivets.

- **Fast Setting**—One man, working from the head of the rivet, can easily set 20-25 rivets per minute.
- **No Refinishing**—There's no need for cutting, trimming or buffing after the rivets are set.
- **Wide Grip Range**—The wide grip range permits the use of one rivet size for fastening varying material thicknesses.
- **Positive Holding Power**—The rivet shank expands to fill the hole completely, insuring tight joints.

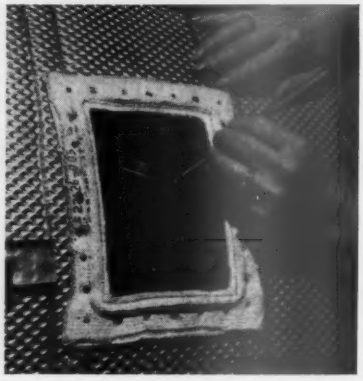

**Final inspection shows** that Du Pont Rivets have firmly secured the asbestos gasket around the access door in the shroud for the afterburner.

Find out how Du Pont Aircraft Blind Expansion Rivets can solve your fastening problems. Call your Du Pont representative or write: E. I. du Pont de Nemours & Co. (Inc.), Explosives Department, Wilmington 98, Delaware.

**DU PONT AIRCRAFT BLIND EXPANSION RIVETS**

DU PONT REG. U.S. PAT. OFF. *A Product of Du Pont Research*

BETTER THINGS FOR BETTER LIVING . . . *THROUGH CHEMISTRY*

# Do you think of pressure transducers?

## The Martin Company does...

and uses Statham Model PA183 pressure transducers in the SeaMaster program.

The Navy's P6M Martin SeaMaster is a 600-mile-per-hour pioneer aircraft of tomorrow's mobile seaplane striking forces.

The Model PA183 pressure transducer is available in ranges from 0-5 to 0-1,000 psi absolute with characteristics ideally suited to flight test. The transducing element is the rugged Statham unbonded strain gage. A feature of the design is that the case permits stacking one instrument upon another.

**WHEN THE NEED IS TO KNOW... FOR SURE SPECIFY STATHAM**

*Please request Bulletin No. PA183TC*

Statham

LABORATORIES

LOS ANGELES 64, CALIFORNIA

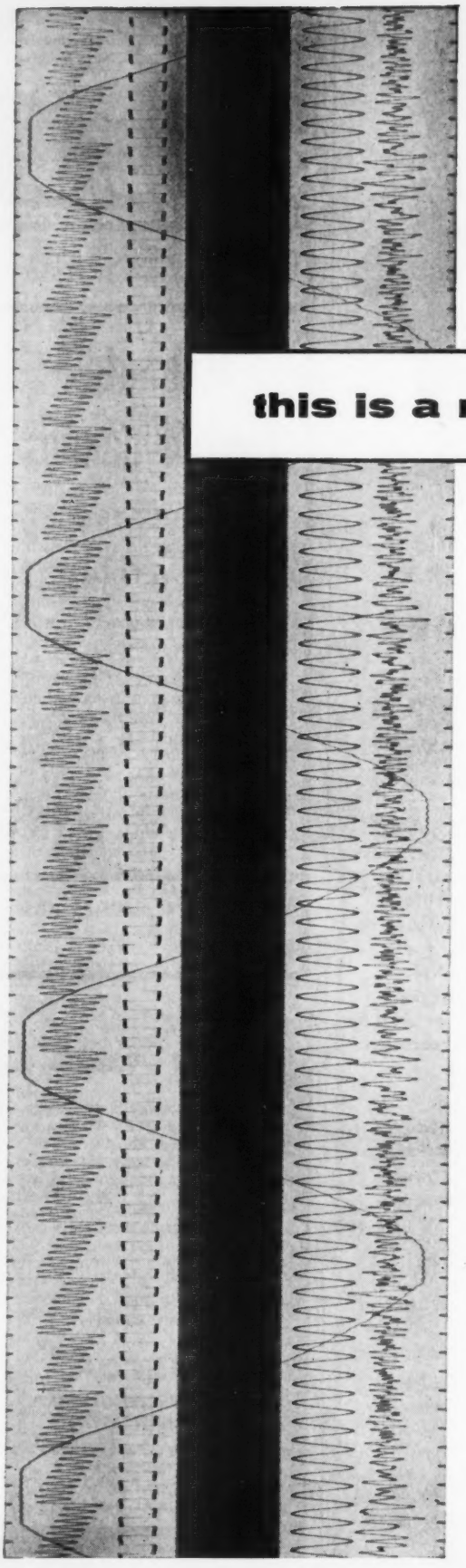

# this is a record of leadership

This Visicorder Oscillograph record* is a symbol of the leadership that is typical of Honeywell engineering. In laboratories all over the world the Visicorder's instantly-readable direct records are showing the way to new advances in rocketry, control, computing, product design and component test, and in nuclear research.

The Model 906 Visicorder is years ahead of the trend. It is the first recording oscillograph that combines the convenience of direct recording with the high frequencies and sensitivities of photographic-type instruments. The Visicorder alone among oscillographs makes it possible for you to monitor high-speed variables as they go on the record.

To record directly the high frequency variables you need to study, use the Visicorder Oscillograph. Call your nearest Minneapolis-Honeywell Industrial Sales Office for demonstation.

*reproduced half size

*Minneapolis-Honeywell Regulator Co., Heiland Division, 5200 East Evans Avenue, Denver 22, Colorado.*

**Reference Data: Write for Visicorder Bulletin**

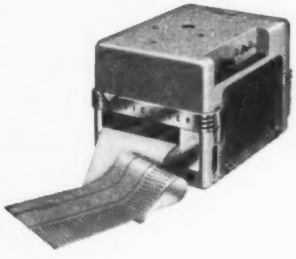

MINNEAPOLIS
**Honeywell**
Heiland Division

# Index to Advertisers